STRUCTURAL TRANSITIONS IN SELF-ASSEMBLED LIPID SYSTEMS DRIVEN BY INDUCED CURVATURE: FROM CELL-PENETRATING PEPTIDES TO PROGRAMMABLE VESICLES

BY

ABHIJIT MISHRA

DISSERTATION

Submitted in partial fulfillment of the requirements
for the degree of Doctor of Philosophy in Materials Science and Engineering
in the Graduate College of the
University of Illinois at Urbana-Champaign, 2010

Urbana, Illinois

Doctoral Committee:

Professor Gerard Wong, Chair and Director of Research
Professor Yi Lu
Professor Kenneth Schweizer
Assistant Professor Jianjun Cheng

ABSTRACT

Arginine rich cell-penetrating peptides are short cationic peptides capable of traversing the plasma membranes of eukaryotic cells. While successful intracellular delivery of many biologically active macromolecules has been accomplished using these peptides, their mechanisms of cell entry are still under investigation. Ionic interactions between the highly cationic peptides and the anionic cell membrane and other anionic molecules on the cell surface are believed to be the initial step in the internalization process.

We examined the interactions of TAT peptide with prototypical cell membranes using confocal microscopy and synchrotron small angle x-ray scattering (SAXS) and studied the effect of membrane charge and intrinsic curvature. We find that the TAT peptide induces negative Gaussian ('saddle-splay') membrane curvature, which is topologically required for pore formation. TAT peptide drastically remodels vesicles into a porous 'sponge-like' bicontinuous manifold. By applying ideas from coordination chemistry, soft condensed matter physics and differential geometry, we propose a geometric mechanism facilitated by both electrostatics and bidentate hydrogen bonding.

We also examined the interactions of other arginine rich cell-penetrating peptides, including Antp and oligoarginine, with model cell membranes, and find that the transduction activity correlates with induction of negative Gaussian curvature. The negative Gaussian membrane curvature is broadly enabling and its

induction can lower the free energy barriers for a range of different entry mechanisms, such as direct translocation as well as endocytotic pathways. Furthermore, we show that the TAT peptide interacts strongly with actin cytoskeleton, which enhances membrane deformation and cytoskeleton reorganization necessary for endocytotic processes. We propose a mechanism that explains how a relatively simple molecule, like the TAT peptide, facilitates direct entry and multiple endocytotic mechanisms.

ACKNOWLEDGEMENTS

I would like to thank my advisor, Prof. Gerard C.L. Wong, for his guidance, support and patience throughout the time I spent at UIUC. I am grateful to him for providing me with numerous opportunities to enhance my knowledge and professional skills. His insights and cooperation have been extremely valuable.

I would also like to thank Prof. Yi Lu for his help and guidance. I am also grateful to Prof. Jianjun Cheng and Prof. Kenneth S. Schweizer for their advice, thoughtful comments and suggestions. I am also thankful to Prof. Tim Deming and Prof. Daniel Kamei at UCLA.

I would like to thank all members of the Wong group for their help, support and friendship – Hongjun Liang, Thomas Angelini, John Butler, Scott Slimmer, Lori Sanders, Rob Coridan, Olena Rudko, Lihua Yang, Nathan Schmidt, Ghee Hwee Lai, Kirstin Purdy, Vernita Gordon, Fan Jin and Max Gibiansky. I am also grateful to Mehmet Yigit, Zehui Cao and Zidong Wang from the Lu lab and Rong Tong and Li Tang from the Cheng Lab.

Finally, I want to thank my family – my parents, brother and sister-in-law – for their support, encouragement and love through the many years of my education.

TABLE OF CONTENTS

CHAPTER 1 INTRODUCTION..... 1

1.1 Structure of lipids..... 3
1.2 Polymorphism of lipids in aqueous solution..... 9
1.3 Cubic phases in lipids..... 16
1.4 Characterization of lipid phases..... 21
1.5 Application of liposomes..... 25
1.6 References..... 27

CHAPTER 2 ARGININE RICH CELL-PENETRATING PEPTIDES..... 39

2.1 TAT peptide as a prototypical example of arginine rich cell penetrating peptides..... 40
2.2 Mechanism of cellular uptake: direct translocation or endocytosis?..... 44
2.3 Interactions between lipid membranes and biomolecules..... 51
2.4 Small angle x-ray scattering (SAXS) measurements for biomolecular samples..... 55
2.5 References..... 60

CHAPTER 3 HIV TAT PEPTIDE FORMS PORES IN MEMBRANES BY INDUCING SADDLE-SPLAY CURVATURE: POTENTIAL ROLE OF BIDENTATE HYDROGEN BONDING..... 69

3.1 Introduction..... 69
3.2 Experimental section..... 70
3.3 Results and discussion..... 72
3.4 Summary..... 85
3.5 References..... 86

CHAPTER 4 MECHANISM FOR CELLULAR UPTAKE OF ARGININE RICH CELL-PENETRATING PEPTIDES..... 88

4.1 Introduction..... 88
4.2 Experimental section..... 90
4.3 Results and discussion..... 93
4.4 Summary..... 114
4.5 References..... 114

CHAPTER 5 INORGANIC MERCURY DETECTION AND CONTROLLED RELEASE OF CHELATING AGENTS FROM ION-RESPONSIVE PEG-LIPOSOMES..... 119

5.1 Introduction.....119
5.2 Experimental section..... 121
5.3 Results and discussion..... 124
5.4 Conclusion..... 133
5.4 References.....133

CHAPTER 1

INTRODUCTION

All cells, in both eukaryotic and prokaryotic organisms, are surrounded by the 'plasma' or 'cell' membrane. This membrane compartmentalizes the intracellular space dividing it into two sub-spaces: the lumina of the various organelles and the cytosol. This enables the individual compartments to specialize for one or several well defined functions creating order within the cell and facilitating the control of such a complex machine. The plasma membrane of animal cells is in general a three layered compound system (Fig 1.1) [1-3]. The center consists of a liquid crystalline lipid/protein layer. The outer surface (called the glycocalix) is covered by a macromolecular film formed by the oligosaccharides of the glycolipid head groups and the branched polypeptide/oligosaccharide head groups of the glycoproteins. At the intracellular side, the bilayer couples to the membrane associated cytoskeleton - the three dimensional macromolecular network of actin filaments in most cells. In cell membranes, lipid bilayers provide a fluidic matrix in which membrane proteins move around [4,5]. The lipid bilayer together with the glycocalix forms a selective filter which controls the transfer of ions, molecules, molecular aggregates and even large particles (such as viruses, bacteria or other cells) between the extracellular space and the cytosol. The bilayer is a multifunctional system which can simultaneously be the site for energy producing processes (such as glycolysis) and for the hormone signal transduction and amplification. The glycocalix acts as receptor for extracellular signals and mediates the

communication between the cell interior and its environment. The lipid protein bilayer together with the cytoskeleton is responsible for the unique combination of flexibility and mechanical stability of cells. The composition of cell membranes involves about a hundred components and thus poses a real challenge for the development of new concepts of the physical basis of self-organization of multi-component systems. However, by reconstituting model membranes from a few lipids and membrane proteins, specific membrane function can be studied on a molecular level [1].

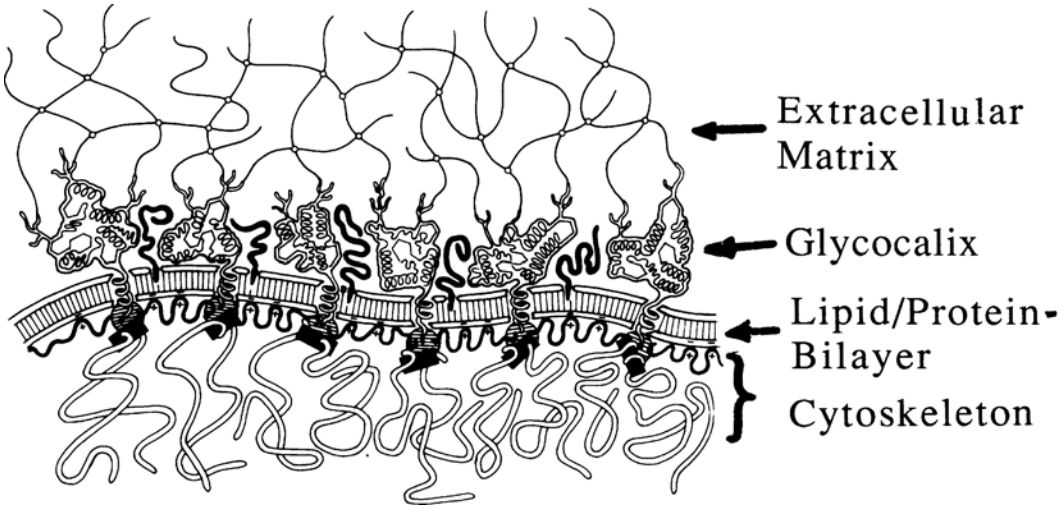


Figure 1.1: Schematic showing the three-layered structure of the cell membrane. The lipid/protein bilayer forms the center. The glycocalix faces the extracellular side and the cytoskeleton, coupled to the bilayer, faces the cytosol. (image adapted from reference [1])

1.1 Structure of lipids

Lipid bilayers are non-covalent structures spontaneously formed by lipid molecules due to their amphiphilic nature, that is, they contain a polar region (hydrophilic headgroup), which prefer high dielectric constant (polar) solvents such as water, and hydrocarbon regions (hydrophobic tails), which prefer non-polar solvents such as oil. The hydrophobic tail is generally composed of one or two fatty acid chains, whereas the head group varies depending on the type of lipid. The various lipids composing the cell membrane can be divided into two main subgroups: one where lipids have a predominantly structural role and other where they play a functional role.

The lipids belonging to the first subgroup are (1) cholesterol, (2) the four major classes of phospholipids: phosphatidylcholine (PC), phosphatidylethanolamine (PE), phosphatidylserine (PS) and sphingomyelin (SPHM) and (3) cerebrosides, which are analogs of sphingomyelin with the phosphocholine group replaced by non-charged sugars such as galactose or glucose.

The second subgroup contains (1) phosphatidylinositol as precursor of the 2nd messengers based on phosphoinositols, (2) phosphatidic acid and phosphatidylglycerol (e.g., as intermediates of lipid synthesis) and many types of gangliosides (a member of the cerebrosides) functioning as carriers of blood group antigens [1-3].

From the physical point of view lipids are characterized by three structural features:

- the size and electrical property of the head groups, which may be charged (as PI, PS, sulfolipids and some gangliosides), zwitterionic (as PC, PE, SPHM) or neutral (as cerebrosides or galactosides)
- the number of carbon atoms (varying between 16 and 24 for the most abundant fatty acids) and the number of double bonds (ranging from 1 to 6)
- the structural difference between the two alkyl chains of each lipid

Phospholipids contain a phosphate group embedded in its molecular backbone. Depending on the alcohol backbone which connects the hydrophobic tail to the hydrophilic head group, phospholipids are classified into two groups: phosphoglyceride constructed from glycerol, and sphingomyelin derived from sphingosine. Phosphoglycerides are the principal type of phospholipids found in cell membranes. Structures of phosphoglycerides have a common backbone: glycerol-3-phosphate. The other two hydroxyl groups at 1 and 2 positions on glycerol are esterified to the carboxyl groups of two fatty acids, which form the hydrophobic moiety of the phospholipid. Besides being connected with glycerol in the backbone, the phosphate group forms a second ester bond with another alcohol, which constructs the hydrophilic head group of the phospholipid

Depending on the alcohol in the hydrophilic head group moiety, the phospholipids can achieve different properties, such as head group size and

charges. Five alcohols are commonly found in phospholipids present in cell membranes: serine, glycerol, inositol, choline, and ethanolamine. The structures of these alcohols are shown in figure 1.2. If the head group of a phospholipid has one serine, glycerol, or inositol attached to its phosphate, the net charge of head group is -1 at physiological pH. When either ethanolamine or choline is esterified to the phosphate, the resultant phospholipid, namely phosphatidylethanoamine or phosphatidylcholine, is zwitterionic with zero net charge at physiological pH.

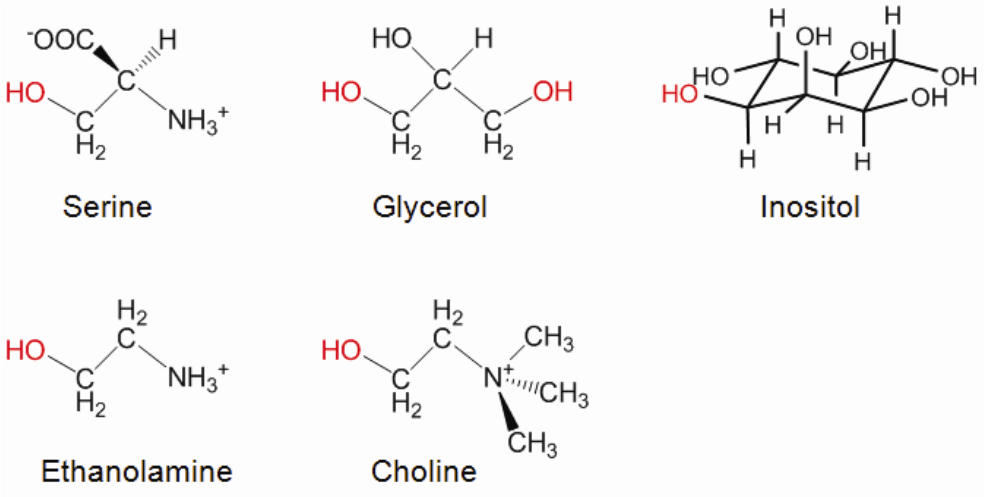


Figure 1.2: Alcohols commonly found in head groups of phospholipids present in cell membranes. The hydroxyl group in red marks possible positions in the alcohols where an ester bond can be formed with the phosphate group (image adapted from reference [2]).

In table 1.1 the lipid compositions of plasma membranes and some intracellular organelles are summarized. We can see from the table that the phospholipids represent greater than 50 weight % of the total lipid mass in most cases, although their relative compositions vary depending on the type of cell. The content of charged lipids is roughly 10 mole % in all membranes and is

highest in the plasma membranes (11–13%). The plasma membranes of mammalian cells have a high content of cholesterol which amounts roughly to 20 weight % of the total lipid [1,6].

Table 1.1: Major lipid components of selected biomembranes (source [7])

	Composition (mol %)			
Source/Location	PC	PE + PS	SM	Cholesterol
Plasma membrane (human erythrocytes)	21	29	21	26
Myelin membrane (human neurons)	16	37	13	34
Plasma membrane (*E. coli*)	0	85	0	0
Endoplasmic reticulum membrane (rat)	54	26	5	7
Golgi membrane (rat)	45	20	13	13
Inner mitochondrial membrane (rat)	45	45	2	7
Outer mitochondrial membrane (rat)	34	46	2	11

The lipid bilayer provides a fluidic matrix in which individual lipid molecules and membrane proteins can move laterally [4]. The lateral diffusion in lipid bilayers can be detected with techniques like fluorescence recovery after photobleaching (FRAP) [8,9], single particle tracking (SPT) [10-12], and optical laser trapping [13]. The diffusion of lipid molecules depends on the host bilayer instead of the lipid probe itself with a diffusion coefficient of 10^{-8}~10^{-7} cm^2/sec [14,15]. The lateral diffusion of integral membrane proteins, on the other hand, depends on the protein itself [5,16]. Some proteins are as mobile as lipid molecules with diffusion coefficients on the order of 10^{-8} cm^2/sec [16,17], whereas others are much slower (diffusion coefficient ~ 10^{-12} ~10^{-11} cm2/sec) or may even stay stationary [5,18]. In addition to lateral diffusion, lipid molecules and membrane proteins may have rotational motion along the molecular axis

perpendicular to the bilayer plane or *librational* motion (wobbling) [19-21]. However, neither rotation nor wobbling is as important as lateral diffusion for biological systems.

Although, lipid molecules can diffuse rapidly in the plane of membrane, it is very hard for them to transverse spontaneously from one leaflet to another. This motion is called "passive transverse diffusion" or "flip-flop". In both artificial and living animal cell membranes, unassisted flip-flop of a lipid molecule from one leaflet to the other occurs once in several hours or even several days [22,23]. However, higher rates of facilitated transmembrane movement of lipid molecules have been detected in both living cells and reconstituted membranes [24-26].

The fluidity of the lipid bilayer depends on the temperature and properties of the composing lipids. In the "fluid" liquid crystalline phase ($L\alpha$), the fatty acid chains are in a relatively flexible and disordered state. If the fatty acid chains are in a rigid and ordered state, the lipid bilayer is in a "gel phase" (L_β). The transition from gel phase (L_β) to the fluid phase (L_α) occurs abruptly at a characteristic temperature, T_m, called the "phase transition temperature" of lipid. Generally, for lipids with same head groups but different lengths of saturated fatty acid chains, those with longer chains tend to have higher T_m. For example, 1,2-Dilauroyl-*sn*-Glycero-3-Phosphocholine (DLPC) with 12 carbon atoms in the fatty acid chain has its *Tm* at -1ºC; while for 1,2-Distearoyl-*sn*-Glycero-3-

Phosphocholine (DSPC), with 18 carbon atoms, the *Tm* increases to 55ºC [27]. Also, for lipids with same length of fatty acid chains, introduction of one or two carbon-carbon double bonds (CH=CH), especially those of *cis*- configuration, into the chain makes the chains more disordered and greatly decreases the phase transition temperature T_m. For example, 1,2-Dioleoyl-*sn*-Glycero-3-Phosphocholine (DOPC), with the same chain length as DSPC but one CH=CH bond in *cis*-configuration in each chain, has a *Tm* of -20ºC, well below that of DSPC [27,28].

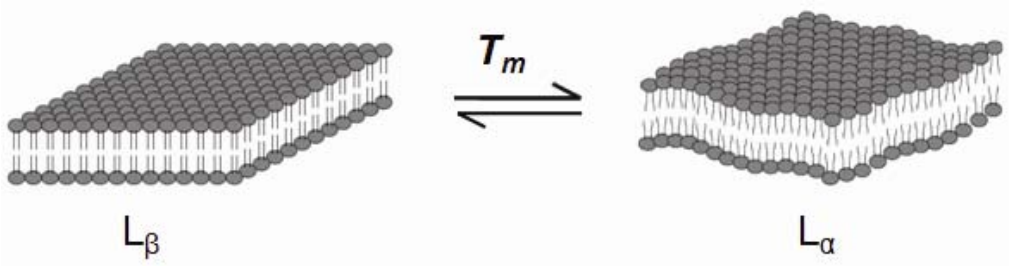


Figure 1.3: Schematic representation of gel-liquid phase transition of lipid membrane (Cartoons are adapted from reference [29]).

1.2 Polymorphism of lipids in aqueous solution

When dispersed in aqueous media, surfactants like lipid molecules tend to organize such that their hydrophilic headgroups stay in contact with the polar solvent while their hydrophobic tails stay in contact with air or other hydrophobic molecules. At low concentration, the surfactant molecules migrate to the air-water or oil-water interface to lower the interfacial tension. Depending on the solubility of the surfactant, they can also exist in monomeric form in bulk solution. As the concentration of the surfactants is increased, the available interfaces become saturated and the interfacial tension becomes a constant. The surfactant molecules no longer migrate to the interface, instead, they self-assemble in the solution to form aggregates. The concentration that leads to the onset of aggregation is called the "critical micelle concentration" (CMC) [30].

Above the CMC, the surfactant molecules form various equilibrium phases that coexist with the critical micellar concentration of monomer surfactant molecules in the solution. The CMC for a double-chain zwitterionic phospholipid is very low (~ 10^{-10} M) while single chain surfactant have higher CMC values [31]. The driving force behind the aggregation of lipids is the hydrophobic effect and the hydrophobic energy is directly proportional to the area of the hydrocarbon-water contact. Thus, the extent of chain-water contact is minimized by forming closed aggregates thereby reducing the chemical potential of the hydrocarbon chains.

The hydrophobic effect by itself favors complete phase separation of the lipid from water. However, the requirement that the hydrophilic headgroups remain in contact with water forces the system to form aggregates such that the headgroups form a continuous interface between water and the hydrophobic tails. For an aggregate composed of N lipids to be in equilibrium with lipid monomers in a binary lipid-water system, the chemical potential of the monomeric and aggregated lipids must be equal:

$$\mu^\circ_N + kT/N \ln(X_N/N) = \mu^\circ_1 + kT/N \ln X_1$$

where, μ° is the free energy per molecule and X is the mole fraction. This assumes that there are no interactions between the aggregates and monomers. When the aggregates are very large ($N \rightarrow \infty$), the equation reduces to:

$$\mu^\circ_N - \mu^\circ_1 = kT \ln(CMC)$$

which relates the free energy of micellisation to the CMC. The distribution function of the aggregate size is given by:

$$X_N = N \cdot X_1^N \exp(-N(\mu^\circ_N - \mu^\circ_1)/ kT)$$

The variation of μ°_N with N dictates the aggregation behavior with lowering of μ°_N as N increases being a necessary condition for aggregation [30-32].

Formation of lipid aggregates is energetically driven by hydrophobic effect, which segregates the hydrocarbon chains away from contact with water. The structures of lipid aggregates are not always the same, even though their formation is due to the same driving force. One successful approach for understanding the polymorphism of lipid aggregates is “geometric packing”

[30,33]. According to this model, each aggregate is composed of two well-defined regimes: (1) a hydrophobic core that contains the hydrocarbon tails, packed such that the monomer density is uniform and liquid like, and (2) a surface region that contains the polar headgroups surrounded by solvent molecules. The two regions are separated by a well-defined interface. The free energy per molecule of the aggregate is the combination of a surface term $f_h(g)$, from the headgroup region and a core term $f_t(g)$, from the hydrocarbon tail packing. The surface term $f_h(g)$ contains contributions from the interfacial tension due to headgroup-headgroup, headgroup-solvent, headgroup-hydrocarbon and hydrocarbon-solvent interactions. These interactions include the steric, electrostatic, hydration, hydrogen-bonding and van der Waals interactions. A simple approximation for $f_h(g)$ is:

$$f_h(g) = \gamma \cdot A + (C/A') = \gamma \cdot (A + (A_h^2 / A'))$$

where, C is a constant, γ is the effective interfacial tension of the water-hydrocarbon interface, A is the area per lipid molecules at the interface, A' is the area per molecule at the center of the headgroup repulsion and A_h is the value of A which minimizes the f_h for a planar layer. When $A = A_h$ the effective surface tension of the flat lipid film vanishes. This is called the Schulman-Montangne condition [34].

The tail term f_t accounts for all the interactions between chain segments inside the hydrophobic core. As described by Israelachvilli and coworkers [30,35,36], $f_t(g)$ is a constant, independent of geometry if the chains are volume

incompressible, no chains protrude into the aqueous exterior and no part of the interior of any aggregate is further away from the hydrocarbon-water interface than a critical length, $l_c = l_{max}$, the all-trans chain length.

For a lipid with hydrophobic carbon tail volume (v), critical hydrocarbon chain length (l_c), and the hydrocarbon-water interfacial area per molecule (A), a dimensionless "*packing parameter*" $p = (v / A \cdot l_c)$ was proposed to understand or predict the most favored geometry aggregates of that lipid could adopt. In the absence of interactions between aggregates, value of the packing parameter p can predict the preferred geometry as shown in table 1.2 [31,35].

Table 1.2: Preferred geometries for different values of the critical packing fraction

Packing fraction (p)	Preferred geometry
0 – 1/3	spheres
1/3 – 1/2	cylinders
1/2 – 1	bilayers

In this model, the structure of the self-assemble aggregate is determined completely by the relative sizes of the hydrophilic headgroups and the hydrophobic tails. While this model is extremely useful in understanding the geometry of lipid aggregates, it has two major limitations. It is unable to predict

the formation of the bicontinuous cubic phases found in many lipid aggregates. Also, it cannot interpret the structure of multi-component lipid aggregates. The major defect of this system is that it completely ignores the effect of geometry. In fact, the free energy contribution of both the headgroup and the hydrocarbon tail regions depend on the interfacial curvature [31].

In an alternate approach, lipid monolayers are used as the building blocks for lipid aggregates and two coupling lipid monolayers influence each other strongly to achieve a balance which determines the final structure lipid aggregates adopt [37-39]. If a membrane were constrained to lie on a surface, the only relevant energy would be due to changes in the average area per molecule of the membrane. However, the membrane can also deform in the normal direction. These out of plane deformations are known as bending or curvature deformations and the free energy associated with them is called the curvature free energy [37]. For a membrane with finite thickness, pure curvature deformations are those perturbations that do not change the overall membrane volume but there may be local stretching and compressions. Also, for membranes of finite thickness, a surface that undergoes no stretching or compression can be chosen to define the interface. The choice of this surface depends on the various elastic constants of the system and is system dependent except for perfectly symmetrical membranes. However, for membrane deformations with wavelengths larger than the membrane thickness, the exact position of the interface is not crucial.

For a point on a surface in the three dimensional space, we can define a 'normal' curvature for all the curves on that surface passing through that point. The two principal curvatures, c_1 and c_2, are the maximum and minimum curvatures among all the normal curvatures going through that point and are perpendicular to each other. The topology of the surface is usually characterized by its mean curvature H and Gaussian curvature K, which are defined as

$$H = \frac{1}{2}(c_1 + c_2)$$

$$K = c_1 \cdot c_2$$

The free energy per unit area associated with bending a membrane, as described by Helfrich [40], can be written as

$$f = \frac{k}{2}(c_1 + c_2 - 2c_0)^2 + k_G c_1 c_2$$

The mean curvature which minimizes the free energy, c_0, is called the 'spontaneous curvature' of the membrane. The 'bending modulus', k, is the energy cost of deviating from the spontaneous curvature and the 'saddle-splay modulus', k_G , measures the energy cost of saddle like deformations.

The shape of the lipid molecules determines the spontaneous curvature. For $c_0 < 0$, the lipids are shaped like traffic cones, with small head groups and bulky tails, and tend to bend toward the hydrophilic side. For $c_0 > 0$, the lipids are shaped like ice-cream cones, with bulky head groups and small tails, and tend to bend toward the hydrophobic side. A 'cylindrical' lipid, whose hydrophilic head

and hydrophobic tail span the same area, will have zero spontaneous curvature, and form flat bilayers.

Different phases have different values of mean and/or Gaussian interfacial curvatures, and these may or may not be uniform at different points on the interface within a single phase. The Gaussian curvature K is a more fundamental property of the interface than H since it determines the qualitative nature of the surface. Surfaces for which K is positive are known as elliptic, and naturally bend round to form closed shells. Micelle or inverse micelles are examples of this. When either of the principal curvatures are zero, the Gaussian curvature is zero, and the surface is known as parabolic. The lamellar and hexagonal phases are examples of this. The third possibility arises when the principal curvatures c1 and c2 are of opposite sign, leading to a negative Gaussian curvature. These surfaces are known as hyperbolic, and an example is the saddle surface. The Gaussian curvature is most negative at the saddle point and increases smoothly to zero at the four apices. When the principal curvatures are everywhere equal in magnitude but opposite in sign, then the surface has zero mean curvature at all points but negative Gaussian curvature. Examples of these are the bicontinuous cubic phases. Figure 1.4 gives a summary on mean curvature and Gaussian curvature of several structures commonly observed in lipid systems [41].

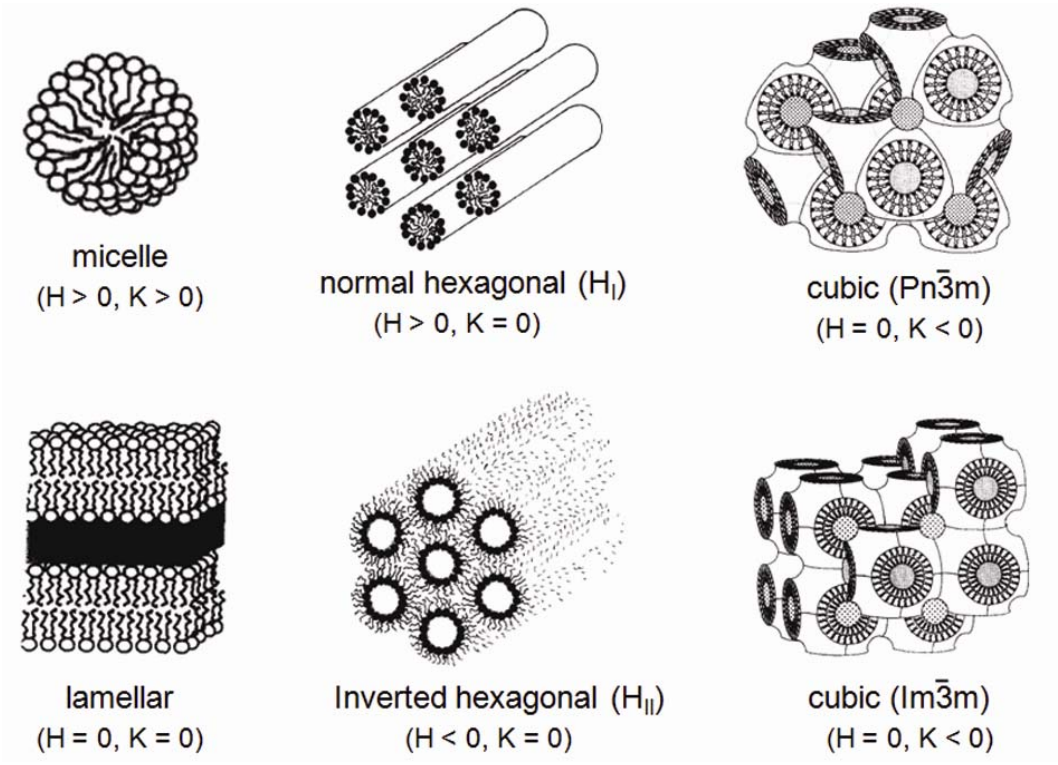


Figure 1.4: Mean curvature *H* and Gaussian curvature *K* of structures commonly observed in lipid systems (Image adapted from references [42,43]).

1.3 Cubic phases in lipids

The cell membrane contains many lipids that promote the formation of non-lamellar phases, including cubic phases. The non-lamellar phases can be subdivided into two types. A type I phase denotes a phase whose structure elements are filled by the apolar moiety and are embedded in a polar matrix (i.e. oil-in-water), whereas a type II phase denotes the reverse (i.e. water-in-oil).

Lipid cubic phases can be sorted in two main classes: 'bicontinuous' and 'micellar'. The bicontinuous phases of type II can be visualized in terms of a highly convoluted lipid bilayer, which subdivides 3D space into two disjointed polar labyrinths separated by an a polar septum. Bicontinuous phases of type I are also known, in which the septum and the two labyrinths are filled by the polar and the non-polar medium, respectively. The bicontinuous cubic phases of type II partition 3D space into two distinct and disjointed polar compartments **(**an inside and an outside) separated from each other by a hydrophobic septum. In lipid-water systems, six cubic structures have been found, Q212, Q223, Q224, Q227, Q229 and Q230. Of these only the Q224 and Q227 phases are stable in the presence of excess water, which is the case for biological membranes [41,44,45].

It has been hypothesized that the bicontinuous cubic phases are based upon underlying periodic minimal surfaces (surfaces that have zero mean curvature at all points) [46-50]. The basis of this is that parallel surfaces on either side of a minimal surface have smaller areas, and hence have non-zero average mean curvatures, directed away from the minimal surface. A lipid bilayer draped onto such a minimal surface will have a net curvature of each monolayer towards the water regions. Thus a system which has a preferred area per headgroup which is smaller than the preferred area per chain(s) can lower its elastic energy by deforming from a planar bilayer to a saddle surface [41]. A minimal surface can be represented (locally) by a set of three integrals called the Wierstrass integrals in which the coordinates of a minimal surface patch is described as integrals of a

complex valued function. It involves two mappings. First the normal direction of each point on the surface is plotted on a unit sphere. This is the Gaussian mapping. These points are subsequently stereographically projected onto an equatorial plane. Under these operations, the minimal surface is transformed into a multi-sheeted covering of the complex plane. Any point on the minimal surface (except fiat points), characterized by cartesian coordinates *(x,y,z)* is described by the complex number ω, which defines its mapped location in the complex plane. The Weierstrass equations allow calculation of the cartesian coordinates *((x,y,z)* with respect to an origin *(x_o,y_o,z_o))* of the minimal surface at all points on the surface - except flat points - in terms of a complex analytic function R(ω). The Weierstrass equations are:

$$x = x_0 + \mathrm{Re}\int_{\omega 0}^{\omega 1} e^{i\theta}\,(1-\omega^2)\,R(\omega)\,d\omega$$

$$y = y_0 + \mathrm{Im}\int_{\omega 0}^{\omega 1} e^{i\theta}\,(1+\omega^2)\,R(\omega)\,d\omega$$

$$z = z_0 - \mathrm{Re}\int_{\omega 0}^{\omega 1} e^{i\theta}\,(2\omega)\,R(\omega)\,d\omega$$

Integration is carried out on an arbitrary path from ω_o to ω_1 in the complex plane, for a fixed value of θ between 0 and π/2. *Any* analytic function R(ω) can be plugged into the equations, to give a minimal surface. Further, the function R(ω) uniquely determines a family of surfaces related by the Bonnet transformation as θ varies. This means that one surface can be transformed into either of the others simply by bending, which leaves the Gaussian curvature at all points unchanged, and preserves all angles, distances and areas on the surface. In terms of minimal surfaces, the inverse bicontinuous cubic phases Ia3d, Pn3m and Im3m are formed

by draping a continuous lipid bilayer onto the G-, D- and P-minimal surfaces, respectively. The D surface has $\theta = 0°$, the G surface has $\theta = 38.015°$ and the P surface has $\theta = 90°$ [44,45].

The Ia3d (= Q230) cubic phase consists of two interwoven yet unconnected chiral networks of water/lipid cylinders, connected coplanarly three by three and separated by the G-minimal surface (Fig 1.5a). Although the two networks are chiral, the cubic phase itself is centrosymmetric. The Pn3m (= Q224) cubic phase consists of two interwoven tetrahedral networks of water channels arranged on a double-diamond lattice, separated by the D-minimal surface (Fig 1.5b). The Im3m (= Q229) cubic phase has orthogonal networks of water channels connected six-by-six, and separated by the P-minimal surface (Fig 1.5c) [41,49,51].

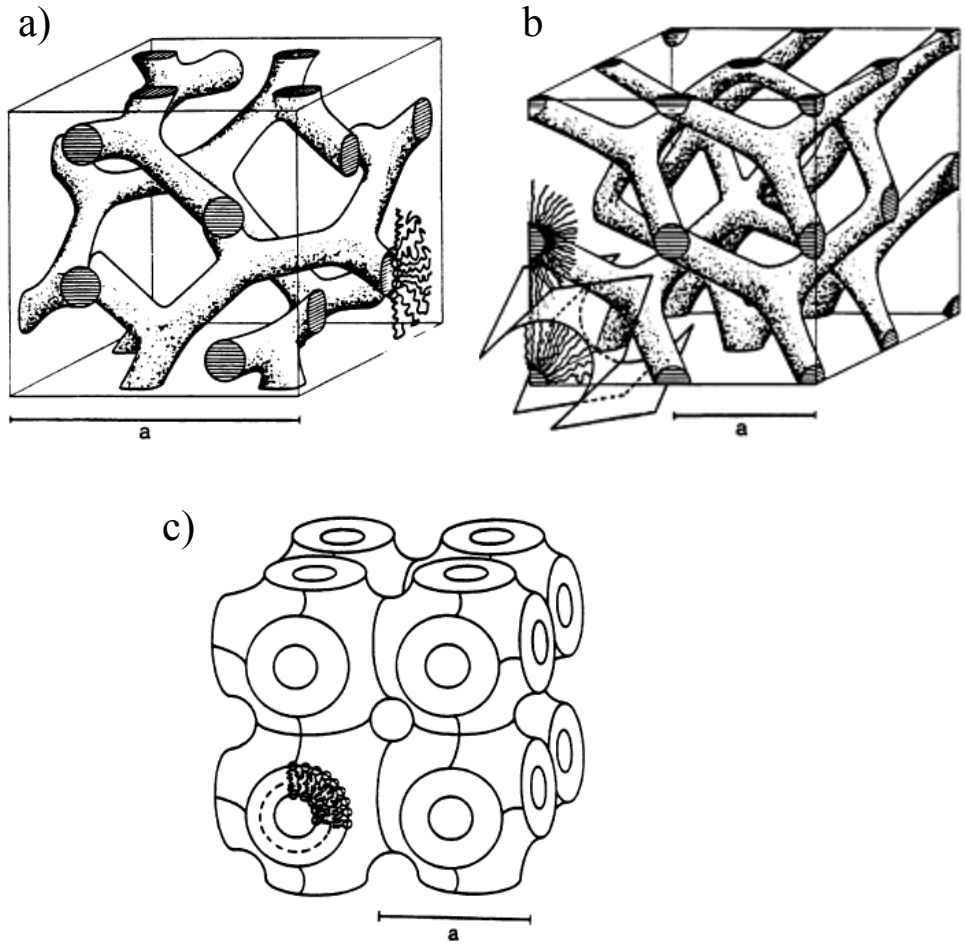


Figure 1.5: Schematics of the inverse bicontinuous cubic phases:
a) Ia3d (= Q230); **b)** Pn3m (= Q224); **c)** Im3m (= Q229).
(image adapted from reference [41])

1.4 Characterization of lipid phases

An understanding of lipid mesomorphism begins with determination of the structures of the phases. X-ray and neutron diffraction, being directly sensitive to the time-averaged arrangement of molecules within a specimen, have yielded much of the known information about lipid phase structure [52-56]. Diffraction is also one of the least ambiguous methods for phase assignment in lipid systems. Freeze-fracture electron microscopy, when used in conjunction with X-ray diffraction, can yield useful complementary data [57]. In the characterization of lipid mesophases by diffraction, there are two regions of the diffraction pattern that are used to identify the phase. The small angle region identifies the symmetry and long range organization of the phase, whereas the wide angle region gives information on the molecular packing, or short range organization of the phase. The signature of a translationally ordered mesophase is the appearance of one or more sharp (Bragg) peaks in the low-angle region of the diffraction pattern.

The lamellar phase shows a series of reflections corresponding to (dominating) one-dimensional periodicity, and from the X-ray data it is possible to determine the thickness of the lipid bilayer, the cross-section per polar head group, and the water layer thickness, assuming a specific sheet geometry. In the same way the diameter of the cylinders in the H_I and H_{II} phases can be determined, as well as the cross-sectional area per polar head group and the distance between adjacent cylinders [41,58].

Cubic lipid phases have a very much more complex architecture than lamellar and hexagonal phases. The lattice type can be identified by the characteristic ratios of the Bragg reflections. It is, then, necessary to determine the crystallographic spacegroup to which the phase belongs, from the pattern of systematic absences in the diffraction pattern. However, this is often not trivial, since usually only a few low-angle Bragg peaks are detected, due to the large thermal disorder inherent in liquid-crystalline phases, which strongly damps the intensities at larger diffraction angles. From unaligned samples it is usually only possible to identify the cubic aspect from the systematic absences, leaving an ambiguity about the precise spacegroup. The intensities of the various Bragg peaks are determined by the distribution of matter (electron density) in the unit cell, which is constrained by the symmetry of the spacegroup. A symmetry-allowed reflection may nonetheless have zero intensity because the unit cell Fourier transform happens to pass through zero at that particular diffraction angle. A further major problem with the characterisation of lipid phases is the difficulty of ensuring that the sample is at equilibrium. In part this may be due to the rate at which a phase comes to equilibrium being very slow. However, a further problem is that the phase itself may be metastable, reverting to more stable forms over a time scale which can span seconds to months [38,41,50,59,60].

It has frequently been suggested that transitions to non-lamellar phases occur via the formation of defects such as inverse micelles [61-63]. In a model developed by Siegel, the first step involves the formation of an ‘inverted micellar

intermediate' between apposed bilayers [64-66]. Two subsequent outcomes are possible (in addition to reversion), depending on the particular lipid system (fig. 1.6). Either the inverted micellar intermediate can fuse with neighbouring ones to form rod-like inverse micelles, or it can fuse with the surrounding monolayers to form an 'interlamellar attachment', a fusion channel between the two bilayers. The former outcome should lead to the formation of the HII phase, whereas the latter should lead to the formation of inverse bicontinuous structures such as cubic phases.

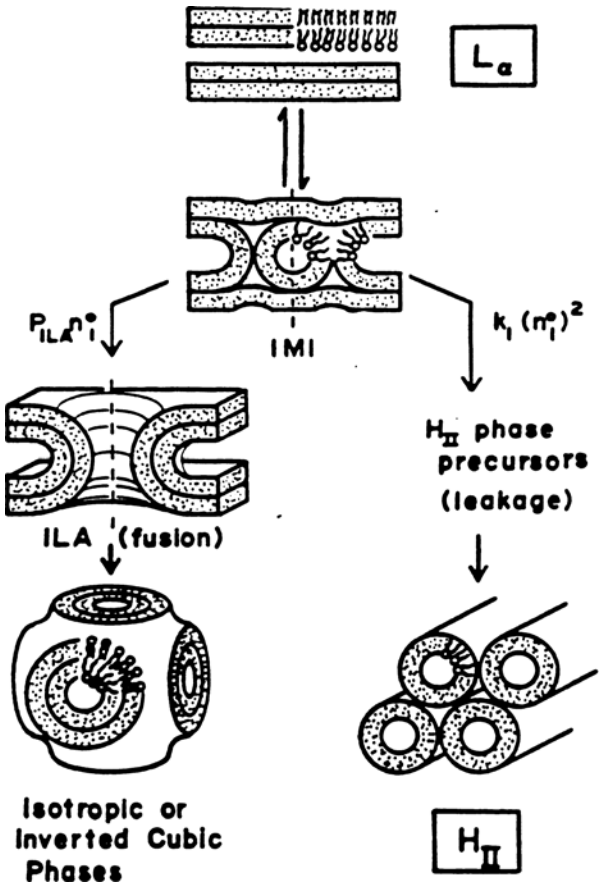


Figure 1.6: Proposed routes for inverse bicontinuous cubic and HII phase formation, via 'inverted micellar intermediates' (image adapted from reference [41])

For lipid systems forming inverse phases, it is known that the L_α–H_{II} transition occurs with the lamellar (001) planes aligned with the (10) planes of the HII phase [67,68]. For the system monooleoyl glycerol, which forms inverse bicontinuous cubic phases, the (001) planes of the lamellar phase were found to be aligned with the (211) planes of the Ia3d cubic phase although occasional alignment with the (220) planes has also been observed [41].

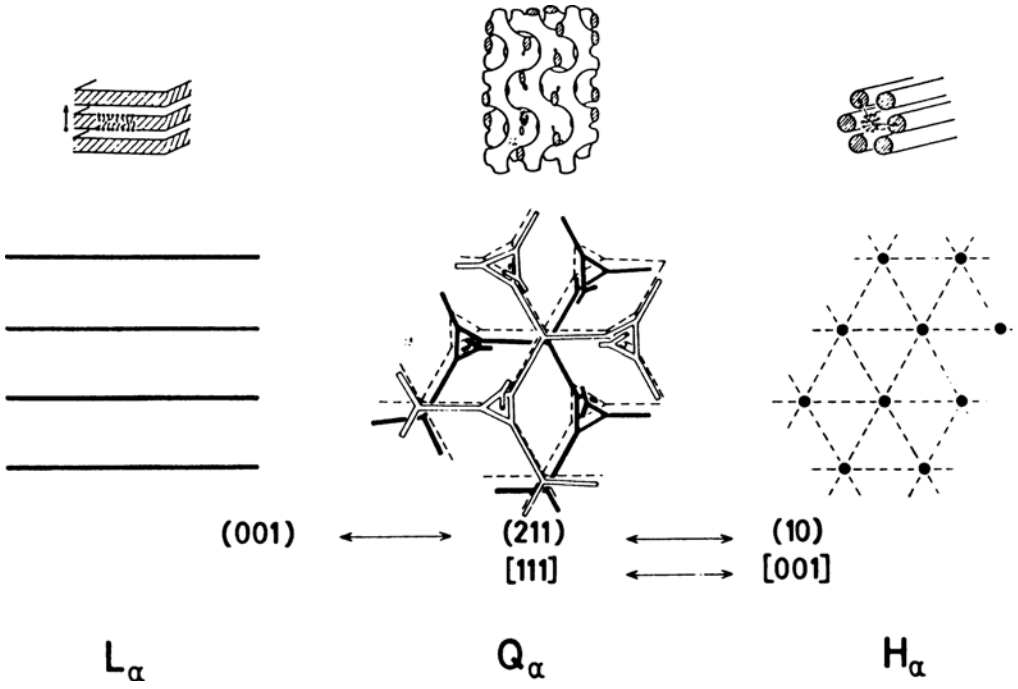


Figure 1.7: Epitaxial relationships between the lamellar L_, type I cubic Q_ (spacegroup Ia3d) and type I hexagonal H_ phases of a polyoxyethylene surfactant (image adapted from [41]).

1.5 Application of liposomes

Liposomes are spherical, self-closed vesicles in which the lipid bilayer sequesters part of the solvent into their interior. Liposomes can be made entirely from naturally occurring substances and are therefore nontoxic, biodegradable and non immunogenic. Liposomes can be used as solubilizers for difficult-to-dissolve substances, dispersants, sustained release systems, delivery systems for the encapsulated substances, stabilizers, protective agents, microencapsulation systems and microreactors. In addition, liposomes can be used use as a model in the basic studies of cell interactions, recognition processes, and of the mode of action of certain substances. [69-71]

Liposomes have proven to be useful drug delivery systems as they offer several advantages over conventional dosage methods. They allow for delivery of hydrophobic or amphiphilic drugs that would otherwise be difficult to administer. They can be used to isolate a bioactive agent, so as to direct the agent away from certain tissues and to deliver the agent to other tissues. This site-specific targeting can be improved by modifying the surface of the liposomes with ligands that bind to specific target cells. In general, liposome encapsulation is considered when drugs are very potent, toxic and have very short life times in the blood circulation or at the sites of local administration. [72-76]

Early liposomal formulations suffered from the fast blood clearance by the reticuloendothelial system (RES). It is now recognized that particle size, surface

charge and liposome composition all have strong influences on the clearance profile. [77-79] Liposomes coated with the poly(ethylene glycol) (PEG) have significantly increased their circulation half-life in the blood, and revolutionized liposome technology. The PEG 'shell' protects the liposomal surface and substantially inhibits protein adsorption and opsonization of the liposomes, as well as minimizes recognition by the RES system. [80-83]

At present, most lipid vesicle mediated bioactive agent delivery is either untargeted or passively targeted. Also, they release the encapsulated agent through passive diffusion from the vesicle or through slow, non-specific degradation of the vesicles. These mechanisms can lead to systemic toxicity and also lack the ability to accurately deliver the bioactive agent to a specific tissue type and/or at a specific time. It would be desirable to have a lipid vesicle system in which the contents of the vesicle are released when the vesicle is in contact with a specific environment, such as a specific tissue.

Antibodies have been used to develop targeted liposome-based delivery systems [84-89]. However, antibody conjugations are difficult to control and typically show poor site-specificity for the conjugation and inconsistent binding affinity. Furthermore, identifying antibodies against molecules that are inherently less immunogenic is difficult. The use of DNA aptamers as alternatives to antibodies can potentially overcome these shortcomings [90]. Aptamers are RNAs and DNAs that have high binding-affinities to specific ligands. Aptamers

are identified by in vitro selection experiments (termed SELEX: systematic evolution of ligands by exponential enrichment), which, starting from random sequence libraries, optimize the nucleic acids for binding to given ligands [91-98]. Aptamers are unstructured in solution but upon associating with their specific ligand fold into molecular architectures in which the ligand becomes an intrinsic part of the nucleic acid structure. Since aptamers are identified through an in vitro process that does not depend on animals, cells, or even in vivo conditions, the properties of aptamers can be changed on demand. Aptamers are produced by chemical synthesis with extreme accuracy and reproducibility. As a result aptamers for molecules that do not induce an immune response can also be identified. Aptamers have been identified that bind to small molecular targets, including metal ions, drugs, antibiotics, nucleotides, and peptides. [90,99-107]

1.6 References

[1] Sackmann, E. (1995) Biological Membranes Architecture and Function. In Structure and Dynamics of Membranes: from Cell to Veiscles (Lipowsky, R. and Sackmann, E., ed.^eds). Elsevier, Amsterdam.

[2] Alberts, B., Johnson, A., Lewis, J., Raff, M., Roberts, K. and Walter, P. (2002) Molecular Biology of the Cell, Garland Science. New York.

[3] Berg, J., Tymoczko, J. and Stryer, L. (2007) Biochemistry, W. H. Freeman and Company. New York.

[4] Singer, S. and Nicolson, G. (1972). The Fluid Mosaic Model of the Structure of Cell Membranes. Science 175, 720-731.

[5] Jacobson, K., Sheets, E. and Simson, R. (1995). Revisiting the Fluid Mosaic Model of Membranes. Science 268, 1441-1442.

[6] Graham, J. and Higgins, J. (1997) Membrane Analysis, BIOS Scientific Publishers Limited. Oxford.

[7] Lodish, H., Berk, A., Zipursky, L., Matsudaira, P., Baltimore, D. and Darnell, J. (2000) Molecular Cell Biology, W. H. Freeman and Company. New York.

[8] Axelrod, D., Koppel, D., Schlessinger, J., Elson, E. and Webb, W. (1976). Mobility measurement by analysis of fluorescence photobleaching recovery kinetics. Biophys. J. 16, 1055-1069.

[9] Jovin, T., Vaz, W., Sidney, F. and Becca, F. (1989) Rotational and translational diffusion in membranes measured by fluorescence and phosphorescence methods. In Methods in Enzymology ed.^eds), pp. 471-513. Academic Press

[10] Geerts, H., De Brabander, M., Nuydens, R., Geuens, S., Moeremans, M., De Mey, J. and Hollenbeck, P. (1987). Nanovid tracking: a new automatic method for the study of mobility in living cells based on colloidal gold and video microscopy. Biophys. J. 52, 775-782.

[11] Ghosh, R. and Webb, W. (1994). Automated detection and tracking of individual and clustered cell surface low density lipoprotein receptor molecules. Biophys. J. 66, 1301-1318.

[12] Saxton, M. and Jacobson, K. (1997). Single Particle Tracking: Applications to Membrane Dynamics. Annual Review of Biophysics and Biomolecular Structure 26, 373-399.

[13] Svoboda, K. and Block, S. (1994). Biological Applications of Optical Forces. Annual Review of Biophysics and Biomolecular Structure 23, 247-285.

[14] Almeida, P., Vaz, W. and Thompson, T. (1992). Lateral diffusion in the liquid phases of dimyristoylphosphatidylcholine/cholesterol lipid bilayers: a free volume analysis. Biochemistry 31, 6739-6747.

[15] Vaz, W., Clegg, R. and Hallmann, D. (1985). Translational diffusion of lipids in liquid crystalline phase phosphatidylcholine multibilayers. A comparison of experiment with theory. Biochemistry 24, 781-786.

[16] Vaz, W., Criado, M., Madeira, V., Schoellmann, G. and Jovin, T. (1982). Size dependence of the translational diffusion of large integral membrane proteins in liquid-crystalline phase lipid bilayers. A study using fluorescence recovery after photobleaching. Biochemistry 21, 5608-5612.

[17] Vaz, W. and Criado, M. (1985). A comparison of the translational diffusion of a monomer and an oligomer of the acetylcholine receptor protein reconstituted into soybean lipid bilayers. Biochimica et Biophysica Acta (BBA) - Biomembranes 819, 18-22.

[18] Sheetz, M., Turney, S., Qian, H. and Elson, E. (1989). Nanometre-level analysis demonstrates that lipid flow does not drive membrane glycoprotein movements. Nature 340, 284-288.

[19] Kinosita, K., Kawato, S. and Ikegami, A. (1984). Dynamic structure of biological and model membranes: Analysis by optical anisotropy decay measurement. Advances in Biophysics 17, 147-203.

[20] Gally, H., Niederberger, W. and Seelig, J. (1975). Conformation and motion of the choline head group in bilayers of dipalmitoyl-3-sn-phosphatidylcholine. Biochemistry 14, 3647-3652.

[21] Jacobson, K. and Wobschall, D. (1974). Rotation of fluorescent probes localized within lipid bilayer membranes. Chemistry and Physics of Lipids 12, 117-131.

[22] Kornberg, R. and McConnell, H. (1971). Inside-outside transitions of phospholipids in vesicle membranes. Biochemistry 10, 1111-1120.

[23] Roseman, M., Litman, B.J. and Thompson, T. (1975). Transbilayer exchange of phosphatidylethanolamine for phosphatidylcholine and N-acetimidoylphosphatidylethanolamine in single-walled bilayer vesicles. Biochemistry 14, 4826-4830.

[24] Langley, K. and Kennedy, E. (1979). Energetics of Rapid Transmembrane Movement and of Compositional Asymmetry of Phosphatidylethanolamine in Membranes of Bacillus megaterium. Proceedings of the National Academy of Sciences 76, 6245-6249.

[25] Donohue-Rolfe, A. and Schaechter, M. (1980). Translocation of Phospholipids from the Inner to the Outer Membrane of Escherichia coli. Proceedings of the National Academy of Sciences 77, 1867-1871.

[26] Huijbregts, R., de Kroon, A. and de Kruijff, B. (1998). Rapid Transmembrane Movement of Newly Synthesized Phosphatidylethanolamine across the Inner Membrane of Escherichia coli. J. Biol. Chem. 273, 18936-18942.

[27] Caffrey, M. (1993) LIPIDAT A Database of Thermo Data and Association Information on Lipid, CRC Press, Inc. Boca Raton, Florida.

[28] Koynova, R. and Caffrey, M. (1998). Phases and phase transitions of the phosphatidylcholines. Biochimica et Biophysica Acta (BBA) - Reviews on Biomembranes 1376, 91-145.

[29] Dowhan, W. (1997). MOLECULAR BASIS FOR MEMBRANE PHOSPHOLIPID DIVERSITY:Why Are There So Many Lipids? Annual Review of Biochemistry 66, 199-232.

[30] Israelachvili, J. (1992) Intermolecular & Surface Forces, Academic Press Inc. London.

[31] Koltover, I. (1998) Structure and interactions in biomaterials based on membrane-biopolymer self-assembly.ed.^eds). University of California at Santa Barbara.

[32] Ben-Shaul, A. and Gelbart, W. (1994) Statistical Thermodynamics of Self-Assembly: Structure and Phase Transitions in Micellar Solutions. In Micelles, Membranes, Microemulsions and Monolayers (Ben-Shaul, A., Gelbart, W. and Roux, D., ed.^eds). Springer, New York.

[33] Evans, D.F. and Wennerström, H. (1999) The Colloidal Domain: Where Physics, Chemistry, Biology, and Technology Meet, Wiley-VCH. New York.

[34] Schulman, J.H. and Montagne, J.B. (1961). FORMATION OF MICROEMULSIONS BY AMINO ALKYL ALCOHOLS. Annals of the New York Academy of Sciences 92, 366-371.

[35] Israelachvili, J., Marčelja, S. and Horn, R. (1980). Physical principles of membrane organization. Q. Rev. Biophys. 13, 121-200.

[36] Israelachvili, J., Mitchell, J. and Ninham, B. (1976). Theory of self-assembly of hydrocarbon amphiphiles into micelles and bilayers. J. Chem. Soc., Faraday Trans. 2 72, 1525 - 1568.

[37] Safran, S. (1994) Statistical Thermodynamics of Surfaces, Interfaces, and Membranes, Addison–Wesley. Reading, MA.

[38] Seddon, J. (1990). Structure of the inverted hexagonal (HII) phase, and non-lamellar phase transitions of lipids. Biochimica et Biophysica Acta (BBA) - Reviews on Biomembranes 1031, 1-69.

[39] Tate, M., Eikenberry, E., Turner, D., Shyamsunder, E. and Gruner, S. (1991). Nonbilayer phases of membrane lipids. Chemistry and Physics of Lipids 57, 147-164.

[40] Helfrich, W. (1973). Elastic properties of lipid bilayers: theory and possible experiments. Naturforsch 28C, 693-703.

[41] Seddon, J. and Templer, R. (1995) Polymorphism of Lipid-Water Systems. In Structure and Dynamics of Membranes: from Cell to Veiscles (Lipowsky, R. and Sackmann, E., ed.^eds). Elsevier, Amsterdam.

[42] Seddon, J.M. (1990). Structure of the inverted hexagonal (HII) phase, and non-lamellar phase transitions of lipids. Biochimica et Biophysica Acta (BBA) - Reviews on Biomembranes 1031, 1-69.

[43] Tate, M.W., Eikenberry, E.F., Turner, D.C., Shyamsunder, E. and Gruner, S.M. (1991). Nonbilayer phases of membrane lipids. Chemistry and Physics of Lipids 57, 147-164.

[44] Landh, T. (1996) Cubic cell membrane architecture. Taking another look at membrane bound cell space.ed.^eds). University of Lund, Lund, Sweden

[45] Hyde, S., Ninham, B., Andersson, S., Blum, Z., Landh, T., Larsson, K. and Lidin, S. (1997) The Language of Shape: The Role of Curvature in Condensed Matter: Physics, Chemistry and Biology, Elsevier. Amsterdam.

[46] Andersson, S., Hyde, S., Larsson, K. and Lidin, S. (2002). Minimal surfaces and structures: from inorganic and metal crystals to cell membranes and biopolymers. Chemical Reviews 88, 221-242.

[47] Scriven, L. (1976). Equilibrium bicontinuous structure. Nature 263, 123-125.

[48] Hyde, S., Andersson, S., Ericsson, B. and Larsson, K. (1984). A cubic structure consisting of a lipid bilayer forming an infinite periodic minimal surface of the gyroid type in the glycerolmonooleatwater system. Z. Krystallogr. 168, 213-219.

[49] Longley, W. and McIntosh, T. (1983). A bicontinuous tetrahedral structure in a liquid-crystalline lipid. Nature 303, 612-614.

[50] Mariani, P., Luzzati, V. and Delacroix, H. (1988). Cubic phases of lipid-containing systems : Structure analysis and biological implications. J. Mol. Biol. 204, 165-189.

[51] Luzzati, V. and Spegt, P. (1967). Polymorphism of Lipids. Nature 215, 701-704.

[52] Luzzati, V. (1968) X-ray diffraction studies of lipid–water systems. In Biological Membranes (Chapman, D., ed.^eds). Academic Press, London.

[53] Gruner, S.M., Cullis, P.R., Hope, M.J. and Tilcock, C.P.S. (1985). Lipid Polymorphism:The Molecular Basis of Nonbilayer Phases. Annual Review of Biophysics and Biophysical Chemistry 14, 211-238.

[54] Levine, Y.K. (1973). X-ray diffraction studies of membranes. Progress in Surface Science 3, 279-352.

[55] Small, D. (1984) Physical Chemistry of Lipids from Alkanes to Phospholipids. In Handbook of Lipid Research (Hanahan, D., ed.^eds). Plenum, New York.

[56] Worcester, D.L. and Franks, N.P. (1976). Structural analysis of hydrated egg lecithin and cholesterol bilayers II. Neutron diffraction. Journal of Molecular Biology 100, 359-378.

[57] Gulik-Krzywicki, T., Aggerbeck, L. and Larsson, K. (1984) The use of freeze-fracture and freezeetching electron microscopy for phase analysis and structure determination of lipid systems. In Surfactants in Solution (Mittal, K. and Lindman, B., ed.^eds). Plenum, New York.

[58] Henry, N. and Lonsdale, K. (1969) International Tables for X-ray Crystallography, The Kynoch Press. Birmingham.

[59] Luzzati, V., Tardieu, A., Gulik-Krzywicki, T., Rivas, E. and Reiss-Husson, F. (1968). Structure of the Cubic Phases of Lipid-Water Systems. Nature 220, 485-488.

[60] Shyamsunder, E., Gruner, S.M., Tate, M.W., Turner, D.C., So, P.T.C. and Tilcock, C.P.S. (2002). Observation of inverted cubic phase in hydrated dioleoylphosphatidylethanolamine membranes. Biochemistry 27, 2332-2336.

[61] Cullis, P., Hope, M., Kruijff, B.d., Verkleij, A. and Tilcock, C. (1985) Structural properties and functional roles of phospholipids in biological membranes. In Phospholipids and Cellular Recognition (Kuo, J., ed.^eds). CRC Press, Boca Raton.

[62] Cullis, P., Hope, M. and Tilcock, C. (1986). Lipid polymorphism and the roles of lipids in membranes. Chem. Phys. Lipids 40, 127-144.

[63] de Kruijff, B., Cullis, P., Verkleij, A., Hope, M., Echteld, C.v. and Taraschi, T. (1985) Lipid polymorphism and membrane function. In The Enzymes of Biological Membranes (Martinosi, A., ed.^eds). Plenum, New York.

[64] Siegel, D.P. (1986). Inverted micellar intermediates and the transitions between lamellar, cubic, and inverted hexagonal lipid phases. I. Mechanism of the L alpha----HII phase transitions. 49, 1155-1170.

[65] Siegel, D.P. (1986). Inverted micellar intermediates and the transitions between lamellar, cubic, and inverted hexagonal lipid phases. II.

Implications for membrane-membrane interactions and membrane fusion. 49, 1171-1183.

[66] Siegel, D.P. (1986). Inverted micellar intermediates and the transitions between lamellar, cubic, and inverted hexagonal amphiphile phases. III. Isotropic and inverted cubic state formation via intermediates in transitions between L[alpha] and HII phases. Chemistry and Physics of Lipids 42, 279-301.

[67] Gruner, S.M., Rothschild, K.J. and Clark, N.A. (1982). X-ray diffraction and electron microscope study of phase separation in rod outer segment photoreceptor membrane multilayers. 39, 241-251.

[68] Gruner, S.M., Rothschild, K.J., DeGrip, W.J. and Clark, N.A. (1985). Co-existing lyotropic liquid crystals : commensurate, faceted and co-planar single hexagonal (HII) domains in lamellar photoreceptor membranes. J. Phys. France 46, 193-201.

[69] Bangham, A.D. (1978). PROPERTIES AND USES OF LIPID VESICLES: AN OVERVIEW. Annals of the New York Academy of Sciences 308, 2-7.

[70] Lasic, D. (1993) Liposomes: From Physics to Applications, Elsevier

[71] Lasic, D.D. (1998). Novel applications of liposomes. Trends in Biotechnology 16, 307-321.

[72] Kaneda, Y. (2000). Virosomes: evolution of the liposome as a targeted drug delivery system. Advanced Drug Delivery Reviews 43, 197-205.

[73] Alving, C.R. (1991). Liposomes as carriers of antigens and adjuvants. Journal of Immunological Methods 140, 1-13.

[74] Sharma, A. and Sharma, U. (1997). Liposomes in drug delivery: Progress and limitations. International Journal of Pharmaceutics 154, 123-140.

[75] Gregoriadis, G. (1995). Engineering liposomes for drug delivery: progress and problems. Trends in Biotechnology 13, 527-537.

[76] Gregoriadis, G., Florence, A. and Patel, H. (1993) Liposomes in Drug Delivery, Harwood Academic Publishers

[77] Allen, T.M. and Chonn, A. (1987). Large unilamellar liposomes with low uptake into the reticuloendothelial system. FEBS Letters 223, 42-46.

[78] Gabizon, A. and Papahadjopoulos, D. (1988). Liposome formulations with prolonged circulation time in blood and enhanced uptake by tumors. Proc. Natl. Sci. Acad. 85, 6949-6953.

[79] Harashima, H., Sakata, K., Funato, K. and Kiwada, H. (1994). Enhanced Hepatic Uptake of Liposomes Through Complement Activation Depending on the Size of Liposomes. Pharmaceutical Research 11, 402-406.

[80] Emanuel, N., Kedar, E., Bolotin, E.M., Smorodinsky, N.I. and Barenholz, Y. (1996). Preparation and Characterization of Doxorubicin-Loaded Sterically Stabilized Immunoliposomes. Pharmaceutical Research 13, 352-359.

[81] Klibanov, A.L., Maruyama, K., Beckerleg, A.M., Torchilin, V.P. and Huang, L. (1991). Activity of amphipathic poly(ethylene glycol) 5000 to prolong the circulation time of liposomes depends on the liposome size and is unfavorable for immunoliposome binding to target. Biochimica et Biophysica Acta (BBA) - Biomembranes 1062, 142-148.

[82] Lasic, D.D., Martin, F.J., Gabizon, A., Huang, S.K. and Papahadjopoulos, D. (1991). Sterically stabilized liposomes: a hypothesis on the molecular origin of the extended circulation times. Biochimica et Biophysica Acta (BBA) - Biomembranes 1070, 187-192.

[83] D. Papahadjopoulos et al. (1991). Sterically stabilized liposomes: improvements in pharmacokinetics and antitumor therapeutic efficacy. Proc. Natl. Sci. Acad. 88, 11460-11464.

[84] Torchilin, V. and Klibanov, A. (1993). Coupling of ligands with liposomes membrane. Drug Target. Del. 2, 227–238.

[85] Bogdanov jr, A.A., Klibanov, A.L. and Torchilin, V.P. (1988). Protein immobilization on the surface of liposomes via carbodiimide activation in the presence of N-hydroxysulfosuccinimide. FEBS Letters 231, 381-384.

[86] Holmberg, E., Maruyama, K., Litzinger, D.C., Wright, S., Davis, M., Kabalka, G.W., Kennel, S.J. and Huang, L. (1989). Highly efficient immunoliposomes prepared with a method which is compatible with various lipid compositions. Biochemical and Biophysical Research Communications 165, 1272-1278.

[87] Martin, F.J., Hubbell, W.L. and Papahadjopoulos, D. (2002). Immunospecific targeting of liposomes to cells: a novel and efficient method for covalent attachment of Fab' fragments via disulfide bonds. Biochemistry 20, 4229-4238.

[88] Leserman, L.D., Barbet, J., Kourilsky, F. and Weinstein, J.N. (1980). Targeting to cells of fluorescent liposomes covalently coupled with monoclonal antibody or protein A. Nature 288, 602-604.

[89] Hansen, C.B., Kao, G.Y., Moase, E.H., Zalipsky, S. and Allen, T.M. (1995). Attachment of antibodies to sterically stabilized liposomes: evaluation, comparison and optimization of coupling procedures. Biochimica et Biophysica Acta (BBA) - Biomembranes 1239, 133-144.

[90] Jayasena, S.D. (1999). Aptamers: An Emerging Class of Molecules That Rival Antibodies in Diagnostics. Clin Chem 45, 1628-1650.

[91] Hermann, T. and Patel, D.J. (2000). Adaptive Recognition by Nucleic Acid Aptamers. Science 287, 820-825.

[92] Tuerk, C. and Gold, L. (1990). Systematic evolution of ligands by exponential enrichment: RNA ligands to bacteriophage T4 DNA polymerase. Science 249, 505-510.

[93] Ellington, A.D. and Szostak, J.W. (1990). In vitro selection of RNA molecules that bind specific ligands. Nature 346, 818-822.

[94] Joyce, G.F. (1994). In vitro evolution of nucleic acids. Current Opinion in Structural Biology 4, 331-336.

[95] Gold, L., Polisky, B., Uhlenbeck, O. and Yarus, M. (1995). Diversity of Oligonucleotide Functions. Annual Review of Biochemistry 64, 763-797.

[96] Lorsch, J.R. and Szostak, J.W. (1996). Chance and Necessity in the Selection of Nucleic Acid Catalysts. Accounts of Chemical Research 29, 103-110.

[97] Li, Y. and Breaker, R.R. (1999). Deoxyribozymes: New players in the ancient game of biocatalysis. Current Opinion in Structural Biology 9, 315-323.

[98] Famulok, M. (1999). Oligonucleotide aptamers that recognize small molecules. Current Opinion in Structural Biology 9, 324-329.

[99] Hofmann, H.P., Limmer, S., Hornung, V. and Sprinzl, M. (1997). Ni2+-binding RNA motifs with an asymmetric purine-rich internal loop and a G-A base pair. RNA 3, 1289-1300.

[100] Ellington, A.D. and Szostak, J.W. (1992). Selection in vitro of single-stranded DNA molecules that fold into specific ligand-binding structures. Nature 355, 850-852.

[101] Jenison, R., Gill, S., Pardi, A. and Polisky, B. (1994). High-resolution molecular discrimination by RNA. Science 263, 1425-1429.

[102] Geiger, A., Burgstaller, P., von der Eltz, H., Roeder, A. and Famulok, M. (1996). RNA aptamers that bind L-arginine with sub-micromolar dissociation constants and high enantioselectivity. Nucl. Acids Res. 24, 1029-1036.

[103] Famulok, M. (2002). Molecular Recognition of Amino Acids by RNA-Aptamers: An L-Citrulline Binding RNA Motif and Its Evolution into an L-Arginine Binder. Journal of the American Chemical Society 116, 1698-1706.

[104] Wallis, M.G., Streicher, B., Wank, H., von Ahsen, U., Clodi, E., Wallace, S.T., Famulok, M. and Schroeder, R. (1997). In vitro selection of a viomycin-binding RNA pseudoknot. Chemistry & Biology 4, 357-366.

[105] Haller, A.A. and Sarnow, P. (1997). In vitro selection of a 7-methyl-guanosine binding RNA that inhibits translation of capped mRNAâ€‰molecules. Proceedings of the National Academy of Sciences of the United States of America 94, 8521-8526.

[106] Sassanfar, M. and Szostak, J.W. (1993). An RNA motif that binds ATP. Nature 364, 550-553.

[107] Williams, K.P., Liu, X.-H., Schumacher, T.N.M., Lin, H.Y., Ausiello, D.A., Kim, P.S. and Bartel, D.P. (1997). Bioactive and nuclease-resistant l-DNA ligand ofâ€‰vasopressin. Proceedings of the National Academy of Sciences of the United States of America 94, 11285-11290.

CHAPTER 2

ARGININE RICH CELL-PENETRATING PEPTIDES

Cellular uptake of biologically active molecules is a major obstacle in pharmaceutical drug design and controlled drug delivery. While a broad range of therapeutic agents, including proteins, peptides and oligonucleotides, have been successfully introduced to target cells using viral vectors[1], and methods such as electroporation, and microinjection, and liposome encapsulation[2], these internalization strategies have a number of drawbacks. Problems include inefficient drug delivery, high variability of drug expression among target cells, cellular damage and toxicity, and restrictions based upon drug and cell type. The first barrier to efficient and controlled intracellular delivery is the plasma membrane which prevents direct translocation of hydrophilic macromolecules. In vivo, the most common pathway for bringing a macromolecule into a cell is through endocytosis. However, the fate of an endocytosed macromolecule is unpredictable; it may remain trapped in endosomes and suffer degradation by the acidic pH and digestive enzymes.

Biology has evolved ways to circumvent these problems as a number of proteins are permeable to mammalian cell membranes. This ability is conferred by a localized region in the protein known as the protein transduction domain. Furthermore the isolated peptide sequence, sometimes referred to as a cell-penetrating peptide, retains the transduction properties of the native protein. These cell penetrating peptides comprise a class of short (<20 amino acid)

cationic peptides that have the ability to traverse the cell membranes of many different types of mammalian cells. A wide variety of macromolecules have been attached to these peptides and subsequently internalized. Moreover, after uptake the cargo maintains its activity. The ability of cell-penetrating peptides to translocate biologically active molecules into cells makes these peptides promising candidates for drug delivery applications.

Among the cell-penetrating peptides, the arginine-rich cell-penetrating peptides have been the most widely studied[3,4]. Examples include the TAT peptide from the HIV transactivator protein TAT, penetratin, a 16 amino acid domain from the Antennapedia protein of *Drosophila*, a flock house virus (FHV) coat peptide (sequence 35-49), and oligoarginines [3,5]. The focus here is on the TAT peptide, partly because it has attracted the most attention, but also because it is a prototypical example that has many of the essential characteristics of the arginine-rich cell-penetrating peptides.

2.1 TAT peptide as a prototypical example of arginine rich cell penetrating peptides

In 1988, Green and Lowenstein [6], and Frankel and Pabo [7], independently discovered that the transactivator of transcription (TAT) protein of the Human Immunodeficiency Virus can penetrate cells and activate the viral genome replication. The TAT protein is an 86 amino acid long protein that is released by infected cells and is an essential regulatory gene for HIV replication [8]. In 1997, Vives *et al* [9] found that a 11-amino acid sequence, TAT (47-57),

known as the TAT peptide or TAT PTD, can not only enter cells but is more efficient than the full length protein. It was observed that the chirality of the peptide backbone has no effect on cellular uptake of TAT peptide; inverse and retro forms were able to enter cells as efficiently as the native peptide, suggesting uptake does not require a specific binding site. The TAT peptide can enter cells efficiently, either alone or linked to macromolecules like proteins, oligonucleotides or liposomes. TAT-mediated delivery appears to be independent of cargo size. Proteins in excess of 100,000 Da, 40 nm nanoparticles and even 200 nm liposomes have been delivered inside cells using TAT peptide. The liposomes were intact inside the cells and remained so even 1 hour after transduction. Conversely, non-conjugated proteins in the incubation media were not able to enter cells [10].

TAT peptide is highly cationic with 6 arginine and 2 lysine residues. Substitution of any basic residue with neutral alanine reduces activity, while substitution of neutral residues has no effect, implying the net positive charge of TAT is necessary for cellular uptake. It has been hypothesized that the utility of being positively charged likely comes from the resulting strong electrostatic interactions with the plasma membranes of eukaryotic cells. Studies on the binding affinities of cationic cell-penetrating peptides indicate these peptides strongly bind electrostatically to the various anionic species present at the extracellular surface of cell membranes, including lipid headgroups, proteins like nucleolin, and proteoglycans such as heparin sulfate [11,12].

Although electrostatic interactions are known to be important for arginine-rich cell penetrating peptides, non-electrostatic effects such as hydrophobicity and peptide structural transitions can also contribute to the binding affinity of amphipathic cell-penetrating peptides to cell membranes [13]. For example, penetratin adopts a random coil structure in solution, and transforms to an α-helical conformation at high lipid to peptide molar ratios [14,15]. Moreover, decreasing the lipid to peptide ratio promotes a higher degree of β-sheet conformation [15]. Both of these secondary structural transitions increase the amphipathicity of Penetratin, allowing its hydrophobic moieties to directly interact with the non-polar interior of the lipid membrane, and several studies have implicated insertion of the hydrophobic portions of Penetratin into the membrane as being important for uptake [16-18]. In contrast, the non-amphipathic TAT peptide is unstructured both in solution and when associated with lipid membranes [19], and TAT associates with the membrane surface since hydrophobic interaction is negligible [11].

It is empirically known that the cationic nature of the peptide is a necessary condition but not a sufficient condition for translocation activity. Although, arginine-rich oligomers can enter cells, similar length polymers of other basic amino acids, lysine, ornithine or histidine, cannot [20]. Branched chain arginine polymer is as efficient as the corresponding linear polymer. However, peptide length is an important factor [21]. The efficiency of cellular uptake depends on the number of arginine residues. Arginine polymers with less

than five amino acids are not as effective as polymers with six or more amino acids. Uptake efficiency increases as the peptide length increases up to 15 amino acids. Peptides with more than 15 arginine residues can still enter cells but with significantly less efficiency [20,22]. The guanidinium headgroup of arginine is the central structural feature required for peptide uptake. Heptamers of citrulline, an isotere of arginine with a nitrogen of guanidine replaced by oxygen, are unable to enter cells [20].

The discovery that the guanidinium residues of arginine are the essential ingredients of a peptide's ability to enter cells has allowed for the design of a range of guanidinium-rich synthetic analogs. Oligoarginine peptoids that have the side chain attached to nitrogen instead of carbon have proved to be more efficient than oligoarginines [21]. Guanidinium-rich oligocarbamates were taken up into cells about three times faster than TAT peptide [23]. Polyguanidino dendrimers, based on diamino acid monomeric units, have also proven to be effective at entering cells [24]. Carbohydrate-based polymers like the guanidinylated neomycin can not only enter cells but can carry large (>300kDa) bioactive macromolecules along [25]. Recently Deming *et al [26]* combined liposome drug delivery system with cell-penetrating peptides by preparing polyarginine-polyleucine block copolymers that self-assemble into vesicles. The vesicles remained intact inside the cells showing their potential to carry large cargoes. Although long polyarginine chains (>20) are thought to be less efficient for intracellular delivery, they facilitated cellular uptake of the vesicles.

2.2 Mechanism of cellular uptake: direct translocation or endocytosis?

The exact molecular mechanism of cellular entry of arginine-rich cell penetrating peptides is currently not fully understood. Initial studies indicated a direct translocation mechanism across the cell membrane that bypassed endocytosis. Fluorescence microscopy and fluorescence activated cell sorting (FACS) studies on cells incubated with fluorescently-labeled peptides showed rapid translocation that was not inhibited when cells were incubated at 4°C. Addition of metabolic or endocytosis inhibitors also seemed to have no effect on cellular internalization. These experiments, along with the finding that inverse and retro forms of the peptide are as effective, led to the belief that cellular uptake involved an energy-independent, non-endocytotic process that was receptor independent.

Most of these early experiments were conducted using microscopy or flow cytometry on fixed cells. In 2003, Richard *et al* [27] showed that a mild fixation of cells with formaldehyde drastically changed the intracellular distribution of TAT peptide. Fixed cells showed nuclear localization of TAT peptide while unfixed cells had the peptide located in cytoplasmic vesicles. Additionally, it was shown that flow cytometry was unable to distinguish between membrane-bound and internalized fluorochrome. In living, nonfixed cells analyzed with FACS, large fraction of the fluorescent peptide was associated with the outer leaflet of the cell membrane instead of being present within the cytoplasm. They demonstrated that trypsin treatment of cells removed surface-bound peptide by

digesting the peptide. FACS analysis following trypsin treatment indicated a relatively slow rate of uptake, comparable to that of classical markers of endocytosis. Since then, many other studies have also observed inhibition of cellular uptake at 4°C and with chemical means that induce energy depletion, indicating an energy-dependent process as the major route for the internalization of cell-penetrating peptides [27-33].

Many groups have proposed that cell membrane heparan sulfate proteoglycans (HSPGs) act as receptors for extracellular TAT uptake. Proteoglycans are negatively charged, and are present on the surface of many cell types. Thermodynamic studies have shown that TAT binds with significantly greater affinity to heparin sulfate than to anionic lipid vesicles [11,12]. That TAT can interact with different components of the membrane suggests that multiple mechanisms are possible. Moreover, it has been observed that interaction with the cell-penetrating peptides results in aggregation of both anionic lipids and proteoglycans, which may provide further clues for the nature of the alternate mechanisms [34,35].

Ligands that bind to proteoglycans can be internalized through an endocytotic pathway. Both TAT protein and TAT peptide were shown to bind strongly to heparin, a sulfated glycosaminoglycan that mimics the heparan sulfate proteoglycans [36,37]. It was also demonstrated that addition of heparin and dextran, another sulfated glycosaminoglycan, inhibits the cellular uptake of TAT

peptide [31,38,39]. Treatment of cells with chemicals that eliminate or cleave the HS proteoglycans resulted in a significant decrease in TAT peptide internalization [40]. Studies with mutant cells that are unable to synthesize glycosaminoglycans showed reduced TAT-mediated transport [39,41,42]. These studies suggest that heparan sulfate can act as a receptor for TAT peptide, and constitute an important pathway for internalization; however, none of the studies have demonstrated complete inhibition of cellular uptake [41]. In addition, polyarginine was able to enter mutant cells that have less than 2% of the wild-type level of heparin sulfate [25]. This suggests the presence of a heparan sulfate-independent pathway in addition to a heparan sulfate-dependent one.

Analysis of peptide uptake by live-cell microscopy has demonstrated the involvement of endocytosis in the cellular internalization of the TAT peptide. Within the broad classification of endocytosis, there are several possible mechanisms of uptake. Studies on TAT peptide uptake in cells with specific endocytotic pathways chemically inhibited have yielded mixed results. Clathrin-mediated endocytosis has been proposed as the primary mechanism of uptake of arginine-rich transporters. Clathrin-mediated endocytosis is the major and best-characterized endocytotic pathway. It involves strong binding of a ligand to a specific cell surface receptor resulting in the clustering of the ligand-receptor complexes in coated pits on the plasma membrane, formed by the assembly of clathrin. The coated pits then invaginate and pinch off from the plasma membrane to form intracellular clathrin-coated vesicles [43]. It has been reported that in

HeLa cells, labeled cell-penetrating peptides colocalize with transferrin, a glycoprotein marker for endocytosis [27,44]. Another study demonstrated that TAT uptake in HeLa cells, in the presence of chlorpromazine, a known inhibitor of clathrin-mediated endocytotic pathway, resulted in a 50% inhibition of peptide uptake, while incubation in a potassium-free buffer resulted in a 40% decrease, indicating the involvement of clathrin-dependent pathway [33]. However, other studies with fluorescently labeled polyarginine conjugates [30,45] and fusion proteins [41,46] showed that it does not colocalize with transferrin. Another study with a TAT-avidin conjugate showed only a modest decrease in uptake upon treatment with hyperosmolar medium, a condition shown to decrease clathrin-dependent endocytosis [47].

Caveolin-dependent endocytosis, a lipid raft-mediated form of endocytosis has likewise been implicated. Caveolae are small, hydrophobic membrane microdomains that are rich in cholesterol and glycosphingolipids. Ligands associate with the cell membrane and then become trapped in relatively stationary caveolae, which then bud off the membrane and form caveosomes. Cholesterol is required for caveolar uptake and drugs that specifically bind to cholesterol perturb internalization through the caveolae [43]. TAT-GFP in HeLa cells [46] and in CHO-K1 and HL3T1 cells [41] has been shown to colocalize with caveolin-1. Both TAT-rhodamine [45] and TAT-GFP [41] complexes have also been shown to colocalize with cholera toxin, which is known to proceed through a caveolin-dependent pathway. However, nystatin, a compound known to inhibit caveolae

formation, and filipin III had little effect on the uptake of fluorescently labeled TAT into HeLa cells or CHO cells [33].

A number of research groups have proposed macropinocytosis as the mechanism of uptake for cell-penetrating peptides. Macropinocytosis involves the formation of large endocytotic vesicles of irregular size and shape, generated by actin-driven envagination of the plasma membrane. Macropinosomes have no coat and do not concentrate receptors. They vary in size, sometimes being as large as 5 μm in diameter [43]. Studies have shown dose-dependent inhibition of TAT peptide uptake when cells are pretreated with amiloride, an inhibitor of the Na^+/H^+ exchange required in macropinocytosis, or cholesterol is removed with β-cyclodextrin [32,48]. Additionally, cytochalasin D, an inhibitor of actin polymerization, and the macropinocytosis inhibitor ethylisopropylamiloride have been shown to significantly suppress uptake of the arginine-rich peptides into HeLa cells [30]. However, Zaro *et al* [49] reported that delivery of oligoarginine in HeLa cells was not inhibited by incubation at 16 °C, or by treatment with amiloride indicating a mechanism different from macropinocytosis.

Although the direct translocation mechanism from earlier studies has been shown to be an artifact of cell fixation and membrane-associated peptide, studies on live, non-fixed cells have indicated the presence of a non-endocytotic mechanism of cellular uptake of cell-penetrating peptides. Maiolo *et al* [50] used confocal microscopy to study the cellular distribution of arginine-rich cell-

penetrating peptides in live cells. They found that the uptake characteristics were a mixture of punctate and diffuse staining. Incubating the cells at 4°C eliminated most of the punctate staining, indicating that it is due to endocytotic uptake. The diffuse staining appeared to be fast and occurred at both 37°C and 4°C, indicating a second, non-endocytotic mechanism. The diffuse staining was not due to the release of peptide from endosomes as it appeared first and the punctate staining later, and it continued to occur at 4°C when endocytosis is inhibited. Several other studies have also reported cellular uptake when the cells have been incubated at 4°C [26,51-53]. It has also been observed that blocking specific endocytotic pathways does not affect the ability of TAT peptide to enter cells.

Examination of translocation of arginine-rich cell-penetrating peptides across unilamellar vesicles as a model system has revealed a range of behavior. Several early studies have indicated that the addition of both TAT peptide [11,54] and Penetratin [55,56] do not induce dye leakage and are not directly translocated in lipid vesicles composed mainly of zwitterionic PC and anionic PG and PS lipids. Membrane potential measurements also indicate that lipid bilayers with similar compositions remain intact [34]. Recent results suggest that the lipid composition of the target membrane is important for transduction activity. We have directly observed TAT peptide entry into giant unilamellar vesicles without any endocytotic machinery, provided that the target membranes have negative intrinsic curvature lipids (such as those with PE headgroups) at concentrations

above a minimum ‘threshold’ concentration [57]. This can also be observed on penetratin, which can also traverse lipid bilayers containing PE lipids [58].

A number of studies have investigated the question of how cell penetrating peptides dissociate from the plasma membrane once they are internalized. For example, it has been shown that the arginine-rich peptide, R_8W, can strongly interact with the anionic cellular cytoskeleton components actin and tubulin, leading to aggregation [59]. The TAT peptide also binds to and condenses DNA. Moreover, the binding constant for the TAT peptide with DNA is 1-2 orders of magnitude higher than for heparin sulfate, leading to the hypothesis that high DNA-binding affinity could facilitate the release of cargo after cellular uptake [60], by promoting competition for the membrane association of poly-cationic peptides.

The debate on the mechanism of cell penetrating peptides, mostly notably TAT, has often been characterized by a type of ‘either/or’ discourse, such as the whether direct translocation or some specific form of endocytosis is most relevant. Since the cellular uptake of arginine-rich peptides is dependent on a variety of factors, including temperature, incubation time, cell type, cargo type and size, linkage type and size, [4,61], comparison between different experiments have been difficult, and has compounded the controversy surrounding the uptake mechanism. It has no doubt been recognized that more than one mechanism may be involved in TAT translocation activity. This recognition accommodates the

broad range of proposed hypotheses, and can potentially conclude the discourse with an artificial consensus. However, an acknowledgement of multiple mechanisms of entry does not explain the central phenomenon: How does a relatively simple molecule like TAT facilitate mechanisms as different as direct entry and the multiple endocytotic mechanisms? Rather than debate the differences between the distinct observed mechanisms, we focus on what these different mechanisms have in common, and relate these common features to what the physical chemistry of cell penetrating peptides allows them to do.

2.3 Interactions between lipid membranes and biomolecules

Lipid membrane is a self-assembled structure held together by the non-covalent interactions between individual lipid molecules. It has two hydrophilic surfaces aligned by lipid head groups on each side and one hydrophobic core where lipid hydrophobic chains are sequestered from water. In aqueous solution, charged lipid membranes and charged biopolymer interact spontaneously through two major pathways which are electrostatic interaction and hydrophobic interactions. Depending on the structural features of the biopolymer, the interactions between lipid membranes and biopolymers can be either dominated by electrostatic interaction or a combination of electrostatic interaction and hydrophobic interaction. If the biopolymer is a polyelectrolyte, like the TAT peptide, the membrane-polyelectrolyte interaction is dominated by electrostatic interactions and, in their self-assembled structure, the polyelectrolyte molecules are associated with the hydrophilic surface of lipid membranes and do not insert

into membrane's hydrophobic region. If the biopolymer is amphipathic with well separated hydrophilic and hydrophobic domains, both electrostatic and hydrophobic interactions contribute and the resultant structure formed by membrane and biopolymer has biopolymer molecules either partially embedded or completely spanning the membrane's hydrophobic core.

2.3.1 Electrostatic interactions between lipid membranes and polyelectrolytes

Electrostatics in aqueous environments is counterintuitive. At physiological conditions, electric fields from charged biopolymers are strongly reduced by the large dielectric constant of water and by screening from ions from dissociated salts. That is not to say that electrostatic interactions are weak. The entropy of ions can result in strong interactions between charged objects in water despite short screening lengths, via coupling between osmotic and electrostatic interactions. For example, the attraction between a cationic cell penetrating peptide and an anionic membrane is driven by the entropy gain from release of condensed counterions.

According to Manning's theory for linear polyelectrolyte solution, the real polyelectrolyte is simplified as an infinite line charge with average axial charge spacing b and, if its Manning parameter $\xi = \frac{l_B}{b}$ is larger than one (l_B is the Bjerrrum length), counterion condensation around the polyelectrolyte chain occurs to reduce ξ to a value just less than one [62]. The Bjerrum length l_B is defined as the length scale where the electrostatic interaction between two unit

charges is equal to the thermal fluctuation energy k_BT. In a solvent with dielectric constant ε, the Bjerrum length l_B is

$$l_B = \frac{e^2}{\varepsilon k_B T} \qquad 2.1$$

where e is the unit charge, k_B is the Boltzman constant, and T is the absolute temperature. In water at 25ºC, the Bjerrum length l_B = 7.1Å.

For a charged plane of infinite size, the counterions condense onto the plane to form the Gouy-Chapman double layer independent of the surface charge density of the plane [63]. The Gouy-Chapmen length l_{GC} is defined as

$$l_{GC} = \frac{\varepsilon \cdot k_B T}{2\pi \cdot e\sigma} = \frac{e}{2\pi \cdot l_B \sigma} \qquad 2.2$$

where ε is the dielectric constant of the solvent, k_B is the Boltzman constant, e is unit charge, σ is the surface charge density of the plane, and l_B is the Bjerrum length.

When charged biopolymers are adsorped onto an oppositely charged membrane, the complementary charge distributions can electrostatically compensate one another. This means that condensed counterions are no longer needed by the membrane and the polymer at the regions of contact, and thus can be released for a large entropic gain. This leads to a strong electrostatic attraction. This type of electrostatic interaction has been observed for self-assembled

complexes between membranes and a variety of anionic polymers, including DNA [64-66], F-Actin [67], microtubules [68], and filamentous phages [69].

When the surface charge densities of the membrane and the charged polymer are similar, as in the case for cationic lipids and DNA complexes, the counterion release is nearly maximal. DNA and cationic lipids in aqueous solution self-assemble into a lamellar structure where one layer of DNA molecules confined between two layers of lipid membranes and distance between DNA molecules within the layer depends the lipid-to-DNA mass ratio [70]. If the concentration of the negative intrinsic curvature lipids, like DOPE, in the membrane is increased, the membrane rigidity decreases and the DNA-membrane complexes undergo a phase transition from lamellar to inverted hexagonal structures where the membrane wraps around the DNA molecules.

For complexes of lipids with Filamentous actin (F-actin), a highly charged polyelectrolyte found in cellular cytoskeleton, the surface charge densities are very different and complete counterion release is sterically impossible. The resulting frustration drives the F-actin and cationic lipid membrane complexes to self-assemble into network of tubules on macroscopic scale (> 100 μm) in which F-actin-membrane form a lamellar structure with one layer of lipid bilayer sandwiched in between two layers of F-actin [71].

2.4 Small angle x-ray scattering (SAXS) measurements for biomolecular samples

X-ray diffraction is one of the major techniques widely used in the determination of material structures. The experiments reported in this thesis have used x-ray diffraction to characterize the structure of self-assembled complexes formed by phospholipid membranes and biopolymers or their synthetic derivatives. These biomolecular systems are different from conventional solid-state crystalline materials in the following aspects: (1), these biomocular samples are often partially ordered, only exhibiting 1-dimensional or 2-dimensional periodic density distribution; (2), these systems are usually fluidic and their periodic density distributions have considerable contributions from thermal fluctuation and static disorder; (3) the length of order in these systems is in the scale of 1-100Å, which confines most of the resultant diffraction pattern to the small angle region (diffraction angles of a few degrees); (4) the biomolecular systems are normally composed of light elements such as carbon, hydrogen, and oxygen, which makes their electron density contrast between the constituent components very low and thus lead to weak diffraction intensities. Therefore, collection of interpretable data from such biomolecular systems requires X-ray beam sources with high intensity and high resolution, which can be easily satisfied by modern synchrotron source.

2.4.1 Fundamental rules of x-ray diffraction

In the classical description, X-rays are transverse electromagnetic waves, where the electric and magnetic fields are perpendicular to each other and to the direction of propagation. It is characterized by its wavelength λ, or its wavenumber k = 2π/λ. From a quantum mechanical perspective, the X-rays can be viewed as a beam of photons, with each photon having an energy ħω and momentum ħ**k**. The intensity of the beam is given by the number if photons passing through a given area per unit time. When X-rays interacts with a free scatterer with charge *q* and mass *m*, the scattered intensity I_{sc} at distance *R* from the scatterer is

$$I_{sc} = I_0 \frac{q^4}{m^2 c^4 R^2}\left(\frac{1+Cos^2 2\theta}{2}\right)$$

where I_0 is the indicent beam intensity, c is the velocity of light, and 2θ is the scattering angle [72-74]. Protons and electrons have the same charge but the mass of a proton is 1836 times larger than that of an electron. The scattered intensity by a proton is, therefore, $(1836)^2$ times smaller than that by an electron. Hence, the X-ray scattering pattern is predominantly contributed by the interactions between x-rays and electrons and the scattering contrast is due to the electron density difference within the system. When electrons scatter X-rays, if the wavelength of the scattered wave is the same as that of the incident one, the scattering process is called *elastic*. However, if energy is transferred to the electron, the scattered photon has a longer wavelength relative to that of the incident photon, and the scattering process is *inelastic* (also known as the Compton effect). The inelastic contribution is mainly due to phonon scattering. As the energy of incident X-ray

photons (~10^4 ev) is significantly larger than that of phonosn (typically < 10^{-1} ev), the energy change is relative negligible compared to energy of the incident beam and the scattering is considered to be quasi-elastic. In practice, special setups with very high energy resolution (~ 10^{-3} ev) are required to detect the energy difference between incident and scattered photons in inelastic scattering.

In an X-ray diffraction experiment, the detectors usually count the number of single photons. The measured intensity, I_{sc} is the number of photons per second recorded by the detector. The differential cross-section $(\frac{d\sigma}{d\Omega})$ can be defined as:

$$\frac{d\sigma}{d\Omega} = \frac{(number\quad of\quad X-ray\ photons\quad scattered\quad per\quad \sec ond\quad in\quad d\Omega)}{(incident\quad flux)\quad d\Omega}$$

where, σ is the scattering cross-section, $d\Omega$ is the solid angle subtend by the detector, and incident flux is the incident beam intensity (I_0) divided by its cross-section area (A_0). The measured intensity, I_{sc}, is related to the differential cross-section $\frac{d\sigma}{d\Omega}$ by

$$\left(\frac{d\sigma}{d\Omega}\right) = \frac{I_{SC}}{(I_0 / A_0)d\Omega}$$

or,

$$I_{sc} = \frac{I_0}{A_0}\left(\frac{d\sigma}{d\Omega}\right)(d\Omega)$$

From the X-ray scattering theory[72-74], the differential cross-section for a system at thermal equilibrium:

$$\frac{d\sigma}{d\Omega} \propto P(q)\cdot |f(q)|^2 \cdot S(q)$$

where, *P(q)* is the polarization factor, *f(q)* is the form factor of the scatterer and *S(q)* is the structure factor for the scatterer lattice. $q=\boldsymbol{k}_s - \boldsymbol{k}_i$, is the scattering vector which measures the photon momentum transfer ($\boldsymbol{k}_i$ and $\boldsymbol{k}_s$ are the wavevectors of the incident and scattered waves, respectively). For elastic X-ray scattering, the scattering vector q is given by:

$$|q| = \frac{4\pi Sin\theta}{\lambda} = \frac{2\pi}{d}$$

where λ is wavelength of the incident X-ray, θ is half of the scattering angle, and d is the periodicity of the electron density fluctuation.

The polarization factor *P(q)* depends on the X-ray source. In a synchrotron source, the electrons orbit in the horizontal plane and hence the emitted x-rays are linearly polarized in the orbit plane but elliptically polarized when viewed out of that plane. So, for synchrotron source, polarization factor *P(q)* = 1 in the vertical scattering plane, while $P(q) = Cos^2 2\theta$ in the horizontal scattering plane where 2θ is the scattering angle. For unpolarized X-ray source, the polarization factor $P(q) = (1 + Cos^2 2\theta)/2$. For the small angle x-ray scattering ($2\theta < 10^0$), the polarization factor is not significantly different from *P(q)* ~ 1.

The static structural factor *S(q)* accounts the geometry of scatterer and contains the structural information of the biomolecular system.

$$S(q) = \frac{1}{N}\sum_{i,j}^{N} <e^{iq\cdot[r_i(0)-r_j(0)]} >= \frac{V}{N}\int drG(r)e^{-iqr}$$

and, $G(r) = \frac{1}{V}\int dr' < \rho(r).\rho(r+r') >$

G(r) is the density-density correlation function with ρ(r) being the electron density distribution of the system.

The form factor *f(q)* of the scatterer is the Fourier Transform of its electron density. For an atom, $f(q) = -r_o f^o(q)$, where r_o is the Thomson scattering length ($r_o = 2.82\times10^{-5}$ Å) and $f^o(q)$ is the atomic form factor given by:

$$f^o(q) = \int \rho(r)e^{iq\bullet r}dr = \begin{cases} z, & for \quad q \to 0 \\ 0, & for \quad q \to \infty \end{cases}$$

where *ρ(r)* is the number density of electron at position *r* around the nucleus in the atom, and z is the total number of electrons in the atom.

For a molecule, the form factor $f^{mol}(q)$ is

$$f^{mol}(q) = -r_o \sum_{r_j} f_j(q)e^{iq\bullet r_j}$$

where $f_j(q)$ is the atomic form factor of the jth atom in the molecule. If $|f^{mol}(q)|^2$ can be determined experimentally with sufficient values of scattering vectors *q*, the position r_j of the jth atom in the molecule can be known. However, even for the very intense x-ray beam provided by modern synchrotron sources, the scattering length of a single molecule is not sufficient to yield measurable scattering signals and the molecules need to be assembled into a crystal.

For a crystal, the form factor $f^{crystal}(q)$ is

$$f^{crystal}(q) = -r_o(\sum_{r_j} f_j^{mol}(q)e^{iq\bullet r_j})(\sum_{R_n} e^{iq\bullet R_n})$$

where the first term is the scattering amplitude from the basis of molecules or atoms contained in the unit cell and is known as "unit cell structure factor" in which r_j is the position of j^{th} molecule or atom in the unit cell, and the second term is a sum over lattice sites and is known as "lattice sum". All the terms in the lattice sum are phase factors located on the unit circle in a complex plane. This lattice sum and as a result the crystal's form factor $f^{crystal}$ is non-vanishing if and only if the scattering vector q coincides with a reciprocal lattice vector G which satisfies $G.R_n = 2\pi \times m$ where m is an integer. This is the Laue condition for the observation of X-ray diffraction. Scattering from a crystal is confined to distinct points in the reciprocal space. The scattering signature can therefore be used to deduce structural information.

2.5 References

[1] Anderson, W.F. (1998). Human gene therapy. Nature 392, 25-30.

[2] Luo, D., and Saltzman, W. (2000). Synthetic DNA delivery systems. Nature Biotech. 18, 33-37.

[3] El-Sayed, A., Futaki, S. and Harashima, H. (2009). Delivery of Macromolecules Using Arginine-Rich Cell-Penetrating Peptides: Ways to Overcome Endosomal Entrapment. The AAPS Journal 11, 13-22.

[4] Wender, P.A., Galliher, W. C., Goun, E. L., Jones, L. R., and Pillow, T. H. (2008). The design of guanidinium-rich transporters and their internalization mechanisms. Adv. Drug Deliv. Rev. 60, 452-472.

[5] Wadia, J., and Dowdy, S. (2005). Transmembrane delivery of protein and peptide drugs by TAT-mediated transduction in the treatment of cancer. Adv. Drug Deliv. Rev. 57, 579-596.

[6] Green, M., and Loewenstein, P. M. (1988). Autonomous functional domains of chemically synthesized human immunodeficiency virus tat trans-activator protein. Cell 55, 1179-1188.

[7] Frankel, A.D., and Pabo, C. O. (1988). Cellular Uptake of the Tat Protein from Human lmmunodeficiency Virus. Cell 55, 1189-1193

[8] Jeang, K., Xiao, H., and Rich, E. (1999). Multifaceted Activities of the HIV-1 Transactivator of Transcription, Tat. J Biol. Chem. 274, 28837-28840.

[9] Vives, E., Brodin, P. and Lebleu, B. (1997). A Truncated HIV-1 Tat Protein Basic Domain Rapidly Translocates through the Plasma Membrane and Accumulates in the Cell Nucleus. J. Biol. Chem. 272, 16010–16017.

[10] Torchilin, V., Rammohan, R., Weissig, V. and Levchenko, T. (2001). TAT peptide on the surface of liposomes affords their efficient intracellular delivery even at low temperature and in the presence of metabolic inhibitores. Proc. Natl. Acad. Sci. 98, 8786-8791.

[11] Ziegler, A., Blatter, X., Seelig, A. and Seelig, J. (2003). Protein Transduction Domains of HIV-1 and SIV TAT Interact with Charged Lipid Vesicles. Binding Mechanism and Thermodynamic Analysis. Biochem. 42, 9185-9194.

[12] Goncalves, E., Kitas, E. and Seelig, J. (2005). Binding of Oligoarginine to Membrane Lipids and Heparan Sulfate: Structural and Thermodynamic Characterization of a Cell-Penetrating Peptide. Biochem. 44, 2692-2702.

[13] Ziegler, A. (2008). Thermodynamic studies and binding mechanisms of cell-penetrating peptides with lipids and glycosaminoglycans. Adv. Drug Deliv. Rev. 60, 580-597.

[14] Caesar, C., Esbjorner, E., Lincoln, P., and Norden, B. (2006). Membrane Interactions of Cell-Penetrating Peptides Probed by Tryptophan Fluorescence and Dichroism Techniques: Correlations of Structure to Cellular Uptake. Biochem. 45, 7682-7692.

[15] Magzoub, M., Eriksson, L., and Graslund, A. (2002). Conformational states of the cell-penetrating peptide penetratin when interacting with phospholipid vesicles: effects of surface charge and peptide concentration. Biochim. Biophys. Acta 1563, 53-63.

[16] Christiaens, B., Symoens, S., Vanderheyden, S., Engelborghs, Y., Joliot, A., Prochiantz, A., Vandekerckhove, J., Rosseneu, M., and Vanloo, B. (2002). Tryptophan fluorescence study of the interaction of penetratin peptides with model membranes. Eur. J. Biochem. 269, 2918-2926.

[17] Dom, G., Shaw-Jackson, C., Matis, C., Bouffioux, O., Picard, J., Prochiantz, A., Mingeot-Leclercq, M., Brasseur, R., and Rezsohazy, R. (2003). Cellular uptake of Antennapedia Penetratin peptides is a two-step process in which phase transfer precedes a tryptophan-dependent translocation. Nucl. Acids Res. 31, 556-561.

[18] Binder, H., and Lindblom, G. (2003). Charge-Dependent Translocation of the Trojan Peptide Penetratin across Lipid Membranes. Biophys J 85, 982-995.

[19] Schwarze, S.R., Hruska, K. A., and Dowdy, S. F. (2000). Protein transduction: unrestricted delivery into all cells? Trends in Cell Biology 10, 290-295.

[20] Mitchell, D.J., Kim, D. T., Steinman, L., Fathman, C. G. & Rothbard, J. B. (2000). Polyarginine enters cells more efficiently than other polycationic homopolymers. J. Pept. Res. 56, 318-325.

[21] Wender, P.A., Mitchell, D. J., Pattabiraman, K., Pelkey, E. T., Steinman, L., and Rothbard, J. B. (2000). The design, synthesis, and evaluation of molecules that enable or enhance cellular uptake: Peptoid molecular transporters. Proc. Natl. Acad. Sci. 97, 13003-13008.

[22] Futaki, S., Suzuki, T., Ohashi, W., Yagami, T., Tanaka, S., Ueda, K., and Sugiura, Y. (2001). Arginine-rich Peptides: An Abundant Source of Membran-Permeable Peptides Having Potential as Carriers for Intracellular Protein Delivery. J Biol. Chem. 276, 5836-5840.

[23] Wender, P., Rothbard, J., Jessop, T., Kreider, E., and Wylie, B. (2002). Oligocarbamate Molecular Transporters: Design, Synthesis, and

Biological Evaluation of a New Class of Transporters for Drug Delivery. J. Am. Chem. Soc. 124, 13382-13383.

[24] Wender, P., Kreider, E., Pelkey, E., Rothbard, J., and VanDeusen, C. (2005). Dendrimeric Molecular Transporters: Synthesis and Evaluation of Tunable Polyguanidino Dendrimers That Facilitate Cellular Uptake. Org. Lett. 7, 4815-4818.

[25] Elson-Schwab, L., Garner, O., Schuksz, M., Crawford, B., Esko, J., and Tor, Y. (2007). Guanidinylated Neomycin Delivers Large, Bioactive Cargo into Cells through a Heparan Sulfate-dependent Pathway. J Biol. Chem. 282, 13585-13591.

[26] Holowka, E.P., Sun, V. Z., Kamei, D. T. and Deming, T. J. . (2007). Polyarginine segments in block copolypeptides drive both vesicular assembly and intracellular delivery. Nature Mater. 6, 52-57.

[27] Richard, J.P., Melikov, K., Vives, E., Ramos, C., Verbeure, B., Gait, M. J., Chernomordik, L. V., and Lebleu, B. . (2003). Cell-penetrating Peptides: A Reevaluation of the Mechanism of Cellular Uptake. J Biol. Chem. 278, 585-590.

[28] Fischer, R., Fotin-Mleczek, M., Hufnagel, H., and Brock, R. (2005). Break on through to the Other Side-Biophysics and Cell Biology Shed Light on Cell-Penetrating Peptides. Chem Bio Chem 6, 2126-2142.

[29] Drin, G., Cottin, S., Blanc, E., Rees, A., and Temsamani, J. (2003). Studies on the Internalization Mechanism of Cationic Cell-penetrating Peptides. J Biol. Chem. 278, 31192-31201.

[30] Nakase, I., Niwa, M., Takeuchi, T., Sonomura, K., Kawabata, N., Koike, Y., Takehashi, M., Tanaka, S., Ueda, K., Simpson, J. C., Jones, A. T., Sugiura, Y., and Futaki, S. (2004). Cellular Uptake of Arginine-Rich Peptides: Roles for Macropinocytosis and Actin Rearrangement. Mol. Therapy 10, 1011-1022.

[31] Fretz, M., Koning, G., Mastrobattista, E., Jiskoot, W., and Storm, G. (2004). OVCAR-3 cells internalize TAT-peptide modified liposomes by endocytosis Biochim. Biophys. Acta 1665, 48-56.

[32] Wadia, J., Stan, R., and Dowdy, S. F. (2004). Transducible TAT-HA fusogenic peptide enhances escape of TAT-fusion proteins after lipid raft macropinocytosis. Nature Med. 10, 310-315.

[33] Richard, J.P., Melikov, K., Brook, H., Prevot, P., Lebleu, B. and Chernomordik, L. V. (2005). Cellular Uptake of Unconjugated TAT Peptide Involves Clathrin-dependent Endocytosis and Heparan Sulfate Receptors. J Biol. Chem. 280, 15300-15306.

[34] Tiriveedhi, V., and Butko, P. (2007). A Fluorescence Spectroscopy Study on the Interactions of the TAT-PTD Peptide with Model Lipid Membranes. Biochem. 46, 3888-3895.

[35] Ziegler, A., and Seelig, J. (2008). Binding and Clustering of Glycosaminoglycans: A Common Property of Mono- and Multivalent Cell-Penetrating Compounds. Biophys. J. 94, 2142-2149.

[36] Rusnati, M., Coltrini, D., Oreste, P., Zoppetti, G., Albini, A., Noonan, D., Fagagna, F., Giacca, M., and Prestai, M. (1997). Interaction of HIV-1 Tat Protein with Heparin. J Biol. Chem. 10, 11313-11320.

[37] Hakansson, S., Jacobs, A. and Caffrey, M. (2001). Heparin binding by the HIV-1 tat protein transduction domain. Protein Sci. 10, 2138-2139.

[38] Ziegler, A., Nervi, P., Durrenberger, M., and Seelig, J. (2005). The cationic cell-penetrating peptide CPP(TAT) derived from the HIV-1 protein TAT is rapidly transported into living fi broblasts: optical, biophysical and metabolic evidence. Biochem. 44, 138-148.

[39] Console, S., Marty, C., Garcia-Echeverria, C., Schwendener, R., and Ballmer-Hofer, K. (2003). Antennapedia and HIV Transactivator of Transcription (TAT) “Protein Transduction Domains” Promote Endocytosis of High Molecular Weight Cargo upon Binding to Cell Surface Glycosaminoglycans. J Biol. Chem. 278, 35109-35114.

[40] Sandgren, S., Cheng, F., and Belting, M. (2002). Nuclear targeting of macromolecular polyanions by an HIV-Tat derived peptide. Role for cell-surface proteoglycans. J Biol. Chem. 277, 38877-38883.

[41] Ferrari, A., Pellegrini, V., Arcangeli, C., Fittipaldi, A., Giacca, M., and Beltram, F. (2003). Caveolae-Mediated Internalization of Extracellular HIV-1 Tat Fusion Proteins Visualized in Real Time. Mol. Therapy 8, 284-294.

[42] Tyagi, M., Rusnati, M., Presta, M., and Giacca, M. (2001). Internalization of HIV-1 Tat Requires Cell Surface Heparan Sulfate Proteoglycans. J Biol. Chem. 276, 3254-3261.

[43] Khalil, I., Kogure, K., Akita, H., and Harashima, H. (2006). Uptake Pathways and Subsequent Intracellular Trafficking in Nonviral Gene Delivery. Pharma. Rev. 58, 32-45.

[44] Potocky, T., Menon, A., and Gellman, S. (2003). Cytoplasmic and Nuclear Delivery of a TAT-derived Peptide and a B-Peptide after Endocytic Uptake into HeLa Cells. J Biol. Chem. 278, 50188-50194.

[45] Jones, S., Christison, R., Bundell, K., Voyce, C., Brockbank, S., Newham, P., and Lindsay, M. (2005). Characterisation of cell-penetrating peptide-mediated peptide delivery. Brit. J. Pharma. 145, 1093-1102.

[46] Fittipaldi, A., Ferrari, A., Zoppe, M., Arcangeli, C., Pellegrini, V., Beltram, F., and Giacca, M. (2003). Cell Membrane Lipid Rafts Mediate Caveolar Endocytosis of HIV-1 Tat Fusion Proteins. J Biol. Chem. 278, 34141-34149.

[47] Säälik, P., Elmquist, A., Hansen, M., Padari, K., Saar, K., Viht, K., Langel, U., and Pooga, M. (2004). Protein Cargo Delivery Properties of Cell-Penetrating Peptides. A Comparative Study. Bioconjugate Chem. 15, 1246-1253.

[48] Kaplan, I.M., Wadia, J. S., and Dowdy, S. F. (2005). Cationic TAT peptide transduction domain enters cells by macropinocytosis. J Control. Release 102, 247-253.

[49] Zaro, J., Rajapaksa, T., Okamoto, C., and Shen, W. (2006). Membrane Transduction of Oligoarginine in HeLa Cells Is Not Mediated by Macropinocytosis. Mol. Pharm. 3, 181-186.

[50] Maiolo, J., Ferrer, M., and Ottinger, E. (2005). Effects of cargo molecules on the cellular uptake of arginine-rich cell-penetrating peptides. Biochim. Biophys. Acta 1712, 161-172.

[51] Ter-Avetisyan, G., Tunnemann, G., Nowak, D., Nitschke, M., Herrmann, A., Drab, M., & Cardoso, M. C. (2009). Cell Entry of Arginine-rich Peptides Is Independent of Endocytosis. J Biol. Chem. 284, 3370-3378.

[52] Iwasa, A., Akita, H., Khalil, I., Kogure, K., Futaki, S., and Harashima, H. (2006). Cellular uptake and subsequent intracellular trafficking of R8-liposomes introduced at low temperature. Biochim. Biophys. Acta 1758, 713-720.

[53] Fretz, M.M., Penning, N., Al-Taei, S., Futaki, S., Takeuchi, T., Nakase, I., Storm, G., and Jones, A. T. (2007). Temperature-, concentration- and cholesterol-dependent translocation of L- and D-octa-arginine across the plasma and nuclear membrane of CD34+ leukaemia cells. Biochem. J. 403, 335-342.

[54] Thoren, P., Persson, D., Lincoln, P., and Norden, B. (2005). Membrane destabilizing properties of cell-penetrating peptides. Biophys. Chem. 114, 169-179.

[55] Drin, G., Demene, H., Temsamani, J., and Brasseur, R. (2001). Translocation of the pAntp Peptide and Its Amphipathic Analogue AP-2AL. Biochem. 40, 1824-1834.

[56] Persson, D., Thoren, P., Herner, M., Lincoln, P., and Norden, B. (2003). Application of a Novel Analysis To Measure the Binding of the Membrane-Translocating Peptide Penetratin to Negatively Charged Liposomes. Biochem. 42, 421-429.

[57] Mishra, A., Gordon, V., Yang, L., Coridan, R., and Wong, G. (2008). HIV TAT Forms Pores in Membranes by Inducing Saddle-Splay Curvature: Potential Role of Bidentate Hydrogen Bonding. Angew. Chem. Intl. Ed. 47, 2986-2989.

[58] Thoren, P.E.G., Persson, D., Karlsson, M., and Norden, B. (2000). The Antennapedia peptide penetratin translocates across lipid bilayers - the first direct observation. FEBS Letters 482, 265-268.

[59] Jones, L., Yazzie, B., and Middaugh, C. (2004). Polyanions and the Proteome. Mol Cell Proteomics 3, 746-769.

[60] Ziegler, A., and Seelig, J. (2007). High Affinity of the Cell-Penetrating Peptide HIV-1 Tat-PTD for DNA. Biochem. 46, 8138-8145.

[61] Brooks, H., Lebleu, B., and Vives, E. . (2005). Tat peptide-mediated cellular delivery: back to basics. Adv. Drug Deliv. Rev. 57, 559.

[62] Manning, G.S. (1969). Limiting Laws and Counterion Condensation in Polyelectrolyte Solutions I. Colligative Properties. The Journal of Chemical Physics 51, 924-933.

[63] Zimm, B.H. and Le Bret, M. (1983). Counter-ion Condensation and System Dimensionality. J. Biomol. Struct. Dyn. 1, 461-471.

[64] Raedler, J.O., Koltover, I., Salditt, T., and Safinya, C. R. (1997). Structure of DNA-cationic liposome complexes: DNA intercalation in multilamellar membranes in distinct interhelical packing regimes. Science 275, 810-814.

[65] Koltover, I., Salditt, T., Raedler, J. O., and Safinya, C. R. (1998). An inverted hexagonal phase of cationic liposome-DNA complexes related to DNA release and delivery. Science 281, 78-81.

[66] Liang, H., Angelini, T., Ho, J., Braun, P., and Wong, G. (2003). Molecular imprinting of biomineralized CdS nanostructures: Crystallographic control using self-assembled DNA-membrane templates. J. Am. Chem. Soc. 125, 11786-11787.

[67] Wong, G., Tang, J., Lin, A., Li, Y., Janmey, P., and Safinya, C. (2000). Hierarchical self-assembly of F-Actin and cationic lipid complexes: Stacked three-layer tubule networks. Science 288, 2035-2039.

[68] Raviv, U., Needleman, D. J., Li, Y., Miller, H. P., Wilson, L., and Safinya, C. (2005). Cationic liposome-microtubule complexes: Pathways to the formation of two-state lipid-protein nanotubes with open or closed ends. Proc. Natl. Acad. Sci. 102, 11167-11172.

[69] Yang, L., Liang, H., Angelini, T., Butler, J., Coridan, R., Tang, J., and Wong, G. (2004). Self-assembled virus-membrane complexes. Nature Mater. 3, 615-619.

[70] Rädler, J.O., Koltover, I., Salditt, T. and Safinya, C.R. (1997). Structure of DNA-Cationic Liposome Complexes: DNA Intercalation in Multilamellar Membranes in Distinct Interhelical Packing Regimes Science 275, 810 - 814.

[71] Wong, G.C.L., Tang, J.X., Lin, A., Li, Y., Janmey, P.A. and Safinya, C.R. (2000). Hierarchical Self-Assembly of F-Actin and Cationic Lipid Complexes: Stacked Three-Layer Tubule Networks Science 288, 2035 - 2039.

[72] Als-Nielsen, J. and McMorrow, D. (2001) Elements of Modern X-ray Physics, John Wiley & Sons, Inc. New York.

[73] Warren, B.E. (1990) X-Ray Diffraction, Dover Publications. New York.

[74] Guinier, A. (1994) X-ray diffraction in crystals, imperfect crystals, and amorphous bodies, Dover. New York.

CHAPTER 3

HIV TAT PEPTIDE FORMS PORES IN MEMBRANES BY INDUCING SADDLE-SPLAY CURVATURE: POTENTIAL ROLE OF BIDENTATE HYDROGEN BONDING

3.1 Introduction

The TAT protein transduction domain (PTD) of the Human Immunodeficiency Virus (HIV-1) can cross cell membranes with unusual efficiency [1], and has many potential biotechnological applications [2-4]. Extant work has provided important clues to the molecular mechanism underlying the activity of this peptide, which consists of 11 amino acids, 8 of which are cationic, and 6 of these are arginines. TAT PTD synthesized with D-amino acids enter cells as efficiently as the native form [5], indicating that the mechanism of transduction is receptor-independent, consistent with recent results that suggest that the TAT PTD may enter cells through receptor-independent macropinocytosis [6]. Substituting any of the PTD's cationic residues with alanine decreases activity, while substitution of neutral residues has no effect [5]. This indicates the importance of electrostatic interactions between cationic TAT PTD and anionic phospholipid membranes. Recent work has shown that the physics of electrostatic interactions can drive a rich polymorphism of self-assembled structures that depend on parameters such as charge density [7,8] and intrinsic membrane curvature [9,10]. However, although arginine-rich polycations can enter cells, cationic polylysine cannot [11]. This shows that electrostatic interactions alone are insufficient for PTD activity and that arginine plays a specific, essential role.

In this chapter, we use confocal microscopy and synchrotron x-ray scattering (SAXS) to study the interaction of the TAT peptide with model membranes at room temperature. We find that the transduction activity correlates with induction of negative Gaussian ('saddle-splay') membrane curvature, which is topologically required for pore formation. Moreover, we show that the TAT peptide can drastically remodel vesicles into a porous bicontinuous phase with analogs in block copolymer systems [12-14], and propose a geometric mechanism facilitated by both electrostatics and bidentate hydrogen bonding. The latter is possible for the TAT peptide but not for similarly-cationic, non-arginated polypeptides.

3.2 Experimental section

3.2.1 Peptide synthesis

The TAT PTD (Tyr-Gly-Arg-Lys-Lys-Arg-Arg-Gln-Arg-Arg-Arg), Rh-TAT (Rhodamine-labeled TAT peptide) and $(Lys)_8$ are synthesized using automated solid-state synthesis.

3.2.2 SUV preparation

The lipids 1,2-Dioleoyl-sn-Glycero-3-[Phospho-L-Serine] (sodium salt) (DOPS), 1,2-Dioleoyl-*sn*-Glycero-3-Phosphocholine (DOPC), 1,2-Dioleoyl-*sn*-Glycero-3-Phosphoethanolamine (DOPE), and 1,2-Dioleoyl-*sn*-Glycero-3-[Phospho-*rac*-(1-glycerol)] (Sodium Salt) (DOPG) are purchased from Avanti Polar Lipids and used without further preparation. Stock solutions of lipids in chloroform are mixed at the desired ratios, dried under N_2 and desiccated under vacuum overnight. The dried lipids are rehydrated with Millipore water to a final concentration of 30 mg/ml at 37 °C

overnight. This solution is sonicated and extruded through a 0.2 μm Nucleopore filter to make liposomes. TAT PTD and $(Lys)_8$ are dissolved in millipore water at 10 mg/ml. Peptides and liposomes are mixed at different peptide-to-lipid molar ratios and salt conditions and subsequently sealed in quartz capillaries.

3.2.3 Synchrotron x-ray scattering

Small angle x-ray scattering (SAXS) data is collected at Stanford Synchrotron Radiation Laboratory (Palo Alto, CA) (BL4–2) and Advanced Photon Source (Argonne, IL, BESSRCAT BL-12ID) using 9-keV and 12-keV x-rays respectively. The scattered intensity is collected using a MAR-Research (Hamburg) charge-coupled device detector (pixel size 79 μm). All experiments are conducted at room temperature. We observe no evidence of radiation damage to the samples. Representative samples are re-measured after several months to ensure that they are fully equilibrated. Absolute electron densities in the unit cell reconstructions are calibrated by using standard measured values for typical head groups and terminal methyl groups.

3.2.4 GUV preparation

The lipids DOPS, DOPE, DOPC, 1-Palmitoyl-2-Oleoyl-*sn*-Glycero-3-Phosphocholine (POPC), and 1-Palmitoyl-2-Oleoyl-*sn*-Glycero-3-Phosphoethanolamine (POPE) are purchased from Avanti Polar Lipids and used without further purification. Lipids in chloroform solution are mixed in the following weight ratios: POPC:DOPS 80:20, DOPE:DOPC:DOPS 20:60:20 and 40:40:20, with the fluorescent membrane dye 2-(4,4-difluoro-5,7-dimethyl-4-bora-3a,4a-diaza-*s*-indacene-3-pentanoyl)-1-hexadecanoyl-*sn*-glycero-3-phosphocholine (BODIPY, purchased from Invitrogen)

incorporated at 0.5 mol%. These solutions are desiccated in a glass vial under vacuum overnight. The resulting film is hydrated with 100 mM NaCl solution containing 1%v/v glycerol to achieve a lipid concentration of 1 mg/mL, refrigerated overnight, and sonicated for 5-10 minutes. The resulting suspension is deposited in 5 μL drops on glass coverslips, dried for 1-2 hours, and rehydrated with 50 μL of 100 mM NaCl solution. Vesicles tens of microns in diameter form and adhere to the glass substrate.

3.2.5 Confocal microscopy

Leica inverted laser scanning confocal microscopes are used for all imaging. Laser lines of 488 nm and 514 nm, respectively, are used sequentially to excite the BODIPY membrane dye and the Rhodamine fluorophore of Rh-PTD, which is added to the sample in successive 1-10 μL drops of 1.4 mM concentration. All experiments are conducted at room temperature.

3.3 Results and discussion

Cell membranes are composed of lipids that have fundamentally different interactions with cationic macroions such as TAT peptide. We examine representative model membranes composed of lipids with different charge and intrinsic curvature: DOPC (1,2-Dioleoyl-*sn*-Glycero-3-Phosphocholine) and DOPE (1,2-Dioleoyl-*sn*-Glycero-3-Phosphoethanolamine) have zwitterionic headgroups while DOPS (1,2-Dioleoyl-*sn*-Glycero-3-[Phospho-L-Serine] (Sodium Salt)) and DOPG (1,2-Dioleoyl-*sn*-Glycero-3-[Phospho-*rac*-(1-glycerol)] (Sodium Salt)) have anionic headgroups. DOPS and DOPC lipids have zero intrinsic curvature ($C_0 = 0$, 'cylinder-shaped') while DOPE

has negative intrinsic curvature ($C_0 < 0$, 'cone-shaped') [15]. Varying the relative amounts of these lipids enables us to independently tune the charge density and intrinsic curvature of the model membrane.

We use confocal microscopy to examine interaction of TAT peptide with Giant Unilamellar Vesicles (GUVs, diameters 5-30 μm) with no endocytotic machinery. When Rhodamine-tagged TAT peptide (Rh-TAT) is applied to the exterior of GUVs with low DOPE content (0% and 20%), Rhodamine fluorescence is seen only outside the GUVs (Fig 3.1a), indicating that the Rh-TAT has not crossed these membranes. However, when Rh-TAT is applied to GUVs with 40% DOPE content, the Rhodamine intensity equilibrates across the membrane over tens of seconds (Fig 3.1b, c). This shows that Rh-TAT has crossed the GUV membranes, which remain intact (Fig 3.1c). Thus, we see that the membrane transduction activity of Rh-TAT requires the presence of a threshold amount of DOPE in the membrane.

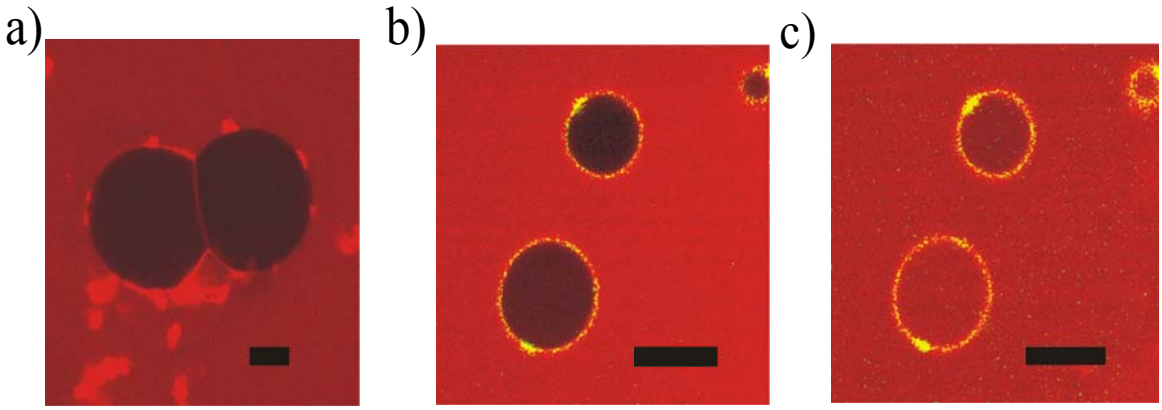


Figure 3.1: Rhodamine-tagged TAT peptide (false-color red) is applied to the exterior of GUVs of different lipid compositions, imaged using confocal microscopy. (**a)** Rh-TAT never enters PS:PC 20:80 membranes. (**b)** Less than 3 seconds after addition, Rh-TAT remains mostly exterior to BODIPY-tagged PS:PC:PE 20:40:40 membranes (false-color green).

Figure 3.1 cont.: (**c**) About 30 seconds later, the vesicle interior has the same brightness as the outside, showing that the Rh-TAT concentration has equilibrated on both sides of the membrane. 5 μm scale bars.

To elucidate the molecular interactions between the TAT peptide and such PE-rich membranes, we use synchrotron SAXS to study complexes formed by this peptide and DOPS:DOPE 20:80 membranes. Before exposure to TAT peptide, we see a broad form factor (Fig 3.2, bottom), as expected for Small Unilamellar Vesicles (SUVs, diameters 15-50 nm). After exposure to the PTD (at peptide:lipid molar ratio of P:L = 1:40), 9 new diffraction peaks are observed (Fig 3.2, middle). The peak positions in q show excellent agreement with those expected for a cubic 'double diamond' Pn3m phase with a lattice constant of a = 15.97 nm (Fig 3a). The same peaks are also observed (Fig 3.2, top) in the presence of HEPES buffer at pH 7.4, indicating that this reconstruction can occur at physiological conditions.

Before making the assignment of a cubic phase to the observed diffraction pattern, the possibility of phase coexistence was considered. This is especially important for cubic phases, from which different subsets of the diffraction peaks can be indexed to simpler phases. In the present case, one can generate a model diffraction pattern using a coexistence of a lamellar phase (q_1 = 1.11 nm^{-1}) and an inverted hexagonal phase (q_{10} =0.96 nm^{-1}), except that it misses the peaks at q = 0.54 nm^{-1} and 0.66 nm^{-1}. This would imply a three-phase coexistence for the present three-component system. Since we see essentially the same diffraction pattern for different peptide/lipid molar ratios, different PS:PE weight ratios, and different temperatures (three degrees of freedom), this

coexistence scheme would violate the Gibbs phase rule and hence, is not possible for a system at equilibrium.

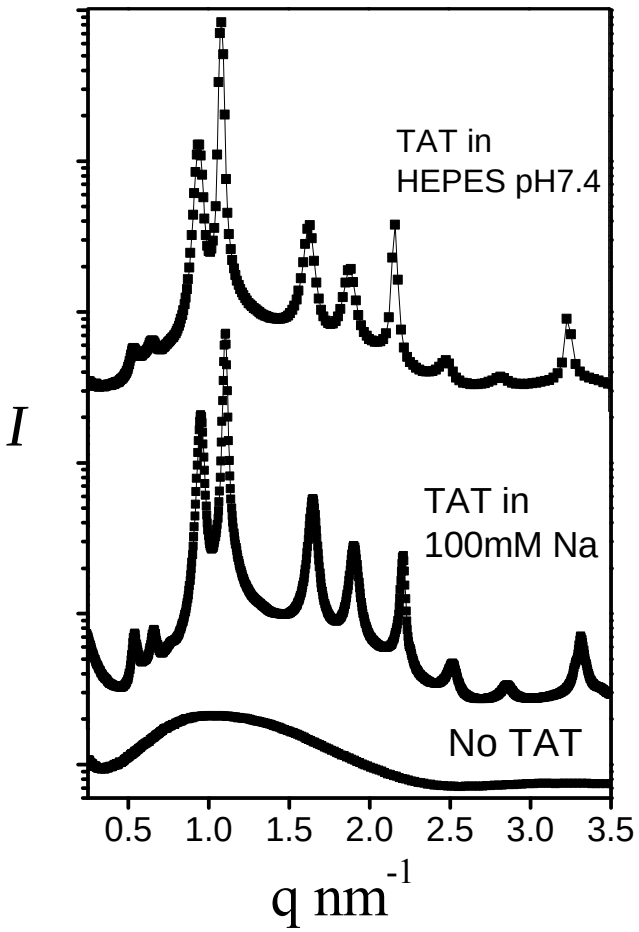


Figure 3.2: SAXS data show that PS:PE 20:80 vesicles (bottom) undergo a topological transformation when complexed with the TAT PTD, to form a cubic 'double-diamond' (Pn3m) phase with two non-intersecting networks of pores ~11 nm in diameter (middle). Addition of the TAT PTD in the presence of HEPES buffer at pH 7.4 results in the same cubic phase (top).

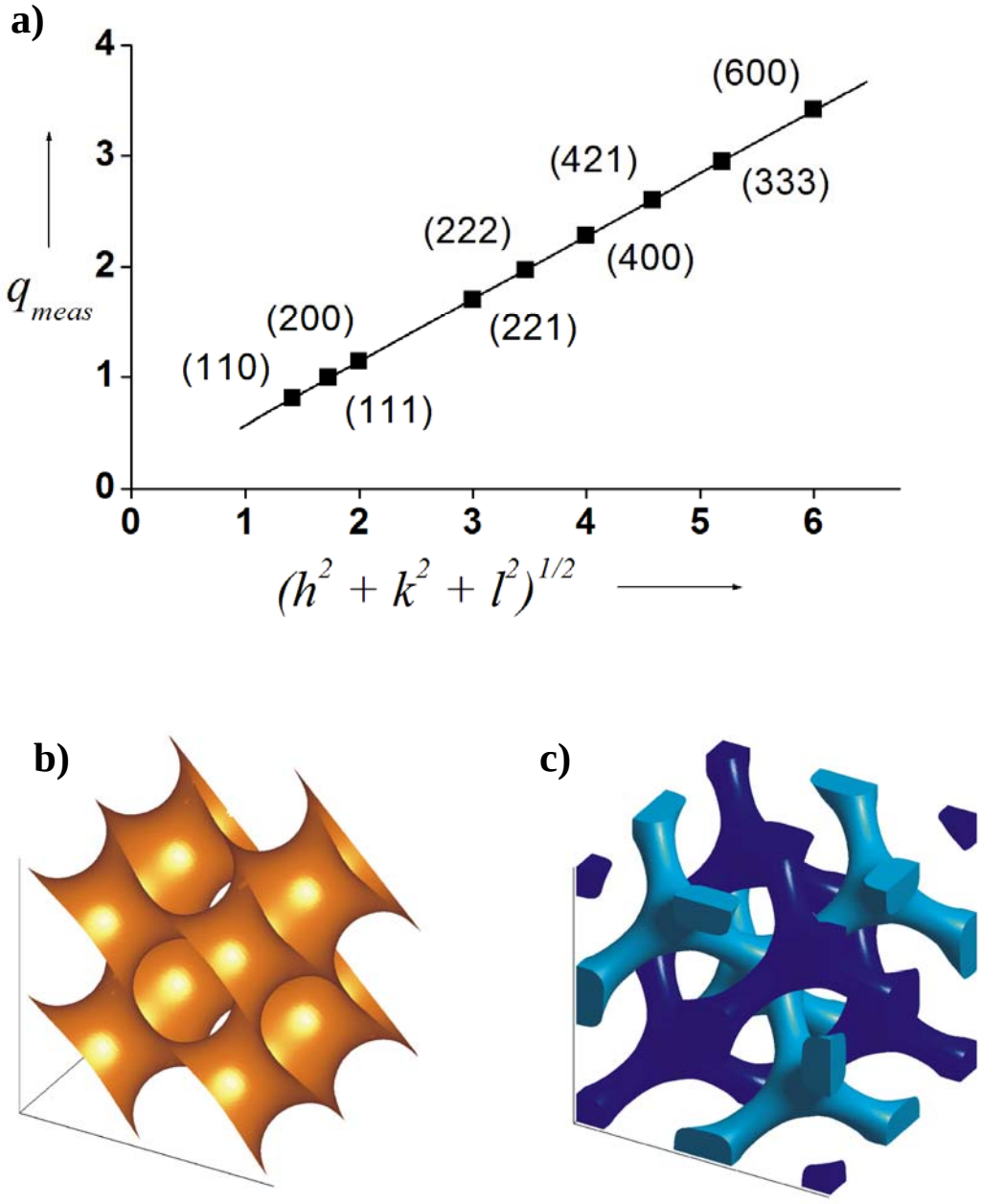


Figure 3.3: **(a)** The agreement between measured peak positions and the corresponding Pn3m cubic indexation, $q_{meas} = 2\pi\sqrt{(h^2+k^2+l^2)}/a$ (where h, k, and l are the Miller indices and a = 15.97 nm is the lattice parameter). Schematic representations of **(b)** the two non-intersecting networks of water pores (blue), and **(c)** the zero-mean-curvature surface at the midplane between the two membrane leaflets (brown).

The cubic Pn3m is a bicontinuous phase characterized by negative Gaussian curvature, threaded with tetrahedral networks of water pores (Fig 3.3b, c). Its presence indicates that the initial SUVs have undergone a drastic topological transformation [12,13]. The lattice constant indicates that the pores in these structures are ~11 nm in diameter. The effect of the TAT peptide on PE-rich membranes is the generation of negative Gaussian curvature, the type of curvature that characterizes the saddle-shaped surfaces inside holes of donuts [15].

Polylysine has the same charge as the TAT peptide but no transduction activity. In complexes formed with polylysine and DOPS:DOPE = 20:80 SUVs (peptide:lipid molar ratio 1:40), SAXS shows three diffraction peaks with peak positions at the 1: $\sqrt{3}$: 2 ratio characteristic of the inverted hexagonal phase (H_{II}) (Fig 3.4). This structural assignment is confirmed by an electron density profile of the unit cell (Fig 3.5a, b) reconstructed from x-ray data via Fourier synthesis. The phases used for the amplitudes at q_{10}, q_{11}, q_{20} are (+,-,-), in agreement with those from previous reconstructions on pure lipid H_{II} phases [16]. Regions of the lowest electron density (green-blue, ~0.169 e/Å^3) correspond to lipid hydrocarbon tails, which surround high-density, hexagonally-coordinated circular rims (red, ~0.410 e/Å^3) corresponding to phospholipid head groups. In turn, these surround intermediate-density channels of the H_{II} phase. For the pure PE H_{II} phase, an electron density of 0.337 e/A^3 is found in these holes, which corresponds well to the electron density of water (Fig 3.5c). For the polylysine-induced PS:PE=20:80 structure, the electron density in the corresponding region is ~0.286 e/A^3, which is consistent with a mixture of water and polypeptide (Fig 3.5b). The density profile shows unambiguously that the complex is in an inverted hexagonal H_{II} phase with the small (2.0 nm diameter)

water channels 'plugged' by polylysine, allowing the cationic polylysine to charge-compensate the anionic DOPS lipid heads. The x-ray experiments above show that the transduction activity of these peptides is correlated to their ability to induce negative Gaussian curvature.

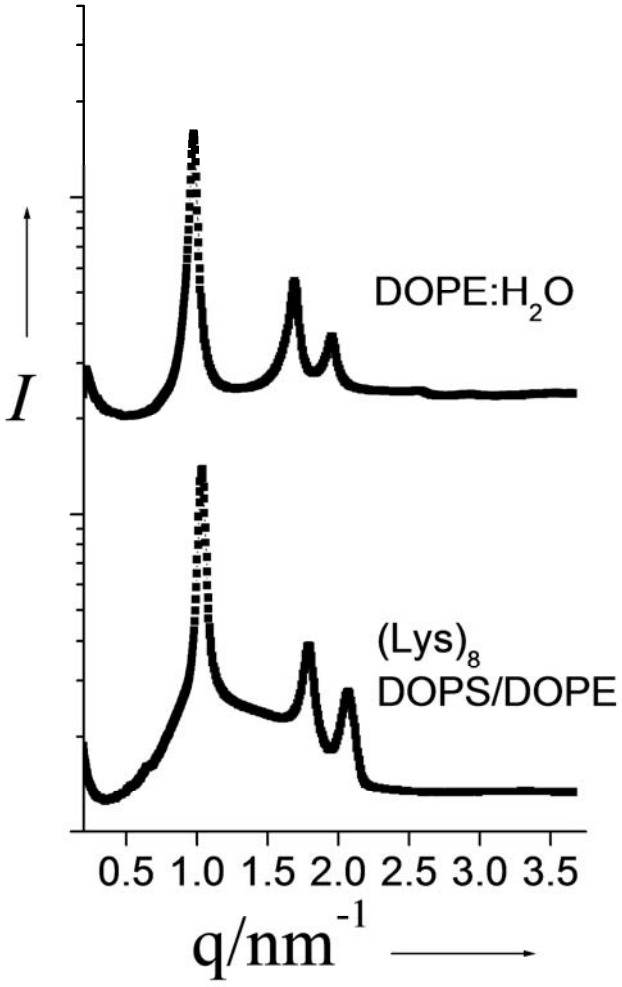


Figure 3.4: SAXS data for polylysine complexed with (bottom) PS:PE 20:80 and (top) PE membranes show peak positions that have the characteristic 1: √3 :2 ratio for an inverted hexagonal (H_{II}) phase.

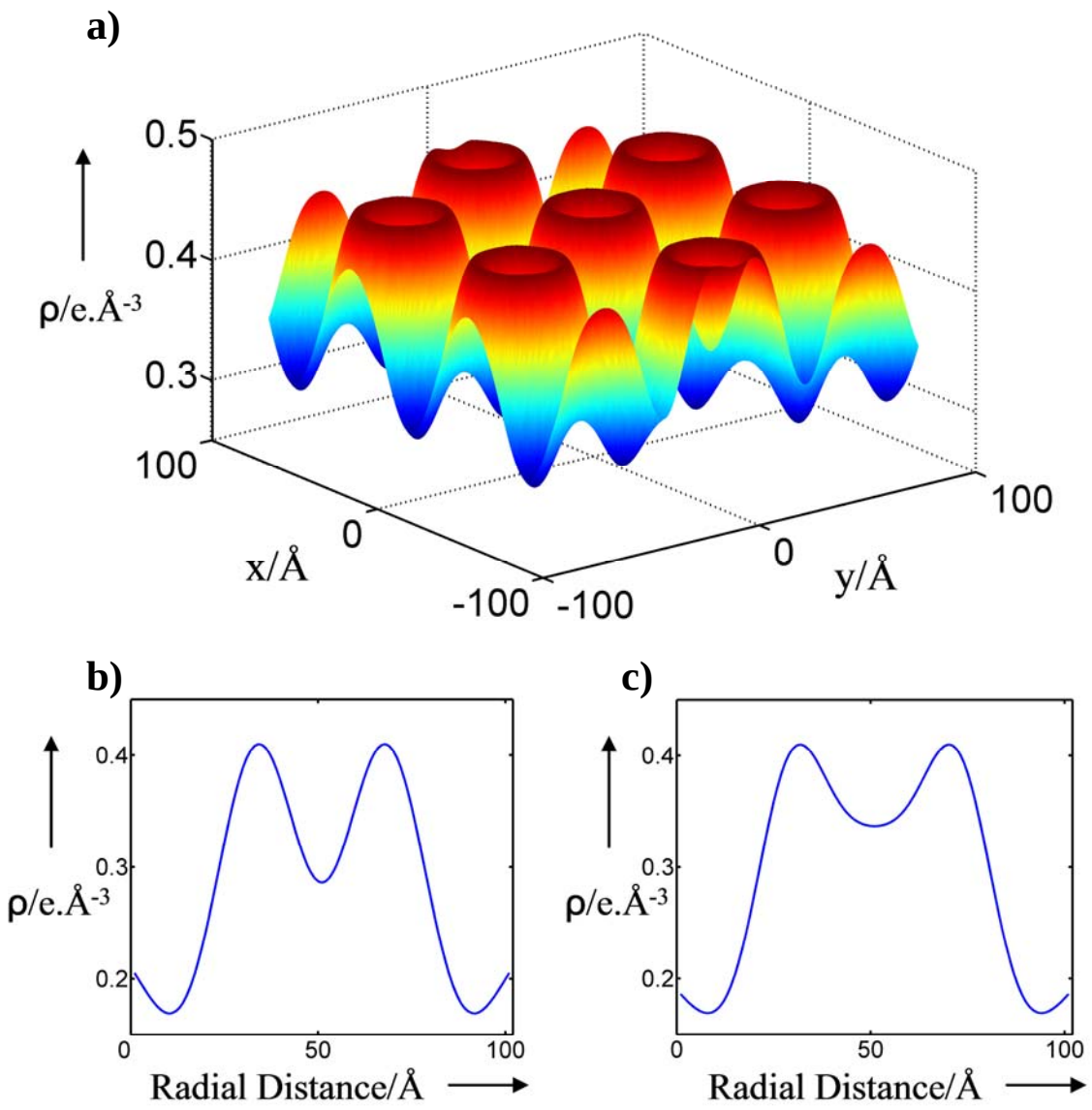


Figure 3.5: **(a)** Electron density reconstruction for polylysine complexed with PS:PE 20:80 membranes. Radial slices of such reconstructions show that the electron density (ρ) in the H_{II} channels formed when **(b)** polylysine is complexed with DOPS:DOPE 20:80 membranes is lower than that in **(c)** pure-DOPE H_{II} phase.

The TAT peptide exhibits a hierarchy of peptide-lipid interactions with different lipid species. The cationic peptide interacts strongly with localized negative charges in both anionic (DOPS) *and* neutral zwitterionic (DOPC) lipids, but does not interact directly with DOPE (Fig 3.6).

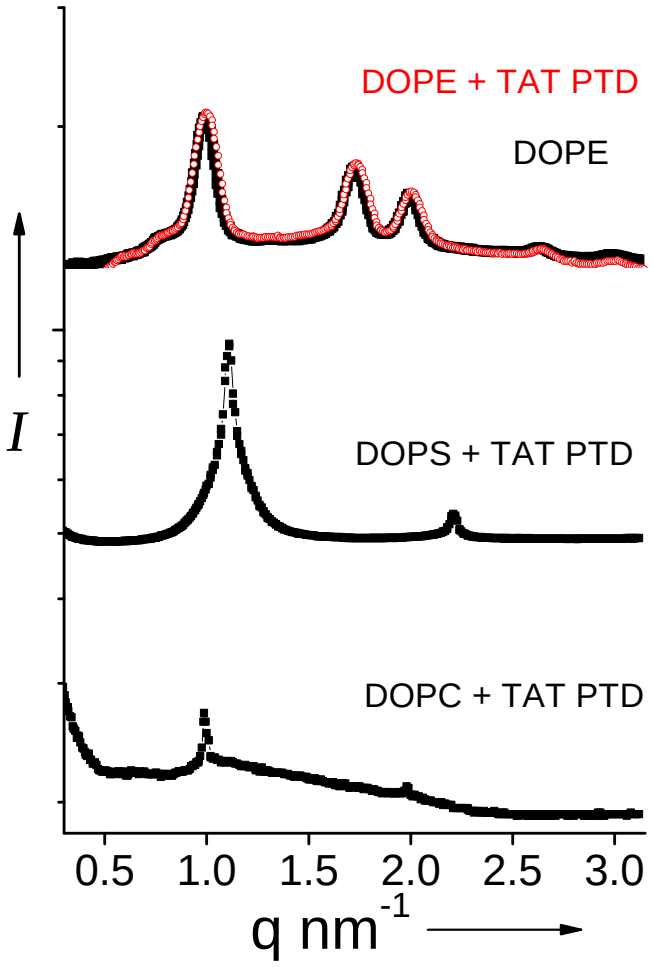


Figure 3.6: SAXS data show that the TAT PTD 'glues' together DOPS (middle) and DOPC (bottom) membranes into a lamellar phase with the PTD intercalated between the bilayers. The native inverted hexagonal diffraction pattern of DOPE (top, black) remains unchanged upon addition of TAT PTD (top, red). The two diffraction patterns can be superimposed.

To identify minimum conditions for Pn3m phase formation, we studied the DOPS:DOPE phase diagram as a function of increasing DOPS fraction and peptide:lipid (P:L) ratio. A single-phase Pn3m cubic appears at DOPS fractions of 20%-30%, which are typical fractions in eukaryotic membranes (Fig 3.7a). Moreover, this occurs for a wide range of P:L ratios. Clearly, DOPS *as well as* DOPE is necessary for the formation of the Pn3m cubic phase. We also systematically isolated the effects of membrane curvature by investigating tertiary DOPS:DOPE:DOPC membranes at different P:L ratios. We varied the DOPE:DOPC ratio while keeping the DOPS concentration constant at a typical eukaryotic value of 20%. This varies the intrinsic curvature without significantly changing the charge density. The resultant phase diagram (Fig 3.7b) shows that a high local concentration of DOPE (70-80%) is necessary for the cubic phase, which can be observed for a wide range of P:L ratios (1:20 to 1:80). For 70% DOPE, coexistence between the lamellar and cubic phases is observed. This is consistent with the observation that TAT peptide requires high DOPE fractions, and suggests that the TAT peptide can induce phase separation in order to organize the Pn3m phase.

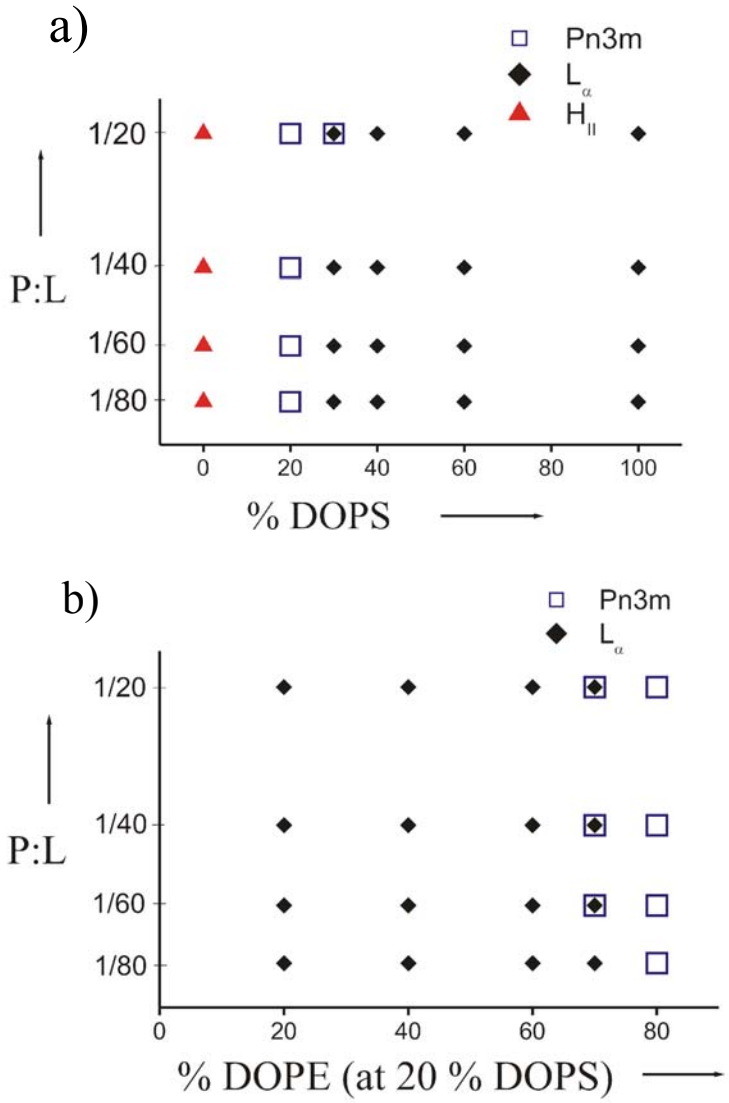


Figure 3.7: **(a)** Phase diagram of TAT-PTD with PS/PE membranes show that TAT-PTD cannot induce pure PE to form the Pn3m phase. PS and PE are both necessary for the Pn3m cubic phase. **(b)** An investigation of self-assembly between TAT PTD with tertiary PS/PE/PC membranes allow us to vary the intrinsic curvature independently of the charge density, and indicates that a high local concentration of negative curvature lipids such as PE (>70%) is necessary for the Pn3m cubic phase

We believe that these structural trends in TAT peptide toward pore formation, the hierarchy of interactions implicit in this trend, as well as the high transduction activity of TAT peptide, can be connected with a simple geometric mechanism. Negative Gaussian curvature is needed topologically to form pores. The TAT peptide is observed to generate negative Gaussian curvature, which indicates that it can simultaneously induce positive curvature along one principal direction and negative curvature in the other to make 'saddle-shaped deformations [15]. In contrast, polylysine only generates negative mean curvature by bending the membrane along one direction to make 'cylinder-shaped' deformations. These geometric observations, along with the importance of negative-curvature DOPE lipids for the TAT peptide's activity and the hierarchy of peptide-lipid interactions combine to suggest a possible molecular mechanism for transduction: Strong electrostatic interactions allow polylysine to generate negative curvature in mixtures of anionic and neutral lipids. This can be seen in the tendency for the membrane sheet to wrap the polypeptide in the direction perpendicular to the peptide axis (Fig 3.8a), creating an H_{II} phase. TAT peptide is mostly polyarginine; arginine is the most basic of all amino acids, because its side chain ends with a guanidinium group. Structurally guanidinium is characterized by a planar Y-shape which acts to delocalize its cationic charge. The result is a moiety with six potential hydrogen bonding sites. The multiple hydrogen bonding abilities as well as its unique shape allow a guanidinium group to direct both electrostatic and hydrogen bonding with anionic and polar molecules [17,18]. When arginine interacts with phospholipids this takes the form of bi-dentate hydrogen bonding from simultaneous association with the phosphates of two lipid head groups (Fig 3.8b). Lysine, in contrast, has an amino group which only forms monodentate hydrogen bonds and

therefore interacts with the phosphate on a single lipid head group. We speculate that because of this, arginine groups are more efficient than lysine groups in crosslinking bulky headgroups of DOPS and DOPC phospholipids. This generates positive curvature along the peptide chain's contour length in addition to negative curvature perpendicular to it, thereby creating negative Gaussian curvature (Fig 3.8c). This generation of negative gaussian curvature is manifested in the TAT peptide induced cubic Pn3m phase. The preferential interaction of the TAT peptide with non-PE lipids suggests that these tendencies may be reinforced via local lipid segregation: Repartitioning of DOPE away from the peptide can concentrate negative curvature perpendicular to the peptide axis, as well as enrich the DOPE content of the inner membrane leaflet not in contact with TAT peptide, thereby increasing positive curvature along the peptide axis.

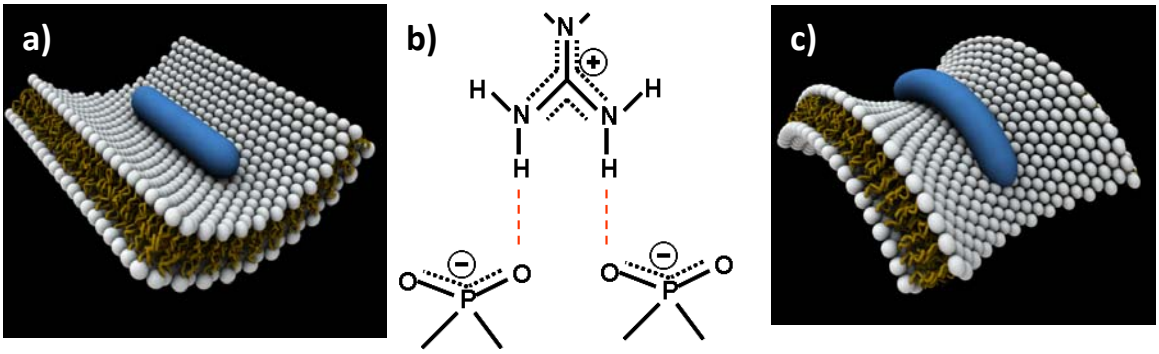


Figure 3.8: Schematic showing the mechanism by which TAT peptide generates negative Gaussian curvature. **(a)** Strong electrostatic attraction induces the membrane sheet to wrap the polypeptide and generate negative curvature in the direction perpendicular to the peptide axis. **(b)** The guanindinium group on the arginine forms bi-dentate hydrogen bonds with the phosphates of two lipid head groups. **(c)** Arginines in TAT peptide efficiently crosslink bulky phospholipid headgroups. This generates positive curvature along the peptide chain's contour length in addition to negative curvature perpendicular to it, thereby creating negative Gaussian curvature

3.4 Summary

The TAT protein of the HIV virus can cross cell membranes with remarkable efficiency. Its 11-amino acid protein transduction domain has been shown to deliver everything from nucleic acids to proteins to nanoparticles. Despite the great potential of TAT peptide as carrier of proteins, nucleic acids, and other bioactive compounds, the precise mechanism of its internalization is not known. Ionic interactions between the highly cationic TAT peptide and the anionic cell membrane and other anionic molecules on the cell surface are believed to be the initial step in the internalization process. We examined the interactions of TAT peptide with prototypical cell membranes using confocal microscopy and synchrotron small angle x-ray scattering (SAXS) and study the effect of membrane charge and intrinsic curvature. We find that the transduction activity correlates with induction of negative Gaussian (‘saddle-splay’) membrane curvature, which is topologically required for pore formation. TAT drastically remodels vesicles into a porous ‘sponge-like’ bicontinuous manifold. This ‘double-diamond’ structure has two non-intersecting tetrahedral networks of 6nm-diameter water pores that can facilitate the direct translocation of most proteins-sized objects, as well as serve as an intermediate state for higher order processes such as receptor-independent forms of endocytosis. By applying ideas from coordination chemistry chemistry, soft condensed matter physics and differential geometry, we propose a geometric mechanism facilitated by both electrostatics and bidentate hydrogen bonding.

3.5 References

[1] Wadia, J.S., & Dowdy, S. F. (2005). Transmembrane delivery of protein and peptide drugs by TAT-mediated transduction in the treatment of cancer. Advanced Drug Delivery Reviews 57, 579-596.

[2] Lewin, M., Carlesso, N., Tung, C. -H., Tang, X. -W., Cory, D., Scadden, D. T., & Weissleder, R. (2000). Tat peptide-derivatized magnetic nanoparticles allow in vivo tracking and recovery of progenitor cells. Nature Biotechnology 18, 410-414.

[3] Schwarze, S.R., Ho, A., Vocero-Akbani, A. & Dowdy, S. F. . (1999). In Vivo Protein Transduction: Delivery of a Biologically Active Protein into the Mouse. Science 285, 1569-1572.

[4] Holowka, E.P., Sun, V. Z., Kamei, D. T. & Deming, T. J. . (2007). Polyarginine segments in block copolypeptides drive both vesicular assembly and intracellular delivery. Nature Materials 6, 52-57.

[5] Wender, P.A., Mitchell, D. J., Pattabiraman, K., Pelkey, E. T., Steinman, L., & Rothbard, J. B. (2000). The design, synthesis, and evaluation of molecules that enable or enhance cellular uptake: Peptoid molecular transporters. Proc. Natl. Acad. Sci. 97, 13003-13008.

[6] Wadia, J.S., Stan, R. V. & Dowdy, S. F. . (2004). Transducible TAT-HA fusogenic peptide enhances escape of TAT-fusion proteins after lipid raft macropinocytosis. Nature Medicine 10, 310-315.

[7] Wong, G.C.L., Tang, J. X., Lin, A., Li, Y., Janmey, P. A., & Safinya, C. R. (2000). Hierarchical Self-Assembly of F-Actin and Cationic Lipid Complexes: Stacked Three-Layer Tubule Networks. Science 288, 2035-2039.

[8] Yang, L., Liang, H., Angelini, T. E., Butler, J., Coridan, R., Tang, J. X., & Wong, G. C. L. (2004). Self-assembled virus–membrane complexes. Nature Materials 3, 615-619.

[9] Koltover, I., Salditt, T., Raedler, J. O. & Safinya, C. R. . (1998). An Inverted Hexagonal Phase of Cationic Liposome–DNA Complexes Related to DNA Release and Delivery. Science 281, 78-81.

[10] Raviv, U., Needleman, D. J., Li, Y., Miller, H. P., Wilson, L., & Safinya, C. R. (2005). Cationic liposome–microtubule complexes: Pathways to the formation of two-state lipid–protein nanotubes with open or closed ends. Proc. Natl. Acad. Sci. 102, 11167-11172.

[11] Mitchell, D.J., Kim, D. T., Steinman, L., Fathman, C. G., and Rothbard, J. B. (2000). Polyarginine enters cells more efficiently than other polycationic homopolymers. J Peptide Research 56, 318-325.

[12] Thomas, E.L., Alward, D. B., Kinning, D. J., & Martin, D. C. (1986). Ordered Bicontinuous Double-Diamond Structure of Star Block Copolymers: A New Equilibrium Microdomain Morphology. Macromolecules 19, 2197-2202.

[13] So, P.T.C., Gruner, S. M. & Erramilli, S. (1993). Pressure-induced topological phase transitions in membranes. Phys. Rev. Lett. 70, 3455-3458.

[14] Garstecki, P., & Holyst, R. (2001). Periodic surfaces of simple and complex topology: Comparison of scattering patterns. Phys. Rev. E 64, 021501.

[15] Ben-Shaul, A., & Gelbart, W. M. (1994) Statistical Thermodynamics of Amphiphilic Self-Assembly: Structure and Phase Transition in Micellar Solutions. In Micelles, Membranes, Microemulsions and Monolayers (Gelbart, W.M., Ben-Shaul, A. & Roux, D., ed.^eds). Springer, New York.

[16] Turner, D.C., & Gruner, S. M. (1992). X-ray Diffraction Reconstruction of the Inverted Hexagonal (HII) Phase in Lipid- Water Systems. Biochemistry 31, 1340-1355.

[17] Rothbard, J.B., Jessop, T. C. & Wender, P. A. . (2005). Adaptive translocation: the role of hydrogen bonding and membrane potential in the uptake of guanidinium-rich transporters into cells. Advanced Drug Delivery Reviews 57, 495-504.

[18] Schug, K.A., Linder, W. (2005). Noncovalent binding between guanidinium and anionic groups: Focus on biological- and synthetic-based arginine/guanidinium interactions with phosph[on]ate and sulf[on]ate residues. Chemical Review 105, 67-113.

CHAPTER 4

MECHANISM FOR CELLULAR UPTAKE OF ARGININE RICH CELL-PENETRATING PEPTIDES

4.1 Introduction

Arginine rich cell-penetrating peptides have proven to be effective carriers for intracellular delivery of therapeutic molecules. These peptides are usually short (< 20 amino acids) and are highly positively charged. Examples include the TAT peptide from the HIV transactivator protein TAT, penetratin, a 16 amino acid domain from the Antennapedia protein of *Drosophila*, a flock house virus (FHV) coat peptide (sequence 35-49), and oligoarginines [1-3]. The guanidinium headgroup of arginine is the central structural feature required for peptide uptake. The importance of the guanidinium group comes from the fact that it is able to form bidentate hydrogen bonds with the phosphate groups on phospholipids [4-6]. A number of guanidinium based synthetic analogs have been developed to enhance therapeutic applications. Examples include guanidinium-rich oligocarbamates, carbohydrate-based polymers like the guanidinylated neomycin, polyguanidino dendrimers based on diamino acid monomeric units, and oligoarginine peptoids with side chains attached to nitrogen instead of carbon. Such analogs have proven to be more effective at entering cells than natural peptides [7-10].

The exact molecular mechanism of cellular entry of arginine-rich cell penetrating peptides is currently not fully understood. The length of the peptide is an important factor with the optimum number of arginine residues between 6 and 15. Peptides with more

than 15 arginine residues can still enter cells but with significantly less efficiency [7,11,12]. Although initial studies indicated a direct translocation mechanism, it was proven to be an artifact of cell fixation [13]. A number of different endocytosis mechanisms have been proposed including heparin sulfate-mediated endocytosis, clatharin-mediated endocytosis and receptor-independent macropinocytosis [13-18]. Also, studies on live, non-fixed cells have indicated the presence of an additional non-endocytotic mechanism of cellular uptake [19-21].

The debate on the mechanism of arginine rich cell-penetrating peptides, has often been characterized by a type of 'either/or' discourse, such as whether direct translocation or some specific form of endocytosis is most relevant. Since the cellular uptake of arginine-rich peptides is dependent on a variety of factors, including temperature, incubation time, cell type, cargo type and size, linkage type and size, comparison between different experiments have been difficult, and has compounded the controversy surrounding the uptake mechanism [1,22]. It has no doubt been recognized that more than one mechanism may be involved in translocation activity. This recognition accommodates the broad range of proposed hypotheses, and can potentially conclude the discourse with an artificial consensus. However, an acknowledgement of multiple mechanisms of entry does not explain the central phenomenon: How does a relatively simple molecule like TAT peptide facilitates mechanisms as different as direct entry and the multiple endocytotic mechanisms? Rather than debate the differences between the distinct observed mechanisms, we focus on what these different mechanisms have in common, and relate these common features to what the physical chemistry of cell penetrating peptides allows them to do.

4.2 Experimental section

4.2.1 Peptide synthesis

The TAT PTD (Tyr-Gly-Arg-Lys-Lys-Arg-Arg-Gln-Arg-Arg-Arg), RPEG-3 (Arg-Arg-Arg-Arg-$(PEG)_3$-Arg-Arg-Arg-Arg), RPEG-5 (Arg-Arg-Arg-Arg-$(PEG)_5$-Arg-Arg-Arg-Arg) and RPEG-27 (Arg-Arg-Arg-Arg-$(PEG)_{27}$-Arg-Arg-Arg-Arg) are synthesized using automated solid-state synthesis. R_9 ($(Arg)_9$) and FITC-labeled TAT are purchased from Anaspec, Inc. R_{34}, R_{46} and R_{60} are provided by Prof. Tim Deming's lab at UCLA.

4.2.2 SUV preparation

The lipids 1,2-Dioleoyl-sn-Glycero-3-[Phospho-L-Serine] (sodium salt) (DOPS), 1,2-Dioleoyl-*sn*-Glycero-3-Phosphocholine (DOPC), 1,2-Dioleoyl-*sn*-Glycero-3-Phosphoethanolamine (DOPE), and 1,2-Dioleoyl-*sn*-Glycero-3-[Phospho-*rac*-(1-glycerol)] (Sodium Salt) (DOPG) are purchased from Avanti Polar Lipids and used without further preparation. Stock solutions of lipids in chloroform are mixed at the desired ratios, dried under N_2 and desiccated under vacuum overnight. The dried lipids are rehydrated with Millipore water to a final concentration of 30 mg/ml at 37 °C overnight. This solution is sonicated and extruded through a 0.2 μm Nucleopore filter to make liposomes. TAT PTD and $(Lys)_8$ are dissolved in millipore water at 10 mg/ml. Peptides and liposomes are mixed at different peptide-to-lipid molar ratios and salt conditions and subsequently sealed in quartz capillaries.

4.2.3 Synchrotron x-ray scattering

Small angle x-ray scattering (SAXS) data is collected at Stanford Synchrotron Radiation Laboratory (Palo Alto, CA) (BL4–2) and Advanced Photon Source (Argonne, IL, BESSRCAT BL-12ID) using 9-keV and 12-keV x-rays respectively. The scattered intensity is collected using a MAR-Research (Hamburg) charge-coupled device detector (pixel size 79 μm). All experiments are conducted at room temperature. We observe no evidence of radiation damage to the samples. Representative samples are re-measured after several months to ensure that they are fully equilibrated. Absolute electron densities in the unit cell reconstructions are calibrated by using standard measured values for typical head groups and terminal methyl groups.

4.2.4 GUV preparation

Giant unilamellar vesicles (GUVs) are prepared using the electroformation process. The chamber is prepared by sealing two ITO-coated microscopic glass slides with a U-shaped Teflon spacer (~ 0.5 mm thick) in between. This gives a chamber volume of about 300 μl. The lipids DOPS, DOPE, DOPC and PEG2k-PE (1,2-dioleoyl-*sn*-glycero-3-phosphoethanolamine-N-[methoxy(polyethylene glycol)-2000]) are purchased from Avanti Polar Lipids and used without further purification. Lipids in chloroform solution are mixed in the following weight ratio: DOPE:DOPC:DOPS 50:30:20 with 2% PEG2k-PE, 5% A23187 (Calcium Ionophore, purchased from Sigma) and 3% fluorescent membrane dye DiO (3,3'-dioctadecyloxacarbocyanine perchlorate, purchased from Invitrogen). Approximately 15 μl of these solutions is spread onto one of the ITO-coated slides and desiccated under vacuum overnight. The swelling solution

contains G-actin, prepared from a lyophilized powder of rabbit skeletal muscle purchased from Cytoskeleton (Denver), in 2 mM citric acid, 10 mM Tris, 100 mM Sucrose (pH = 8). Rhodamine phalloidin (Rh-phalloidin, purchased from Cytoskeleton) is used to stain actin. The electroformation chamber is connected to a function generator and subjected to the following cycle:

10 Hz sine wave: - 5 min, 0.11 Vpp

- 20 min, 0.93 Vpp

- 70 min, 2.3 Vpp

4 Hz square wave: - 70 min, 2.3 Vpp

Vesicles tens of microns in diameter form and are diluted in 2 mM citric acid, 10 mM Tris, 160 mM glucose (pH = 8).

4.2.5 Confocal microscopy

Leica inverted laser scanning confocal microscopes are used for all imaging. Laser lines of 488 nm and 514 nm, respectively, are used sequentially to excite the DiO membrane dye and the Rhodamine fluorophore of Rh-phalloidin labeled actin. All experiments are conducted at room temperature.

4.3 Results and discussion

4.3.1 Arginine-rich cell-penetrating peptides induce negative gaussian curvature

We have seen that the TAT peptide induces negative Gaussian curvature and its membrane transduction activity is related to the ability to generate such curvature [6]. We also examined two other naturally occurring arginine-rich cell-penetrating peptides Antp and pVEC [23]. When these peptides are added to 20:80 DOPS:DOPE small unilamellar vesicles, the diffraction pattern changes drastically from the initial broad form factor (Fig 4.1a). The new peaks observed for both Antp and pVEC can be indexed to the same Pn3m cubic phase induced by TAT peptide. The lattice constant of the cubic phase induced by Antp and pVEC is 15.9 nm and 16.9 nm, respectively. These results suggest that the ability to generate negative Gaussian curvature is general for arginine-rich cell penetrating peptide.

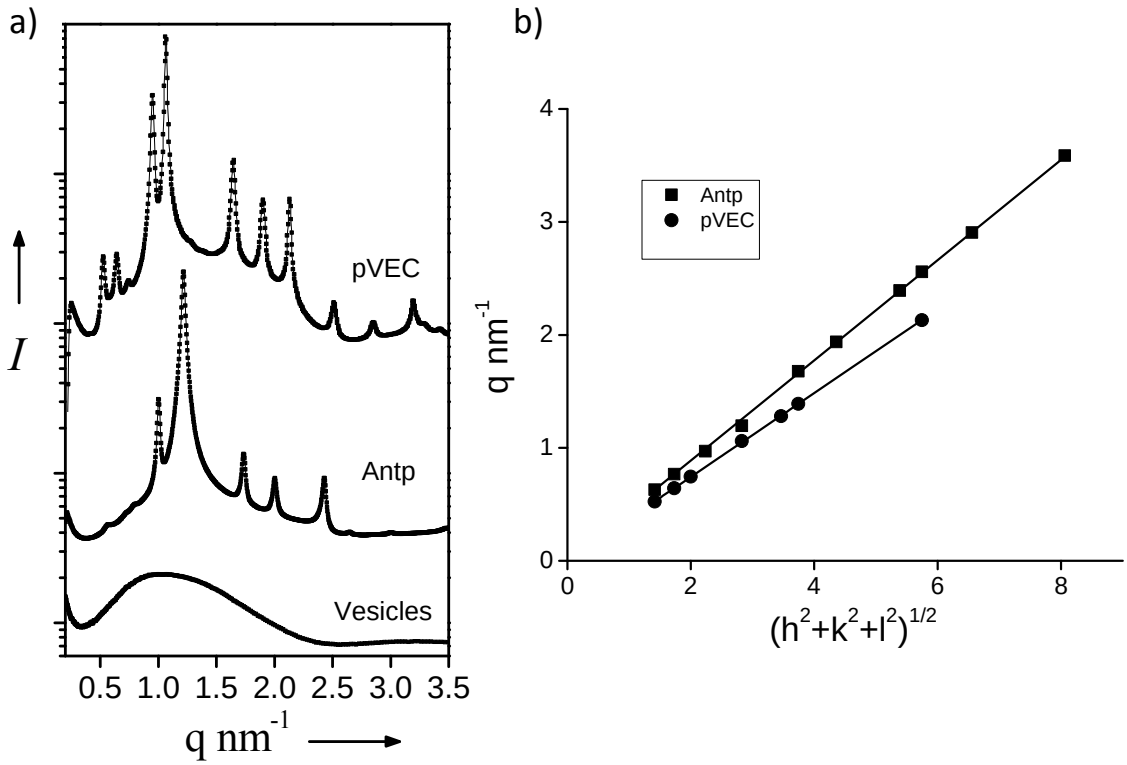


Figure 4.1: **(a)** SAXS data show that when PS:PE 20:80 vesicles (bottom) are complexed with Antp (middle) or pVEC (top), undergo topological transformation and form the cubic Pn3m phase. **(b)** The cubic indexation shows that the lattice constants are 15.9nm and 16.9nm for Antp and pVEC, respectively.

It is known that the number of arginine residues in polyarginine is important for its transduction ability. Polyarginines with less than 5 arginine residues are unable to enter cells; while peptides with more than 15 arginine residues can enter cells but with significantly less efficiency [11]. We incubated HeLa cells with fluorescently labeled peptides with 4, 9, 34, 46 and 60 arginine residues. The longer polyarginines, R34, R46 and R60, were toxic to cells at the experimental conditions (12.5 μM for 15 minutes) that worked well for the shorter peptides. Decreasing the concentration and incubation times made the cells more viable with the longer peptides. The cells were analyzed with

confocal microscopy after incubation. Confocal images show that cells incubated with R4 do not have detectable fluorescence inside them (Fig 4.2a). Cells incubated with R9 demonstrated high fluorescence intensity indicating efficient translocation (Fig 4.2c). The longer peptides, R34, R46 and R60, were also able to enter cells; however, the fluorescence associated with the cells was less intense compared to R9 (Fig 4.2d, e, f). These results are consistent with previous observations [7,11,12].

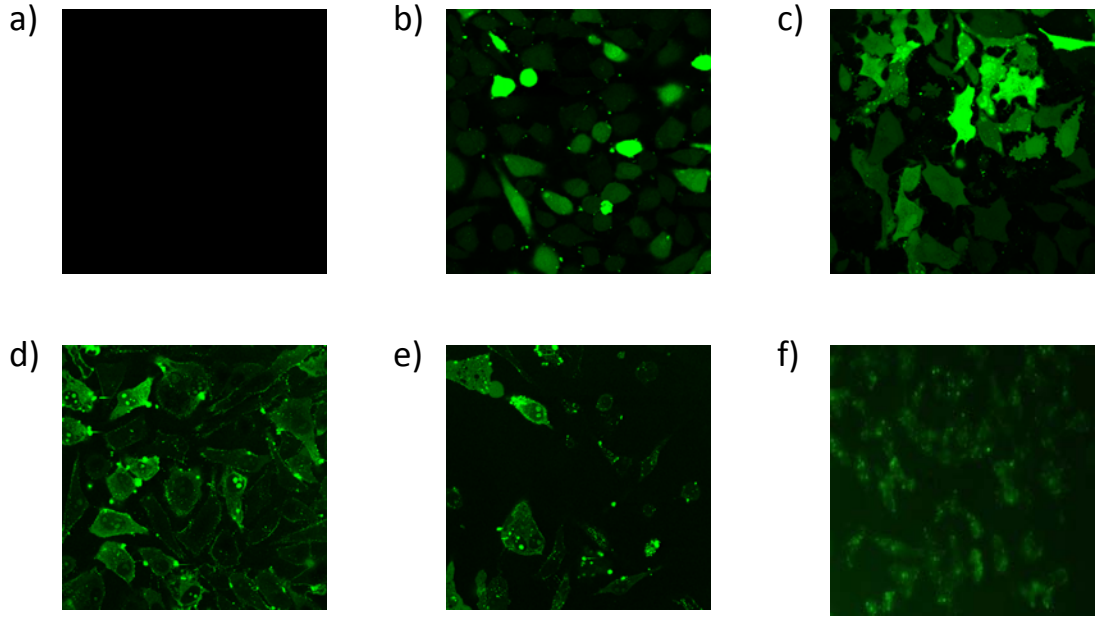


Figure 4.2: Confocal microscopy analysis of HeLa cells incubated with (a) R_4, (b) TAT peptide, (c) R_9, (d) R_{34}, (e) R_{46}, and (f) R_{60}. The images show that R_4 is unable to enter cells. TAT peptide and R_9 enter cells efficiently. The longer peptides, R_{34}, R_{46} and R_{60}, are also able to enter cells but not as efficiently as TAT peptide or R_9.

We studied the interaction of the polyarginines with model membranes using SAXS. The diffraction results show that R_4 with 20:80 DOPS:DOPE forms an inverted hexagonal phase with a coexisting lamellar phase (4.3a). The lattice constant of the

inverted hexagonal phase is 7.7 nm, with the pore size of ~3 nm. These results indicate that R_4, like polylysine, generates negative mean curvature rather the negative Gaussian curvature. On the other hand, R_9 induces negative Gaussian curvature. It forms the cubic Pn3m phase with the 20:80 DOPS:DOPE model membranes. It exhibits a similar phase behavior as the TAT peptide [6]. The longer arginine polymers, R_{34}, R_{46} and R_{60}, are also able to induce the Pn3m cubic phase but only over a much narrower range of peptide to lipid molar ratios (P/L) as compared to R_9 or TAT peptide. The lattice parameter of the induced Pn3m cubic phase increases as the number of arginine residues increases (Fig 4.3b). These results suggest that the ability of a peptide to generate negative Gaussian curvature may be used as an indicator for its transduction activity.

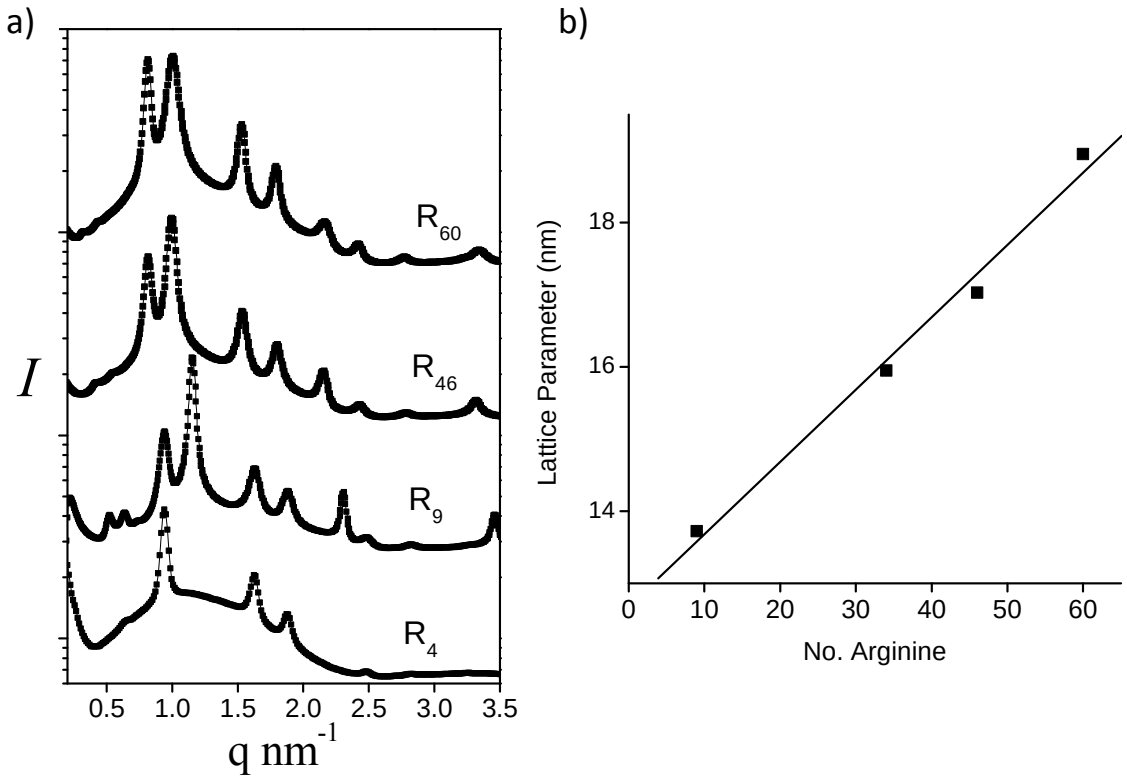


Figure 4.3: **(a)** SAXS data show that R_4 induces an inverted hexagonal phase with 20:80 PS:PE vesicles (bottom). The longer polyarginines form the cubic Pn3m phase. **(b)** The lattice parameter of the induced cubic phases increases with increasing number of arginine residues.

Arginine-rich cell penetrating peptides that are found in nature do not necessarily have all their arginine residues contiguous. Peptides such as penetratin or pVEC, have other amino acids separating the arginine rich domains. We use peptides with two R_4 domains separated by different lengths of polyethylene glycol (PEG) spacers to understand the effect of separation distance on transduction activity. The peptides used were RPEG-5, which has the R_4 domains separated by 5 monomers of PEG, and RPEG-27, where the R_4 domains are separated by 27 monomers of PEG. The separation distance

between the R_4 domains in these peptides is 1.5 nm for RPEG-5, and 4.6 nm for RPEG-27. The synchrotron diffraction results for the interaction of these peptides with 20:80 DOPE:DOPE model membranes is shown in fig 4.4. The results show that RPEG-27, which has the R_4 domains separated by the largest distance, forms an inverted hexagonal phase with a coexisting lamellar phase. The lattice constant of the inverted hexagonal phase is similar to that induced by R_4 only. The difference in the lamellar spacing in the RPEG-27 induced phase and the lamellar spacing in the R_4 only lamellar phase is similar to the size of the PEG spacer. These results indicate that RPEG-27 essentially acts as unconnected R_4 peptides, with the PEG spacer only swelling the membranes in lamellar phase. On the other hand, the peptide with the smaller PEG spacers, RPEG-5, induces the cubic Pn3m phase with 20:80 DOPS:DOPE. The diffraction peaks and the indexing for the two peptides are shown in fig. The lattice constant of the Pn3m phase for RPEG-5 is 16.2 nm.

The above results show that peptides with the arginine rich domains separated by a PEG spacer approximately the size of amino acids (on the order of 1 nm), behave as a single long polyarginine molecule. However, peptides which have the arginine rich domains separated by PEG spacers about the thickness of the lipid bilayers (~ 4.5 nm) behave as independent short arginine peptides.

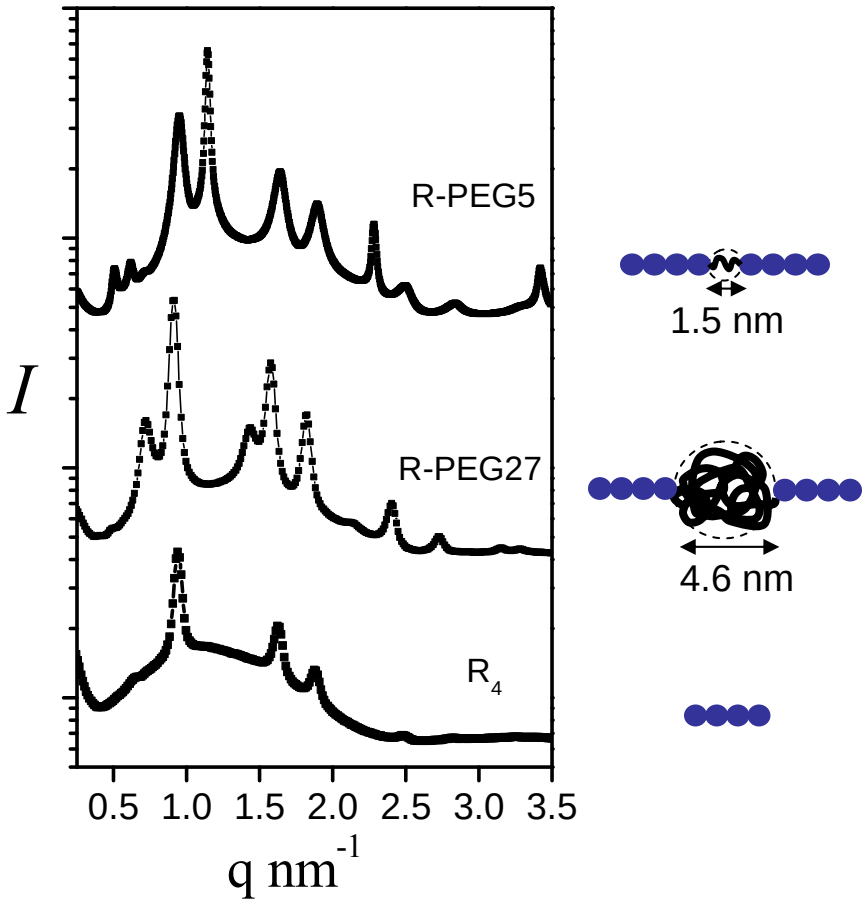


Figure 4.4: SAXS data for peptides with two R_4 domains separated by PEG spacers. R-PEG27 forms coexisting lamellar and inverted hexagonal phases while R-PEG5 induces the cubic Pn3m phase. Schematics of the peptides shown on the right.

4.3.2 Significance of gaussian membrane curvature for pore formation and other cellular processes

The formation of a pore in a membrane requires the generation of negative Gaussian curvature ($K<0$). The Gaussian Curvature, K, at a point on the membrane is the product of the two principle axes of curvature at that point. Therefore, $K<0$ implies the principle axes of curvature at a given point must curve in opposite directions, so that the membrane is locally shaped like a saddle (fig 4.5a). This is the type of curvature seen objects with holes, for example a torus: the 'hole' of the torus is composed of regions with saddle-shaped curvature. In contrast, objects such as spheres have no holes, and have $K>0$ everywhere on their surface (fig 4.5b).

In a more general compass, it can be seen that negative Gaussian curvature is broadly enabling. While negative Gaussian curvature is topologically necessary for pore formation it can be seen in other processes. From fig 4.5, it can be seen that generation of negative Gaussian membrane curvature is a necessary condition for the dimples for caveoli-based endocytosis, for the cytoskeleton-driven protrusions in macropinocytosis, as well as for pore formation. The Gauss-Bonnet theorem shows that if pores do not form, the net change in the global Gaussian curvature of the membrane is zero, i.e. $\Delta\int K \cdot dA = 0$: If one region of the membrane develops positive Gaussian curvature then some other region will develop negative Gaussian curvature to exactly compensate for the distortion. Examples of this balance of curvatures constrained by topology can be seen in proposed types of TAT entry mechanisms. The invaginations in a cell's plasma membrane surface during endocytosis display negative Gaussian curvature along the rim of the enclosure while the 'pocket' is sphere-shaped with positive Gaussian curvature.

For cellular uptake processes such as macropinocytosis, the positive Gaussian curvature at the tip of protrusions is countered by the negative Gaussian curvature found at the base of the extension.

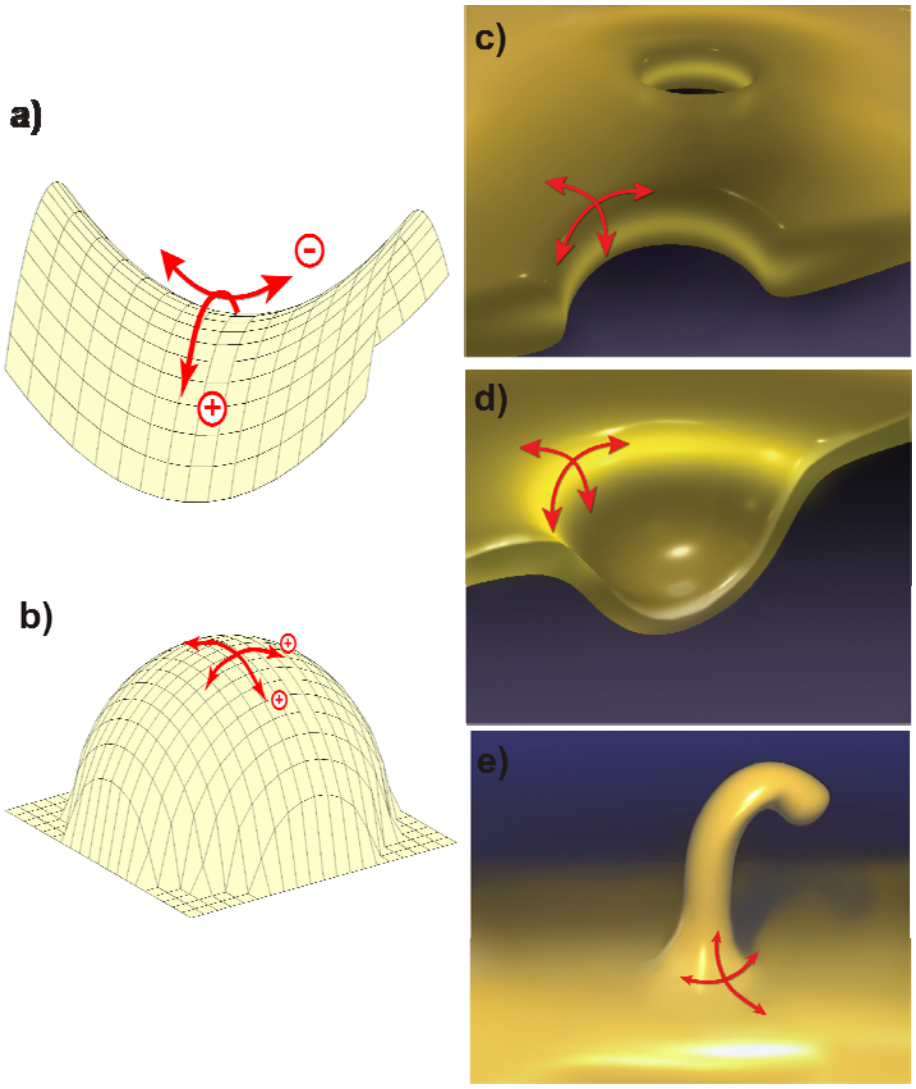


Figure 4.5: Examples of **(a)** negative Gaussian curvature and **(b)** positive Gaussian curvature. The former is saddle shaped and found in objects with holes such as a donut. The latter is found on objects like spheres or ellipsoids, and do not have holes. Negative Gaussian curvature is topologically necessary for the formation of **(c)** membrane pores, **(d)** membrane dimples or invaginations (such as those in endocytosis), and **(e)** membrane protrusions (such as those in macropinocytosis).

4.3.3 Role of cholesterol

Cholesterol is present in eukaryotic membranes in significant amount. The structure of cholesterol consists of four fused carbon rings. They make the hydrophobic part of cholesterol very rigid. The hydroxyl group is the polar part of cholesterol. The large hydrophobic tail and the small hydrophilic head give cholesterol its negative intrinsic curvature while making it highly insoluble in water. Cholesterol is accommodated rapidly in membranes and forms liquid-ordered domains, called 'lipid rafts'. High cholesterol membrane content has been shown to accompany receptor independent endocytosis mechanisms implicated in cell-penetrating peptide uptake.

In order to understand the role of cholesterol in TAT peptide uptake, we studied the interaction of TAT peptide with membranes containing cholesterol. We fixed the DOPS content at 20% by weight and varied the amounts of DOPE, DOPC and cholesterol. The phase diagram of TAT peptide-membrane interaction with increasing cholesterol content is shown in fig 4.6. For membranes that do not contain cholesterol, the cubic Pn3m phase is observed only with a high amount of DOPE (>70%). However, adding cholesterol decreases the amount of DOPE required to form the cubic Pn3m phase. These results indicate that the presence of cholesterol enhances the ability of cell-penetrating peptides to generate the Pn3m cubic phase.

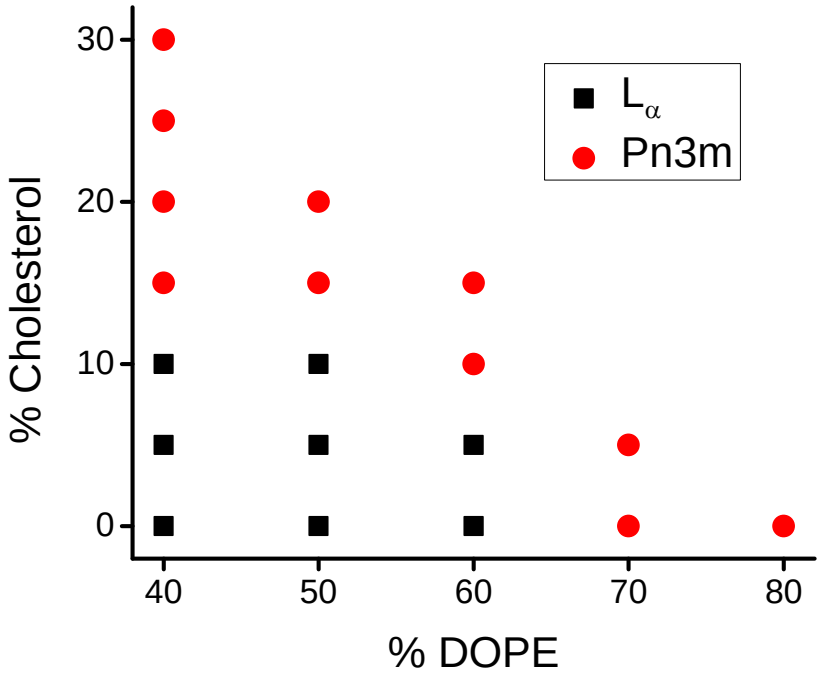


Figure 4.6: Phase diagram of TAT-PTD with PS/PE/PC/Cholesterol membranes show that addition of cholesterol decreases the threshold concentration of DOPE required to form the cubic Pn3m phase.

The x-ray data show a strong dependence of the phase behavior on membrane lipid composition. The phase diagram indicates that the Pn3m cubic phase is generated by TAT peptide in membranes enriched with negative intrinsic curvature lipids ($c_0 < 0$), like PE and cholesterol. Substitution with PC ($c_0 = 0$) makes the intrinsic curvature of the membrane monolayers less negative which results in the loss of the negative gaussian curvature-rich Pn3m phase. Moreover, direct translocation of TAT peptide into the interior of giant unilamellar vesicles (GUVs) was shown to depend on a threshold amount of negative intrinsic curvature lipid, PE.

Formation of a hydrophilic or toroidal pore in a membrane results in a change in Gaussian curvature in the membrane. From the Gauss-Bonnet theorem it can be shown that the change is given by $\Delta\int K \cdot dA = -4\pi$. It follows that the free energy change from pore formation is $E = \kappa_G \int K \cdot dA = -4\pi\kappa_G$, where κ_G is the Gaussian curvature modulus of the bilayer. It can be shown [24]:

$$\kappa_G = 2\kappa_G{}^m - 4\kappa^m c_o{}^m \delta$$

Here $\kappa_G{}^m$ (< 0, from the lateral stress profile of a membrane monolayer [25]) is the Gaussian curvature modulus of the monolayer, κ^m (>0) is the monolayer bending modulus, and δ (>0) is the distance from the middle of the bilayer to the monolayer pivot point.

Typically the negative value of the monolayer Gaussian curvature modulus ensures that κ_G likewise remains negative preventing pore formation. However, negative intrinsic curvature lipids such as PE and cholesterol decrease $c_o{}^m$, the intrinsic curvature of the membrane monolayer, shifting the bilayer Gaussian curvature modulus toward positive values. The decreased energetic barrier to changes in membrane topology toward porous phases enhances the negative Gaussian curvature generation abilities of cell penetrating peptides thereby enhancing their transduction ability.

4.3.4 Effect of transport inhibitors on cellular uptake

Lipid-raft mediated endocytosis processes, like macropinocytosis and caveolae-mediated endocytosis, have been implicated in the membrane transduction mechanism of cell-penetrating peptides [16,17,26]. Macropinocytosis involves the formation of large endocytotic vesicles (macropinosomes) of irregular size and shape, generated by actin-driven envagination of the plasma membrane. Caveolae are small, hydrophobic membrane microdomains, rich in cholesterol and glycosphingolipids that trap membrane-associated ligands and bud off the membrane, forming caveosomes [27]. Transport inhibition experiments were performed to examine the cellular uptake of TAT peptide in the presence of specific inhibitors. The nuclei of the HeLa cells were stained with DAPI. The cells were pretreated with cytochalasin D or nystatin, chemicals that inhibit macropinocytosis and caveolae-dependent endocytosis respectively. The pretreated cells were then incubated with fluorescently-labeled TAT peptide at 12.5 uM for 15 minutes.

Figure 4.7 shows the representative confocal images of the HeLa cells. Fluorescence signal was observed throughout the control cells (cells not treated with transport inhibitors), indicating that the TAT peptide has crossed the cell membrane (Fig 4.7a). While treating the cells with nystatin had a negligible effect (Fig 4.7b), cytochalasin D significantly reduced the uptake of TAT peptide (Fig 4.7c). Similar results are obtained when the HeLa cells are incubated with R_9 (Fig 4.7d, e, f). These results indicate that macropinocytosis is important for TAT transduction.

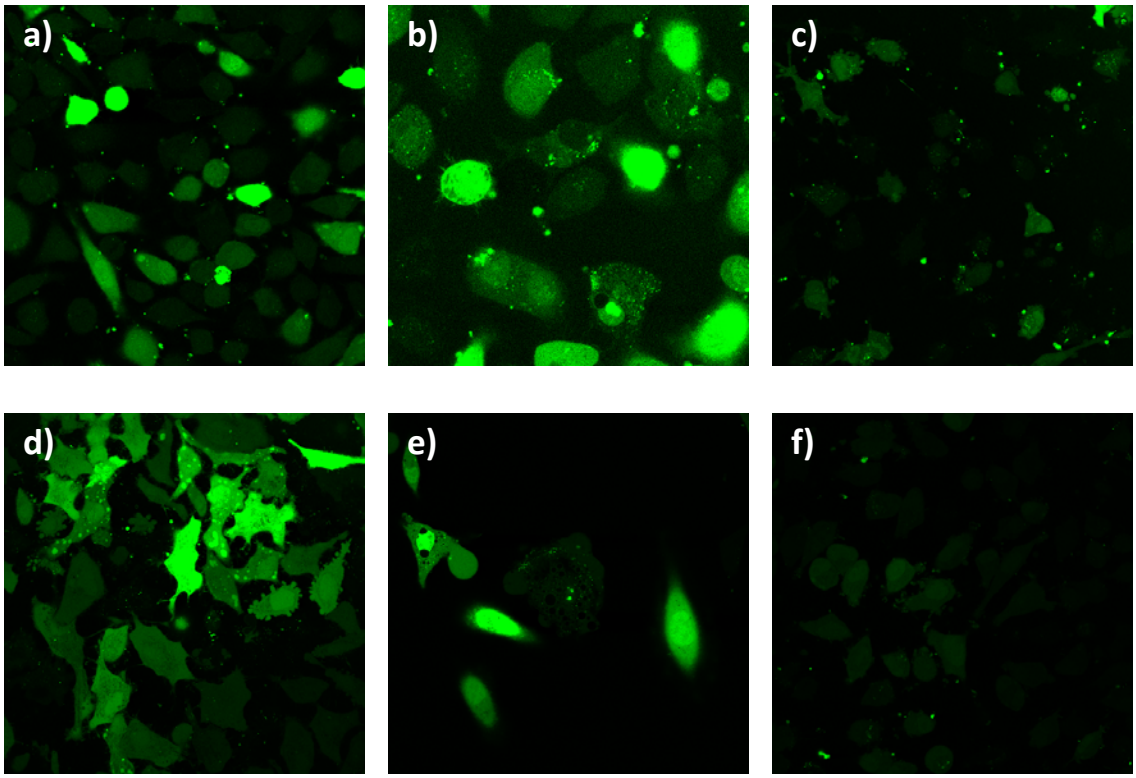


Figure 4.7: Confocal microscopy images of HeLa cells incubated with TAT peptide (top row) and R_9 (bottom row). **(a)** & **(d)** Control cells. **(b)** & **(e)** Cells pretreated with nystatin. **(c)** & **(f)** Cells pretreated with cytochalasin D.

4.3.5 TAT peptide induced reorganization of cytoskeleton

The cellular uptake of TAT peptide is reduced when the cells are treated with cytochalasin D, an inhibitor of actin polymerization. This implies an important role for actin polymerization. Actin is one of the principal structural proteins in eukaryotic cells. The actin cytoskeleton dynamically maintains the structural integrity of the plasma membrane and plays important roles in a number of membrane-associated events, such as cell adhesion, cell motility, and regulation of integral membrane protein distributions. This versatility is afforded by actin's ability to dynamically adjust its degree of polymerization from monomeric G-actin (35 Å by 55 Å by 55 Å) to polymeric F-Actin, which is a linear chain of G-actin subunits. The polymerization process is reversible and depends on the ionic strength of the solution. F-Actin filaments are helical and very stiff; with a persistence length of ≈ 10 μm. Actin has an approximate average linear charge density of $1e^-/2.5Å$ at pH 7. In the presence of multivalent cations, F-actin filaments condense into close-packed bundles [28].

Small angle X-ray diffraction pattern shows that when TAT peptide is complexed with F-actin, it condenses the actin filaments into close-packed bundles (Fig 4.8a, top). Two correlation peaks are observed at q = 0.83 nm^{-1} and 1.34 nm^{-1}. The ratio of the peak positions differs slightly from that expected for an exact hexagonal lattice. This diffraction pattern is similar to the pattern observed when F-actin is condensed by high concentration of divalent Ba^{2+} ions [29]. The same diffraction is observed when TAT peptide is complexed with the G-actin monomers (Fig 4.8a, bottom). This indicates that the TAT peptide can not only condense actin filaments into bundles but also polymerize actin monomers.

It is known that reorganization of the cytoskeleton drives membrane deformations during processes like cell motility and endocytosis. Polymerization of actin filaments and microtubules in giant unilamellar vesicles (GUV) show that membrane curvature fluctuations can influence formation of protrusions from the protein network [30,31]. We have seen that the TAT peptide can induce negative Gaussian curvature in membranes as well as polymerize and condense actin. Now we look at the effect of TAT peptide on spherical GUVs with encapsulated evolving cytoskeleton.

The GUVs encapsulate monomeric G-actin and Rh-phalloidin which specifically binds to filamentous F-actin. When a multivalent salt, like $MgCl_2$, is added to the solution, the Mg^{2+} ions pass through the Calcium ion-channels in the membrane and induce polymerization of actin and promote the formation of a network of F-actin bundles. However, this does not deform the membrane and the vesicle remains spherical (Fig 4.8b). The TAT peptide has a dual effect when it is added to the vesicles. It not only changes the curvature of the membrane, but also enters the vesicle and encourages actin bundling. This deforms the vesicle and induces blebbing or fingering which are stabilized by the encapsulated and growing actin network (Fig 4.8c, d). In some cases, the actin network aligns and grows in a certain orientation deforming the spherical vesicle into an elongated structure (Fig 4.8e). These results indicate that the TAT peptide can enhance membrane deformation and cytoskeleton reorganization necessary for endocytotic processes.

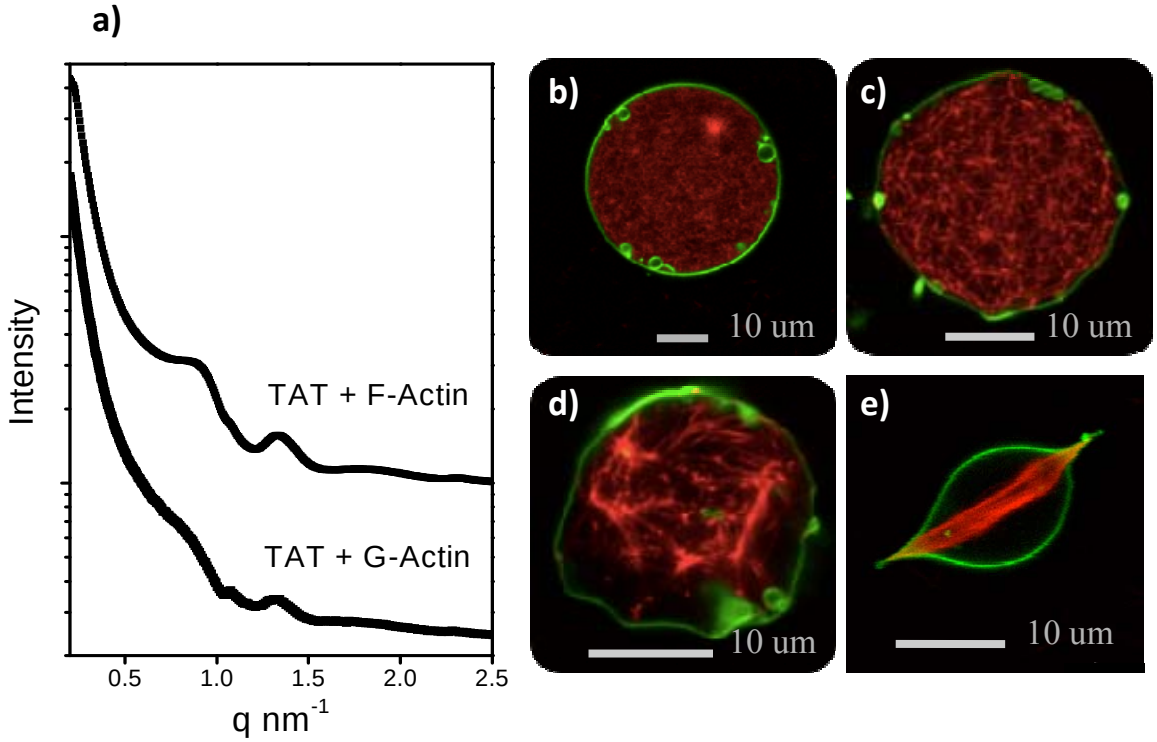


Figure 4.8: **(a)** SAXS data show that the TAT peptide condenses F-actin filaments into close-packed bundles (top). It also polymerizes and condenses G-atin monomers (bottom). **(b)** Addition of $MgCl_2$ to G-actin encapsulated GUVs induces polymerization and formation of actin network without any accompanying deformation of vesicle. **(c)** & **(d)** Addition of TAT peptide induces blebbing or fingering stabilized by the growing actin network. **(e)** Growth of actin network leads to elongated vesicles in some cases.

4.3.6 Effect of cargo size

The size of the cargo attached to the TAT peptide appears to determine the mechanism of uptake. It has been shown that complexes or fusions of TAT with large 20 nm quantum dots or proteins (> 50 amino acids) enter cells primarily through an endocytotic, vesicle-associated pathway whereas a small peptide (< 50 amino acids) cargo can transduce cells through an additional, non-endocytotic pathway. In addition, the specific endocytotic pathway also appears to depend on the cargo size. It was observed that when fluorescent beads attached to TAT peptide are less than 200 nm in diameter, cellular uptake is primarily through clatharin-mediated endocytosis. As the size of the beads increases the mode of uptake becomes increasingly caveolae-mediated with the caveolae pathway dominating for beads of 500 nm in diameter [1].

We look at the effect of cargo size on the ability of TAT peptide to enter giant vesicles. For the bulky cargo we use PLA nanoparticles roughly 30 nm in diameter. These naoparticles are modified to have maleimide groups on the surface which are used to conjugated TAT peptides with a cysteine residue at the end. The nanoparticles are stained with Cy5 dye. As we have seen earlier, when TAT peptide (with no bulky cargo attached) is added to vesicles containing PE lipids above a certain threshold, it enters the vesicles and the peptide concentration equilibrates across the membrane (Fig 4.9a). When the PLA nanoparticles, with no conjugated TAT peptide, are added to the same vesicles, they are unable to enter the vesicles and remain equally distributed in the solution (Fig 4.9b). Nanoparticles conjugated to TAT peptide are also unable to enter vesicles; however, they aggregate around the periphery of GUVs, causing an enhancement of fluorescence intensity at the lipid bilayer (Fig 4.9c). These results suggest that although

large nanoparticles conjugated to TAT peptide are unable to enter lipid vesicles, the TAT peptide anchors the nanoparticles to the membrane.

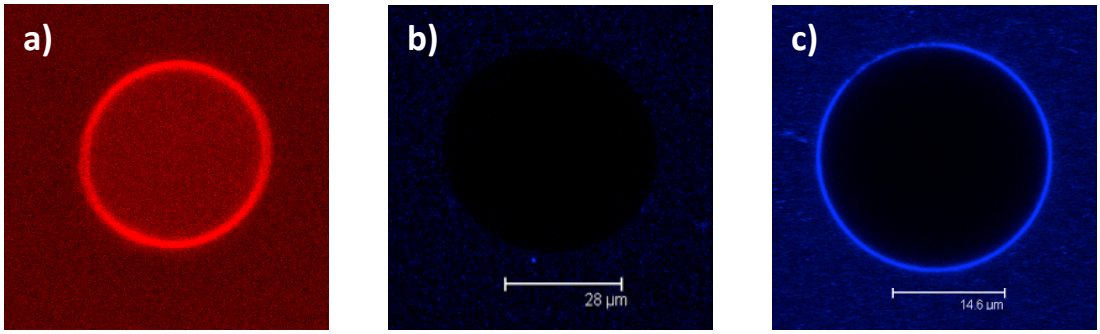


Figure 4.9: **(a)** Rhodamine-tagged TAT peptide (false-color red) applied to the exterior of PS:PC:PE 20:40:40 GUVs crosses the membrane with the vesicle interior having the same brightness as the outside, showing that the Rh-TAT concentration has equilibrated on both sides of the membrane. **(b)** Cy5-tagged PLA nanoparticles (blue) never enter the GUVs and remain distributed outside. **(c)** Cy5-tagged PLA nanoparticles conjugated to TAT peptide (blue) aggregate around the periphery of GUVs, causing an enhancement of fluorescence intensity at the lipid bilayer.

4.3.7 Mechanism for transduction

We believe the above results can explain how a simple molecule like the TAT peptide can utilize various endocytotic and non-endocytotic mechanisms for cellular transduction. When the TAT peptide approaches the cellular membrane, it can interact with either a receptor, like heparin sulfate, or directly with the membrane. If the TAT peptide interacts with heparin sulfate, it binds to it with high affinity and gets internalized by endocytosis. If the TAT peptide does not bind to any receptor but interacts directly with the lipid membrane, it induces negative Gaussian curvature locally. This type of

curvature is a necessary condition for the dimples for caveoli- or clatharin-based endocytosis, for the cytoskeleton-driven protrusions in macropinocytosis, as well as for pore formation. The mechanism by which TAT peptide generates such curvature has been explained earlier, and involves the guanidinium group forming bidentate hydrogen bonds. Presence of negative intrinsic lipids, like DOPE and Cholesterol, enhance the ability of the peptide to generate negative Gaussian curvature. If the cargo attached to the TAT peptide is small enough, it can be directly translocated into the cells. However, bulky cargoes get anchored to the membrane by the TAT peptide (Fig 4.10). Since the TAT peptide generates negative Gaussian curvature, it makes it easier for the cell to internalize the attached bulky cargo by one of the various endocytosis processes. In addition, the TAT peptide encourages actin polymerization and bundling, thereby, enhancing macropinocytosis.

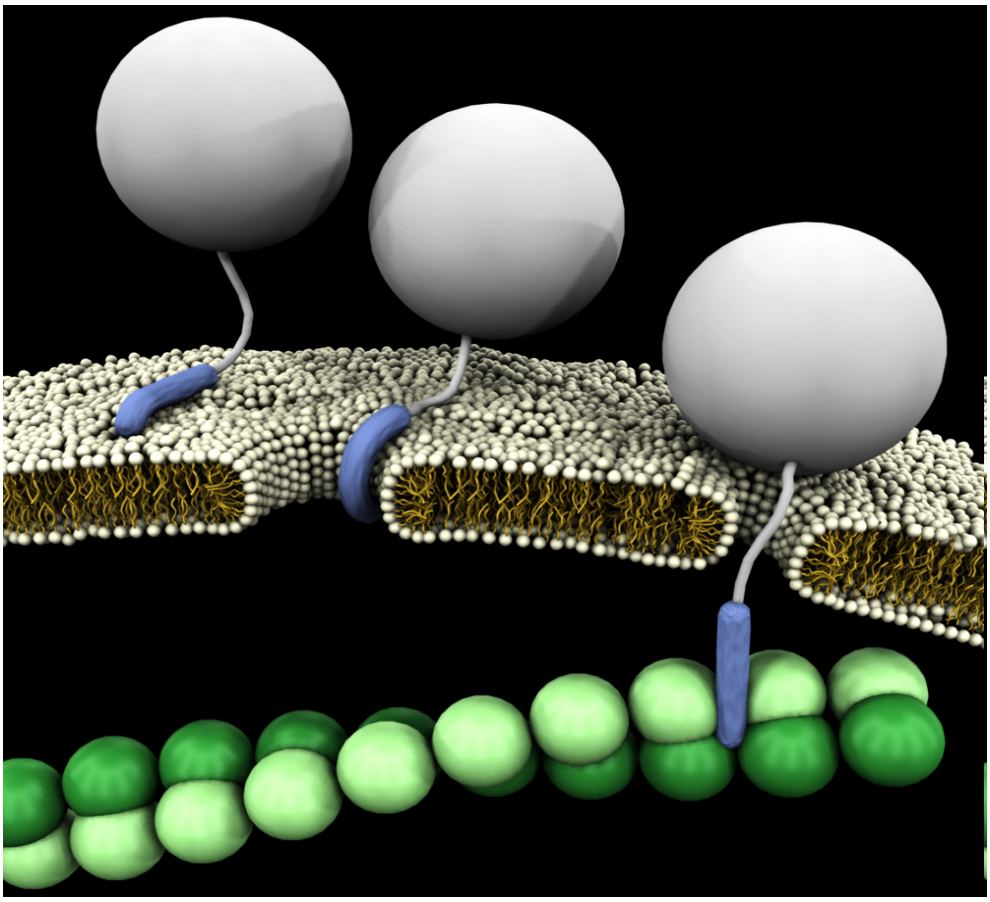


Figure 4.10: Schematic showing mechanism of transduction for TAT peptide coupled to bulky cargos. The TAT peptide lands on the membrane, generates negative Gaussian curvature and anchors the cargo. Internalization occurs via one of the various endocytosis processes including macropinocytosis.

4.4 Summary

Arginine rich cell-penetrating peptides are short cationic peptides capable of traversing the plasma membranes of eukaryotic cells. While successful intracellular delivery of many biologically active macromolecules has been accomplished using these peptides, their mechanisms of cell entry are still under investigation. We used synchrotron small angle x-ray scattering (SAXS) to study the interactions of arginine rich peptides with model cell membranes and find that the transduction activity correlates with induction of negative Gaussian ('saddle-splay') membrane curvature. The negative Gaussian membrane curvature is broadly enabling and its induction can lower the free energy barriers for a range of different entry mechanisms, such as direct translocation as well as endocytotic pathways. Moreover, the peptides have strong electrostatic interactions with different components of the cell besides the cell membrane, in ways that contribute to their activity. Finally, we connect the observations with a mechanism that explains how a relatively simple molecule, like the TAT peptide, facilitates mechanisms as different as direct entry and the multiple endocytotic mechanisms.

4.5 References

[1] Wender, P.A., Galliher, W. C., Goun, E. L., Jones, L. R., and Pillow, T. H. (2008). The design of guanidinium-rich transporters and their internalization mechanisms. Adv. Drug Deliv. Rev. 60, 452-472.

[2] El-Sayed, A., Futaki, S. and Harashima, H. (2009). Delivery of Macromolecules Using Arginine-Rich Cell-Penetrating Peptides: Ways to Overcome Endosomal Entrapment. The AAPS Journal 11, 13-22.

[3] Wadia, J., and Dowdy, S. (2005). Transmembrane delivery of protein and peptide drugs by TAT-mediated transduction in the treatment of cancer. Adv. Drug Deliv. Rev. 57, 579-596.

[4] Schug, K.A., and Linder, W. (2005). Noncovalent binding between guanidinium and anionic groups: Focus on biological- and synthetic-based arginine/guanidinium interactions with phosph[on]ate and sulf[on]ate residues. Chemical Review 105, 67-113.

[5] Rothbard, J.B., Jessop, T. C., and Wender, P. A. (2005). Adaptive translocation: The role of hydrogen bonding and membrane potential in the uptake of guanidinium-rich transporters into cells. Adv. Drug Deliv. Rev. 57, 495-504.

[6] Mishra, A., Gordon, V., Yang, L., Coridan, R., and Wong, G. (2008). HIV TAT Forms Pores in Membranes by Inducing Saddle-Splay Curvature: Potential Role of Bidentate Hydrogen Bonding. Angew. Chem. Intl. Ed. 47, 2986-2989.

[7] Wender, P.A., Mitchell, D. J., Pattabiraman, K., Pelkey, E. T., Steinman, L., and Rothbard, J. B. (2000). The design, synthesis, and evaluation of molecules that enable or enhance cellular uptake: Peptoid molecular transporters. Proc. Natl. Acad. Sci. 97, 13003-13008.

[8] Wender, P., Rothbard, J., Jessop, T., Kreider, E., and Wylie, B. (2002). Oligocarbamate Molecular Transporters: Design, Synthesis, and Biological Evaluation of a New Class of Transporters for Drug Delivery. J. Am. Chem. Soc. 124, 13382-13383.

[9] Wender, P., Kreider, E., Pelkey, E., Rothbard, J., and VanDeusen, C. (2005). Dendrimeric Molecular Transporters: Synthesis and Evaluation of Tunable Polyguanidino Dendrimers That Facilitate Cellular Uptake. Org. Lett. 7, 4815-4818.

[10] Elson-Schwab, L., Garner, O., Schuksz, M., Crawford, B., Esko, J., and Tor, Y. (2007). Guanidinylated Neomycin Delivers Large, Bioactive Cargo into Cells through a Heparan Sulfate-dependent Pathway. J Biol. Chem. 282, 13585-13591.

[11] Mitchell, D.J., Kim, D. T., Steinman, L., Fathman, C. G. & Rothbard, J. B. (2000). Polyarginine enters cells more efficiently than other polycationic homopolymers. J. Pept. Res. 56, 318-325.

[12] Futaki, S., Suzuki, T., Ohashi, W., Yagami, T., Tanaka, S., Ueda, K., and Sugiura, Y. (2001). Arginine-rich Peptides: An Abundant Source of Membran-Permeable Peptides Having Potential as Carriers for Intracellular Protein Delivery. J Biol. Chem. 276, 5836-5840.

[13] Richard, J.P., Melikov, K., Vives, E., Ramos, C., Verbeure, B., Gait, M. J., Chernomordik, L. V., and Lebleu, B. . (2003). Cell-penetrating Peptides: A Reevaluation of the Mechanism of Cellular Uptake. J Biol. Chem. 278, 585-590.

[14] Drin, G., Cottin, S., Blanc, E., Rees, A., and Temsamani, J. (2003). Studies on the Internalization Mechanism of Cationic Cell-penetrating Peptides. J Biol. Chem. 278, 31192-31201.

[15] Fischer, R., Fotin-Mleczek, M., Hufnagel, H., and Brock, R. (2005). Break on through to the Other Side-Biophysics and Cell Biology Shed Light on Cell-Penetrating Peptides. Chem Bio Chem 6, 2126-2142.

[16] Nakase, I., Niwa, M., Takeuchi, T., Sonomura, K., Kawabata, N., Koike, Y., Takehashi, M., Tanaka, S., Ueda, K., Simpson, J. C., Jones, A. T., Sugiura, Y., and Futaki, S. (2004). Cellular Uptake of Arginine-Rich Peptides: Roles for Macropinocytosis and Actin Rearrangement. Mol. Therapy 10, 1011-1022.

[17] Kaplan, I.M., Wadia, J. S., and Dowdy, S. F. (2005). Cationic TAT peptide transduction domain enters cells by macropinocytosis. J Control. Release 102, 247-253.

[18] Richard, J.P., Melikov, K., Brook, H., Prevot, P., Lebleu, B. and Chernomordik, L. V. (2005). Cellular Uptake of Unconjugated TAT Peptide Involves Clathrin-dependent Endocytosis and Heparan Sulfate Receptors. J Biol. Chem. 280, 15300-15306.

[19] Maiolo, J., Ferrer, M., and Ottinger, E. (2005). Effects of cargo molecules on the cellular uptake of arginine-rich cell-penetrating peptides. Biochim. Biophys. Acta 1712, 161-172.

[20] Ter-Avetisyan, G., Tunnemann, G., Nowak, D., Nitschke, M., Herrmann, A., Drab, M., & Cardoso, M. C. (2009). Cell Entry of Arginine-rich Peptides Is Independent of Endocytosis. J Biol. Chem. 284, 3370-3378.

[21] Fretz, M.M., Penning, N., Al-Taei, S., Futaki, S., Takeuchi, T., Nakase, I., Storm, G., and Jones, A. T. (2007). Temperature-, concentration- and cholesterol-dependent translocation of L- and D-octa-arginine across the plasma and nuclear membrane of CD34+ leukaemia cells. Biochem. J. 403, 335-342.

[22] Brooks, H., Lebleu, B., and Vives, E. . (2005). Tat peptide-mediated cellular delivery: back to basics. Adv. Drug Deliv. Rev. 57, 559.

[23] Lundberg, P. and Langel, Ü. (2003). A brief introduction to cell-penetrating peptides. Journal of Molecular Recognition 16, 227-233.

[24] Helfrich, W. (1973). Elastic properties of lipid bilayers: theory and possible experiments. Naturforsch 28C, 693-703.

[25] Templer, R., Khoo, B., and Seddon, J. . (1998). Gaussian curvature modulus of an amphiphilic monolayer. Langmuir 14, 7427-7434.

[26] Ferrari, A., Pellegrini, V., Arcangeli, C., Fittipaldi, A., Giacca, M., and Beltram, F. (2003). Caveolae-Mediated Internalization of Extracellular HIV-1 Tat Fusion Proteins Visualized in Real Time. Mol. Therapy 8, 284-294.

[27] Khalil, I., Kogure, K., Akita, H., and Harashima, H. (2006). Uptake Pathways and Subsequent Intracellular Trafficking in Nonviral Gene Delivery. Pharma. Rev. 58, 32-45.

[28] Wong, G.C.L., Lin, A., Tang, J.X., Li, Y., Janmey, P.A. and Safinya, C.R. (2003). Lamellar Phase of Stacked Two-Dimensional Rafts of Actin Filaments. Physical Review Letters 91, 018103.

[29] Angelini, T.E., Liang, H., Wriggers, W. and Wong, G.C.L. (2003). Like-charge attraction between polyelectrolytes induced by counterion charge density waves. Proceedings of the National Academy of Sciences of the United States of America 100, 8634-8637.

[30] Liu, A.P., Richmond, D.L., Maibaum, L., Pronk, S., Geissler, P.L. and Fletcher, D.A. (2008). Membrane-induced bundling of actin filaments. Nat Phys 4, 789-793.

[31] Fygenson, D.K., Marko, J.F. and Libchaber, A. (1997). Mechanics of Microtubule-Based Membrane Extension. Physical Review Letters 79, 4497.

CHAPTER 5

INORGANIC MERCURY DETECTION AND CONTROLLED RELEASE OF CHELATING AGENTS FROM ION-RESPONSIVE PEG-LIPOSOMES

5.1 Introduction

Liposomes are assemblies of lipid molecules in the form of closed spherical bilayers. They have been used extensively for drug delivery applications. Liposome based delivery systems can be used to isolate a bioactive agent, so as to direct the agent away from certain tissues and to deliver the agent to other tissues. Since the lipid bilayer separates the encapsulated content from the external environment, efficient encapsulation of a broad range of cargo is possible.[1,2] It has been shown that inorganic mercury binds to phosphatidylethanolamine (PE) lipid headgroups strongly and can reorient them (Figure 1A inset).[3] PE lipids have negative intrinsic curvature; hence, liposomes of 100% PE are not possible. However, we can form and stabilize vesicles of such lipids by incorporating polymeric bulky headgroups, like polyethylene glycol (PEG), on the hydrophilic side. We hypothesized that such PE-based PEG-liposomes may be used to develop a mercury sensing and controlled release platform.

Mercury exposure has been linked to a number of health problems, such as damage to the central nervous system, endocrine system, brain, kidney and fetus development.[4] Since inorganic mercury is found in water, soil, food sources, as

well as a broad range of environments, there is a substantial need for both sensitive detection and efficient detoxification of mercury just like we do for sensing other biologically important metal ions.[5-9] To meet the need, a number of mercury sensors have been developed based on small organic molecules,[10-19] oligonucleotides,[20,21] conjugated polymers,[22] foldamers,[23], micelles,[24] genetically engineered cells,[25], membranes,[26] electrodes,[27] enzymes,[28] antibodies,[29] proteins,[30,31] DNAzymes,[32,33], functionalized nanotubes, [34] and nanoparticles.[35,36] Despite the progress of mercury detection in organic solvents, there remains a need for sensors with high sensitivity and selectivity that can detect mercury in water,[11,12,17,37-41] and no single platform can detect and detoxify mercury at the same time. Moreover, the distribution of mercury can be location- and time-specific, a systemic dose of detoxifying agents can be inefficient in dealing with various concentrations of mercury, while a large dose can potentially lead to undesirable side effects.

In collaboration with Mehmet Yigit and Prof. Yi Lu, we developed a novel liposome-based system that can detect and respond to the presence of mercury with a concentration as low as 10 nM, the maximum contamination level defined by the U.S. Environmental Protection Agency for mercury in drinking water. In particular, we were able to modulate the release profile of Hg chelators by the local concentration of Hg so that more chelators are released in regions with high concentration Hg and low or no chelators are released in regions of low concentration. This ‘budgeted’ release profile will be particularly useful in

situations in which the local levels of Hg contamination vary, or if such contamination is time-dependent.

5.2 Experimental section

5.2.1 Materials

The lipids 1,2-dioleoyl-sn-glycero-3-phosphoethanolamine (DOPE), and 1,2-dioleoyl-sn-glycero-3-phosphoethanolamine-n-methoxy(polyethyleneglycol)-2000](ammonium salt) (PEG-PE) were purchased from Avanti Polar Lipids. Stock solutions of lipids in chloroform at 30 mg/ml were freshly prepared. Column buffer was prepared by addition of 24 ml of 500 mM HEPES buffer at pH 7.4 and 15 ml of 2 M NaCl into 160 ml of distilled water. 1 mM, 100 μM and 10 μM stock solutions of Hg(ClO4)2 were prepared. 200 mM and 1 mM stock solution of divalent metal ions were prepared for further use.

5.2.2 Liposome preparation

The PEG-PE and DOPE were mixed at the 20% w/w ratio. The solution was dried under N2 and desiccated under vacuum overnight. The dried lipids are rehydrated with 1 ml of 50 mM of fluorescein in 100 mM of NaCl and 50 mM of HEPES buffer at pH 7.4. The hydrated mixture is incubated at 37 °C for one day. The resultant solution is extruded 11 times in a mini-extruder through 1 μm polycarbonate membrane. The resulting vesicles are purified by PD-10 desalting column against column buffer. 1300 μl of liposome solution is collected from PD-10 column. The liposome solution is diluted to 4500 μl in column buffer.

5.2.3 Detection of mercury by fluorescence

2 µl of stock solution of 1, 2.5, 5, 10 or 100 µM of Hg(ClO4)2 was added into 200 µl of fluorescein encapsulated liposomes for detection of final concentration of 10, 25, 50, 100 or 1000 nM Hg2+. The fluorescence change with the addition of inorganic mercury is monitored by fluorimeter (λex = 495 nm and λem = 520 nm) over 15 minutes using disposable glass cuvettes. In order to check the effect of other divalent metal ions, 2 µl of stock solution of various concentrations of metal salts was added into 200 µl of fluorescein encapsulated liposomes. The change in fluorescence is monitored using the same parameters in monitoring the effect of Hg2+. The fluorescent measurements are performed in triplicate.

5.2.4 Encapsulation of meso-DMSA and fluorescein in liposomes

The DOPE and PEG-PE were mixed at the four to one ratio, dried under N2 and desiccated under vacuum overnight. The dried lipids are rehydrated with 1 ml of 50 mM fluorescein with 0, 100, 1000 or 2000 µM meso-DMSA in 100 mM of NaCl and 50 mM of HEPES buffer at pH 7.4 for in vitro experiments. The dried lipids are rehydrated with 1 ml of 2 µM meso-DMSA in 100 mM of NaCl and 50 mM of HEPES buffer at pH 7.4 for HeLa cell experiments. The hydrated mixture is incubated at 37 °C for one day. The resultant solution is extruded 11 times in a mini-extruder through 1 µm polycarbonate membrane. The resulting vesicles are purified by PD-10 desalting column against column buffer. 1300 µl of

liposome solution is collected from PD-10 column. The liposome solution is diluted to 4500 µl in column buffer.

5.2.5 HeLa cell experiments

HeLa cells are cultured following ATCC's recommendation, in Eagle's Menimum Essential Medium, supplemented with 100 units/mL aqueous penicillin G, 100 µg/mL streptomycin, and 10% fetal bovine serum.The HeLa cells were grown in 96-well plates with medium at concentrations to allow 70% confluence in 24 h. At the experiment day, cells were washed with PBS buffer and incubated with prewarmed Opti-MEM medium (phenol red reduced) for 30 minutes at 37 oC. After the addition of different formulations of liposomes (with or without meso- DMSA (2µM, 80µL)), cells was incubated for 8 hours and then washed with 100 µL/well PBS twice. Cells were further treated with 0, 0.2, 0.4, 0.6, 0.8 or 1.0 µM final concentrations of Hg using stock solution of 20, 40, 60, 80 or 100 µM of Hg(ClO4)2 in prewarmed fresh growth medium for 48 h. Cell viability was assessed colorimetrically with the MTT reagent (Sigma-Aldrich) following the standard protocol provided by the manufacturer. The absorbance was read with a microplate reader at 570 nm.

5.3 Results and discussion

PEG-liposomes, encapsulating both fluorescent molecules and mercury-specific chelators, were designed to rupture in the presence of mercury, thus releasing the encapsulated fluorophores and the chelators. Since the self-quenching of the fluorophores inside of the liposome is reversed upon liposome rupture, the fluorescent signal increases, thereby providing a read-out of the release profile (Figure 5.1a). Importantly, as the chelators are released to reduce the concentration of free mercury (Figure 5.1b), the release of chelators is down regulated, so that the PEG-liposomes can be maximally available to interact with free mercury elsewhere.

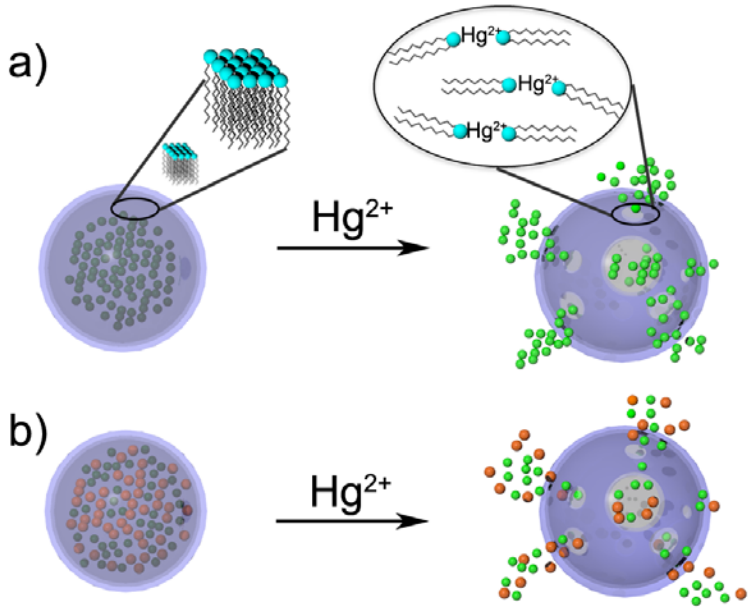


Figure 5.1: Interaction of inorganic mercury with **a)** fluorescein encapsulated DOPE liposomes and **b)** *meso*-DMSA and fluorescein encapsulated DOPE liposomes. Green and orange circles represent fluorescein and *meso*-DMSA, respectively. Enlarged areas show lipid molecules on the liposome surface and their interaction with Hg^{2+} that destabilizes liposomes.

To demonstrate the rupture of liposomes in the presence of Hg^{2+}, liposomes were prepared using 1,2-dioleoyl-*sn*-glycero-3-phosphoethanolamine (DOPE) and PEG-PE (PEG MW 2000Da) as the building blocks. Liposomes consisting of 100% DOPE are not stable due to the negative intrinsic curvature of PE lipids. However, we found that by incorporating 20% w/w of PEG we were able to achieve stable liposomes. Fluorescein was encapsulated in the liposome with a concentration of 50 nM, which is sufficiently high to ensure fluorescence self-quenching and detection. The interaction of mercury ions with DOPE headgroups, and the resultant induced reorientation of the headgroups, can in principle lead to rupture of the vesicles, thereby releasing and unquenching the fluorescein. When 1 μM of $Hg(ClO_4)_2$ was added to the liposomes, a significant increase in the fluorescence was indeed observed (Figure 5.2a). The fluorescein release at this concentration of mercury is determined to be the maximum by comparing it to the fluorescein release by Triton-X (a detergent), which should rupture all lipid vesicles in the solution. To further quantify this effect, different amounts of Hg^{2+} were added into the liposome solution and the change in fluorescence spectra was monitored over a 15 minutes time period. The fluorescence increase with 10, 25, 50, 100 nM and 1 μM Hg^{2+} was determined as 20.66 ± 6.88 %, 24.66 ± 7.54 %, 59.8 ± 19.74 %, 74.28 ± 5.85 % and 97.83 ± 3.05 %, respectively. As shown in Figure 5.2b, fluorescence increased with increasing concentration of Hg^{2+}, which is consistent with the hypothesis that mercury is the inducing agent for liposome rupture and fluorescein release. At 10

nM of Hg^{2+}, the maximum contamination level defined by the US EPA, the system can still display signal above the background (Figure 5.3).

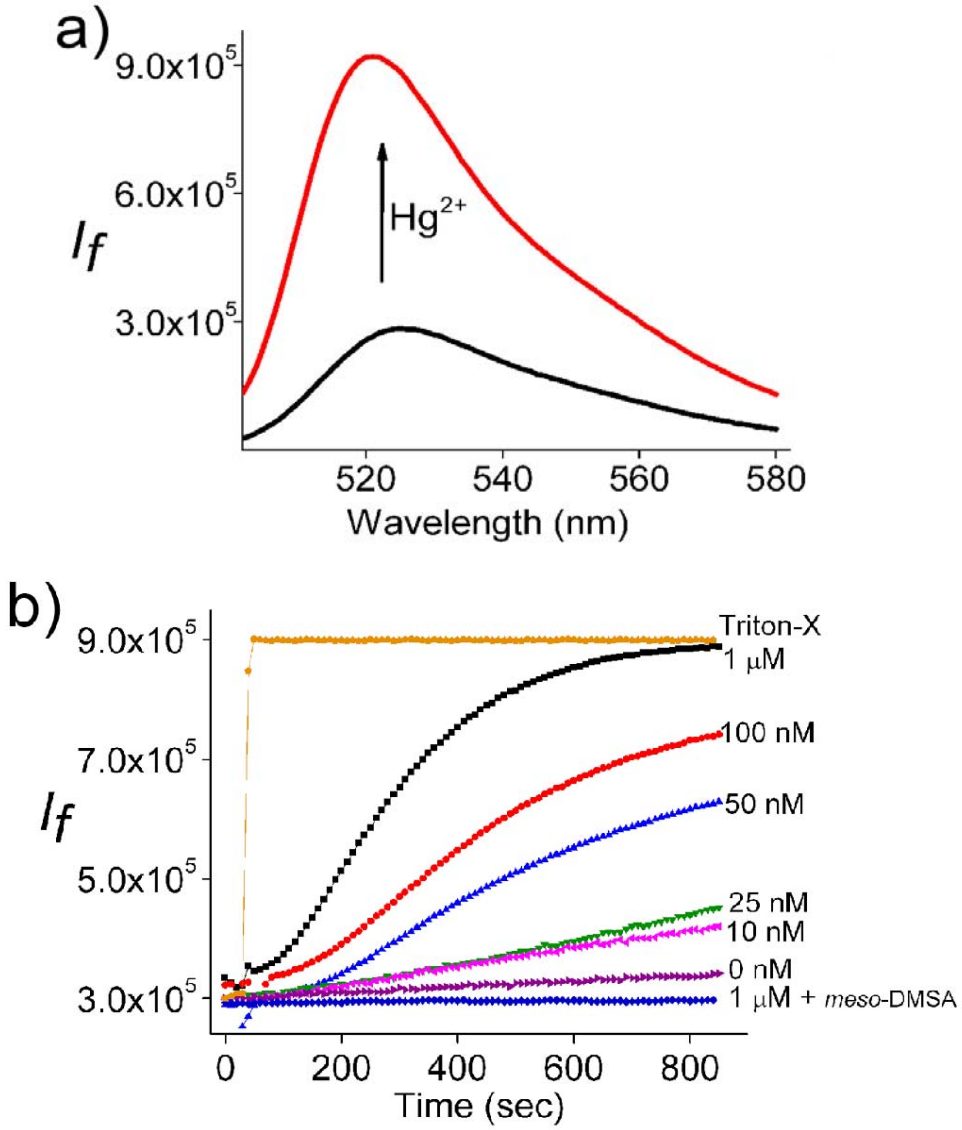


Figure 5.2 **a)** Fluorescence spectra of fluorescein encapsulated liposomes before (black) and after (red) addition of 1 μM Hg^{2+}, λ_{ex}=495 nm, **b)** Time-dependent fluorescence change after addition of 10, 25, 50, 100, 1000 nM Hg^{2+} or 1 μM Hg^{2+} chelated with *meso*-DMSA (1 μM + *meso*-DMSA).

To test whether Hg^{2+}-lipid interaction can be used to make ion-responsive liposomes for the 'budgeted' release of chelating agents, *meso*-2,3-dimercaptosuccinic acid (*meso*-DMSA), a molecule routinely used in clinic for the treatment of mercury exposure, was encapsulated in the liposome in order to chelate mercury. *Meso*-DMSA is one of the most commonly used chelators as it is water-soluble, odorless, stable and nearly non-toxic.[42] It binds to the inorganic mercury and forms non-toxic metal-chelator complex.[43-46] To test the efficiency of *meso*-DMSA chelation, we incubated Hg^{2+} with *meso*-DMSA for five minutes and then added it to the fluorescein-encapsulated liposomes for a final concentration of 1 μM of Hg^{2+}. In contrast to high the fluorescence intensity (97.83 $\pm$ 3.05 %) at the same concentration of Hg^{2+} in the absence of *meso*-DMSA, the fluorescence intensity remained unchanged in the presence of *meso*-DMSA (Figure 5.2b, 1μM + *meso*-DMSA). This experiment indicates that the mercury ions that bind to meso-DMSA can *no longer* interact with new lipid headgroups and therefore do not break up liposomes that encapsulate additional chelators.

In order to quantify the detection and budgeted chelation of Hg^{2+} simultaneously, we encapsulated 50 mM fluorescein with 0, 100, 1000 or 2000 μM *meso*-DMSA in the liposomes. The liposomes were then incubated with 1μM Hg^{2+} for 15 min. As shown in the inset of Figure 5.3, the concentration of *meso*-DMSA is inversely correlated with the fluorescence intensity inside of the liposomes. This result indicates that when the liposomes interact with the

mercury ions, some liposomes rupture and release the encapsulated dye and *meso*-DMSA. The released dye results in the increase in fluorescence intensity while the released *meso*-DMSA binds to the mercury ions; the resulting complex is unable to rupture the liposomes. As the concentration of *meso*-DMSA increases, fewer liposomes are ruptured resulting in smaller increase in fluorescence. This result further demonstrates that the liposomes comprise a single delivery platform that can be used for both Hg^{2+} detection and efficient Hg^{2+} chelation via the budgeted release of *meso*-DMSA from ion-responsive liposomes. Clearly, the rate of liposome rupture depends on the Hg^{2+} concentration. This important property allows for tuning the response of these liposomes by encapsulating different doses of the chelators. Since only a fraction of the liposomes are ruptured in this controlled chelation scheme, only as much chelators are released as necessary, leaving the rest intact for further detection and chelation of mercury contamination.

It is known that different ions can also interact with lipids, and potentially lead to adventitious interactions with liposomes. To test selectivity of the present system for mercury, we added 10 μM of different divalent metal ions and 1 mM Mg^{2+} and Ca^{2+} to the system. The increase in the fluorescence upon addition of 10 μM of essentially all other divalent metal ions and 1 mM of Ca^{2+} or Mg^{2+} is drastically lower compared to the increase on addition of only 10 nM of Hg^{2+} (see Figure 5.3). This result suggests that the system in not only sensitive but also selective to Hg^{2+}.

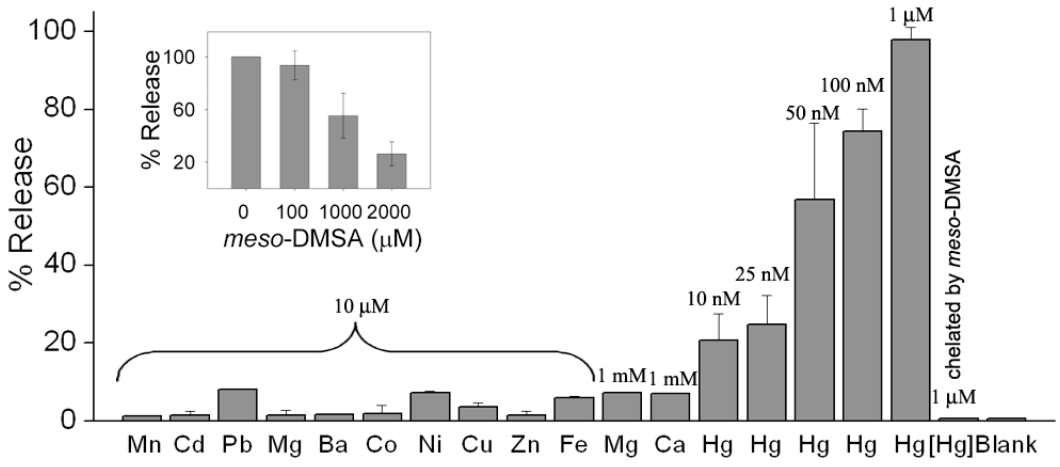


Figure 5.3 Fluorescence change in fluorescein encapsulated liposomes with various divalent metal ions and different concentrations of Hg^{2+}. Inset: fluorescence increase with fluorescein and various concentration of *meso*-DMSA encapsulated DOPE liposomes with 1 μM Hg^{2+}. The [Hg] indicates mercury chelated with *meso*-DMSA. Experiments are performed in triplicate.

To find out if such selectivity is maintained not only when individual metal ion is tested, as shown in Figure 5.3, but also when mixtures of metal ions are used, we compared the increase in fluorescence intensity between the liposome encapsulating fluorescein alone and the liposome encapsulating both fluorescein and *meso*-DMSA in the presence of 1μM Hg^{2+} and 10 μM Mn^{2+}, Cd^{2+}, Ba^{2+}, Co^{2+} or Cu^{2+}. As shown in Figure 5.4, the liposomes containing fluorescein and *meso*-DMSA has significantly less fluorescent increase than the liposomes containing only fluorescein, suggesting that Hg^{2+} effect are maintained in the presence of excess of other metal ions.

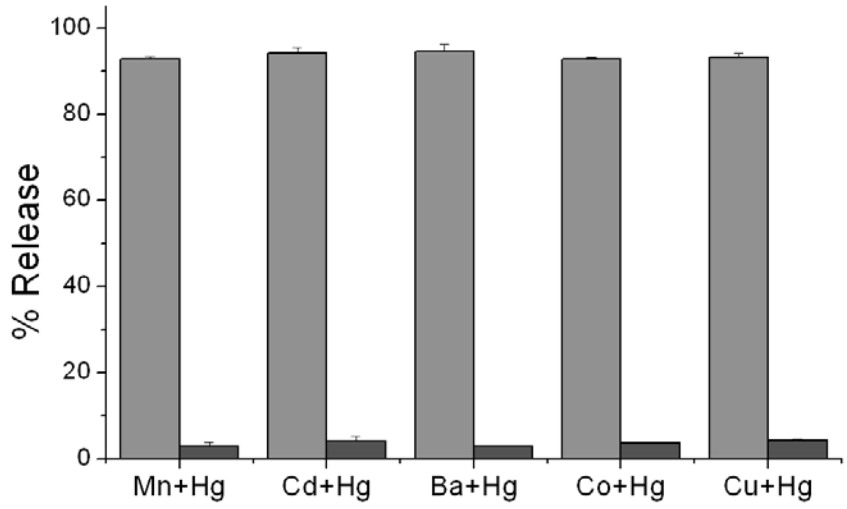


Figure 5.4: Fluorescence change in 50 mM fluorescein encapsulated (light gray) or 50 mM fluorescein and 3 mM *meso*-DMSA encapsulated liposomes with 10 μM Mn^{2+}+ 1 μM Hg^{2+},10 μM Cd^{2+}+ 1 μM Hg^{2+}, 10 μM Ba^{2+}+ 1 μM Hg^{2+}, 10 μM Co^{2+}+ 1 μM Hg^{2+} or 10 μM Co^{2+}+ 1 μM Hg^{2+}. Experiments are performed in triplicate.

After demonstrating the controlled and budgeted release of a Hg^{2+} chelator *in vitro*, we assessed whether this approach can be used in a biological systems. First, we utilized the HeLa cells in this study and checked the viability of the HeLa cells in the presence of Hg^{2+} at a concentration of 0, 0.2, 0.4, 0.6, 0.8 and 1.0 μM. As shown in the Figure 5.5a, the cell viability decreased dramatically to 35.7% in the presence of 0.2 μM Hg^{2+} and further decreased to 24.0 % in the presence of 0.4 μM Hg^{2+}, which confirmed the toxicity of Hg^{2+} to the cells. Incubating the HeLa cells with liposomes without any chelator resulted in almost identical toxicity profiles as the cells in the absence of liposome, indicating that the liposomes cannot interact with Hg^{2+} to reduce its toxicity. In contrast, when 2 μM *meso*-DMSA-containing liposome was incubated with the HeLa cells,

substantially improved viabilities were observed. The cell viabilities improved 56.8% and 43.1% when 2 μM *meso*-DMSA was added to the cell culture media containing 0.2 and 0.4 μM Hg^{2+}, respectively, than those without *meso*-DMSA (Figure 5.5a). The cell viability did not improve beyond 0.6 μM of Hg^{2+}, probably due to the limitation of amount of 2 μM *meso*-DMSA that can be encapsulated into liposome and their incomplete release. To provide further evidence for dosage-dependence protection, we carried out the same experiment in the presence of a constant concentration of 0.4 μM Hg^{2+} and used HeLa cells that were pretreated with increasing concentrations of either liposome alone (LP) or liposome with *meso*-DMSA (LP-*meso*-DMSA). As shown in Figure 5.5b, different concentrations of liposome-treated cells without chelator inside have little effect on cell viability, while increasing concentrations of liposome encapsulated *meso*-DMSA resulted in higher cell viability (from 24.0% to 49.4%), indicating the effects of controlled and budgeted release of a Hg^{2+} chelator in cellular environment.

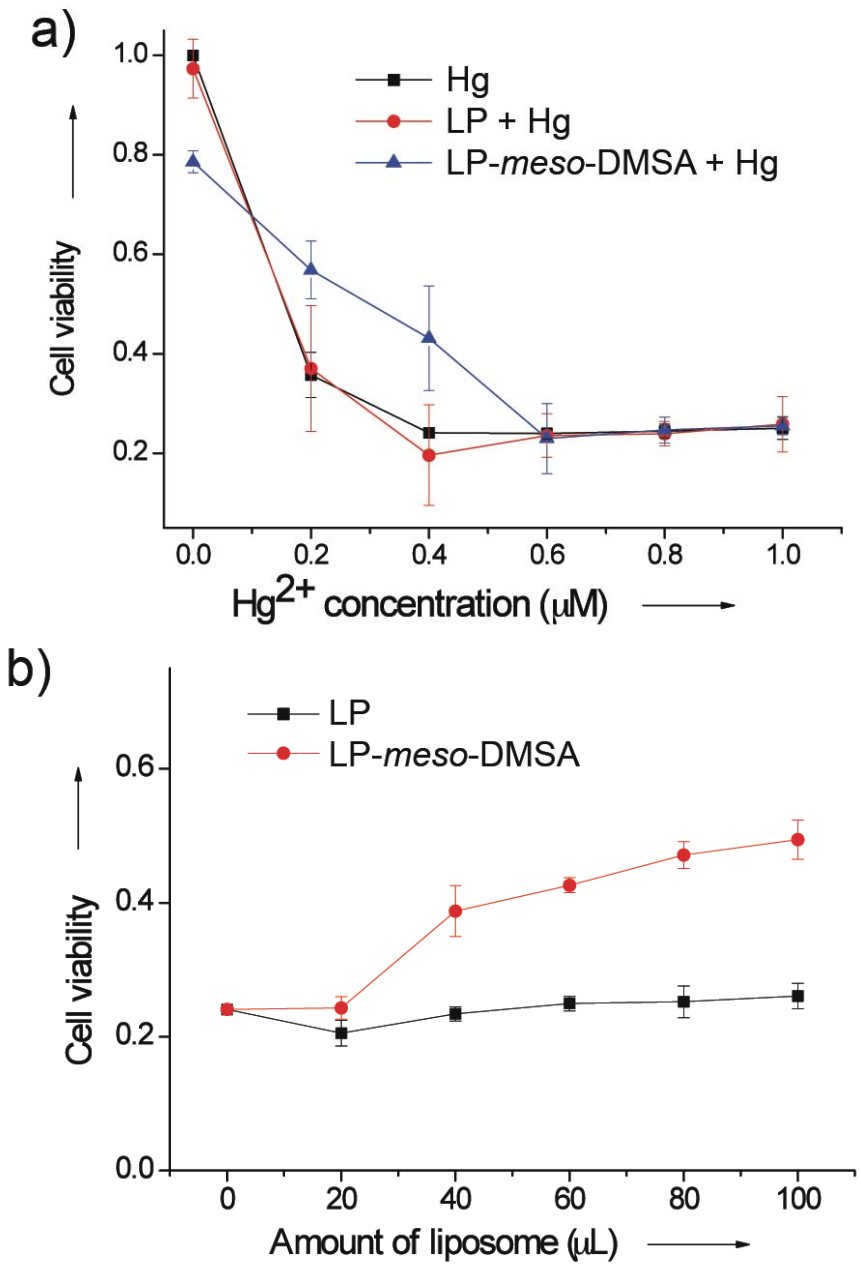


Figure 5.5: HeLa cells viability assays in the presence of different Hg^{2+} concentrations. **a)**, HeLa cells alone (Hg), HeLa cells initially treated with liposomes (LP +Hg), or with liposomes containing *meso*-DMSA (LP- meso-DMSA + Hg); **b)** 0.4 μM Hg^{2+}, were first treated with liposomes loaded with *meso*-DMSA (LP- *meso*-DMSA + Hg), or with no *meso*-DMSA (LP +Hg). Cell viability measured at Day 2 of liposome/cell incubation by MTT cytotoxicity assays.

5.4 Conclusion

Mercury is a highly toxic and widespread pollutant in the environment. Therefore, the strategy or the system that allows for both sensitive detection and efficient detoxification of mercury is in great demand. For this reason a number of mercury sensor related papers have been published recently. However, no single platform can detect and detoxify mercury at the same time. More importantly, since the distribution of mercury can be location- and time-specific, a single dose of mercury detoxification agent may be inefficient in dealing with various concentrations of Hg, and too high a concentration of the agent can potentially lead to side-effects.

We have demonstrated a multiple-use, liposome based system that can simultaneously detect and detoxify inorganic mercury, both in vitro and in HeLa cells, by controlled and budgeted release of both a fluorophore for sensing and a chelating agent for detoxification. This system is highly selective for mercury, and is able to detect mercury as low as 10 nM, the maximum contamination level defined by the US EPA. This budgeted release profile will be particularly useful in situations where the local levels of Hg contamination vary in a location- and time- dependent manner.

5.5 References

[1] Samad, A., Sultana, Y. and Aqil, M. (2007). Liposomal drug delivery systems: an update review. Current Drug Delivery 4, 297-305.

[2] Dass, C.R. (2008). Drug delivery in cancer using liposomes. Methods in Molecular Biology 437, 177-182.

[3] Girault, L., Lemaire, P., Boudou, A., Debouzy, J.-C. and Dufourc, E.J. (1996). Interactions of inorganic mercury with phospholipid micelles and model membranes. A 31P-NMR study. European Biophysics Journal 24, 413-421.

[4] Harris, H.H., Pickering, I.J. and George, G.N. (2003). The chemical form of mercury in fish. Science 301, 1203.

[5] Nolan, E.M. and Lippard, S.J. (2003). A "Turn-On" fluorescent sensor for the selective detection of mercuric ion in aqueous media. Journal of the American Chemical Society 125, 14270-14271.

[6] Kikuchi, K., Komatsu, K. and Nagano, T. (2004). Zinc sensing for cellular application. Current opinion in chemical biology 8, 182-191.

[7] Komatsu, K., Kikuchi, K., Kojima, H., Urano, Y. and Nagano, T. (2005). Selective zinc sensor molecules with various affinities for Zn2+, revealing dynamics and degional distribution of synaptically released Zn2+ in hippocampal slices. Journal of the American Chemical Society 127, 10197-10204.

[8] Wang, T. and Guo, Z. (2006). Copper in medicine: homeostasis, chelation therapy and antitumor drug design. Current Medicinal Chemistry 13, 525-537.

[9] Qian, F., Zhang, C., Zhang, Y., He, W., Gao, X., Hu, P. and Guo, Z. (2009). Visible light excitable Zn2+ fluorescent sensor derived from an intramolecular charge transfer fluorophore and its in vitro and in vivo application. Journal of the American Chemical Society 131, 1460-1468.

[10] Yoon, J., Ohler, N.E., Vance, D.H., Aumiller, W.D. and Czarnik, A.W. (1997). A fluorescent chemosensor signaling only Hg(II) and Cu(II) in water. Tetrahedron Lett. 38, 3845-3848.

[11] Guo, X., Qian, X. and Jia, L. (2004). A highly selective and sensitive fluorescent chemosensor for Hg2+ in neutral buffer aqueous solution. Journal of the American Chemical Society 126, 2272-2273.

[12] Caballero, A. et al. (2005). Highly selective chromogenic and redox or fluorescent sensors of Hg2+ in aqueous environment based on 1,4-

disubstituted azines. Journal of the American Chemical Society 127, 15666-15667.

[13] Yoon, S., Albers, A.E., Wong, A.P. and Chang, C.J. (2005). Screening mercury levels in fish with a selective fluorescent chemosensor. Journal of the American Chemical Society 127, 16030-16031.

[14] Yang, Y.-K., Yook, K.-J. and Tae, J. (2005). A rhodamine-based fluorescent and colorimetric chemodosimeter for the rapid detection of Hg2+ ions in aqueous media. Journal of the American Chemical Society 127, 16760-16761.

[15] Nolan, E.M., Racine, M.E. and Lippard, S.J. (2006). Selective Hg(II) detection in aqueous solution with thiol derivatized fluoresceins. Inorganic Chemistry 45, 2742-2749.

[16] Kim, S.H., Kim, J.S., Park, S.M. and Chang, S.-K. (2006). Hg2+-selective OFF-ON and Cu2+-selective ON-OFF type fluoroionophore based upon cyclam. Organic letters 8, 371-374.

[17] Ha-Thi, M.-H., Penhoat, M., Michelet, V. and Leray, I. (2007). Highly selective and sensitive phosphane sulfide derivative for the detection of Hg2+ in an organoaqueous medium. Organic letters 9, 1133-1136.

[18] Nolan, E.M. and Lippard, S.J. (2007). Turn-On and ratiometric mercury sensing in water with a red-emitting probe. Journal of the American Chemical Society 129, 5910-5918.

[19] Yoon, S., Miller, E.W., He, Q., Do, P.H. and Chang, C.J. (2007). A bright and specific fluorescent sensor for mercury in water, cells, and tissue. Angewandte Chemie, International Edition 46, 6658-6661.

[20] Ono, A. and Togashi, H. (2004). Molecular sensors: Highly selective oligonucleotide-based sensor for mercury(II) in aqueous solutions. Angewandte Chemie, International Edition 43, 4300-4302.

[21] Wang, Z., Heon Lee, J. and Lu, Y. (2008). Highly sensitive "turn-on" fluorescent sensor for Hg2+ in aqueous solution based on structure-switching DNA. Chem Commun (Camb), 6005-6007.

[22] Liu, X., Tang, Y., Wang, L., Zhang, J., Song, S., Fan, C. and Wang, S. (2007). Optical detection of mercury(II) in aqueous solutions by using conjugated polymers and label-free oligonucleotides. Advanced Materials 19, 1471-1474.

[23] Zhao, Y. and Zhong, Z. (2006). Tuning the sensitivity of a foldamer-based mercury sensor by its folding energy. Journal of the American Chemical Society 128, 9988-9989.

[24] Pallavicini, P., Diaz-Fernandez, Y.A., Foti, F., Mangano, C. and Patroni, S. (2007). Fluorescent sensors for Hg(2+) in micelles: a new approach that transforms an ON-OFF into an OFF-ON response as a function of the lipophilicity of the receptor. Chemistry (Weinheim an der Bergstrasse, Germany) 13, 178-187.

[25] Virta, M., Lampinen, J. and Karp, M. (1995). A luminescence-based mercury biosensor. Analytical Chemistry 67, 667-669.

[26] Chan, W.H., Yang, R.H. and Wang, K.M. (2001). Development of a mercury ion-selective optical sensor based on fluorescence quenching of 5,10,15,20-tetraphenylporphyrin. Analytica Chimica Acta 444, 261-269.

[27] Widmann, A. and van den Berg, C.M.G. (2005). Mercury detection in seawater using a mercaptoacetic acid modified gold microwire electrode. Electroanalysis 17, 825-831.

[28] Frasco, M.F., Colletier, J.-P., Weik, M., Carvalho, F., Guilhermino, L., Stojan, J. and Fournier, D. (2007). Mechanisms of cholinesterase inhibition by inorganic mercury. FEBS Journal 274, 1849-1861.

[29] Matsushita, M., Meijler, M.M., Wirsching, P., Lerner, R.A. and Janda, K.D. (2005). A blue fluorescent antibody-cofactor sensor for mercury. Organic letters 7, 4943-4946.

[30] Chen, P. and He, C. (2004). A general strategy to convert the MerR family proteins into highly sensitive and selective fluorescent biosensors for metal ions. Journal of the American Chemical Society 126, 728-729.

[31] Wegner, S.V., Okesli, A., Chen, P. and He, C. (2007). Design of an emission ratiometric biosensor from MerR family proteins: A sensitive

and selective sensor for Hg2+. Journal of the American Chemical Society 129, 3474-3475.

[32] Vannela, R. and Adriaens, P. (2007). In vitro selection of Hg (II) and As (V)-dependent RNA-cleaving DNAzymes. Environmental Engineering Science 24, 73-84.

[33] Liu, J. and Lu, Y. (2007). Rational design of "Turn-On" allosteric DNAzyme catalytic beacons for aqueous mercury ions with ultrahigh sensitivity and selectivity. Angewandte Chemie International Edition 46, 7587-7590.

[34] Heller, D.A., Jeng, E.S., Yeung, T.-K., Martinez, B.M., Moll, A.E., Gastala, J.B. and Strano, M.S. (2006). Optical Detection of DNA Conformational Polymorphism on Single-Walled Carbon Nanotubes. Science 311, 508-511.

[35] Lee, J.-S., Han, M.S. and Mirkin, C.A. (2007). Colorimetric detection of mercuric ion (Hg2+) in aqueous media by DNA-functionalized gold nanoparticles. Angewandte Chemie, International Edition 46, 4093-4096.

[36] Xue, X., Wang, F. and Liu, X. (2008). One-step, room temperature, colorimetric detection of mercury (Hg2+) using DNA/nanoparticle conjugates. Journal of the American Chemical Society 130, 3244-3245.

[37] Prodi, L., Bargossi, C., Montalti, M., Zaccheroni, N., Su, N., Bradshaw, J.S., Izatt, R.M. and Savage, P.B. (2000). An effective fluorescent chemosensor for mercury ions. Journal of the American Chemical Society 122, 6769-6770.

[38] Szurdoki, F., Ren, D. and Walt, D.R. (2000). A combinatorial approach to discover new chelators for optical metal ion sensing. Analytical Chemistry 72, 5250-5257.

[39] Liu, B. and Tian, H. (2005). A selective fluorescent ratiometric chemodosimeter for mercury ion. Chemical Communications (Cambridge, United Kingdom), 3156-3158.

[40] Song, K.C., Kim, J.S., Park, S.M., Chung, K.-C., Ahn, S. and Chang, S.-K. (2006). Fluorogenic Hg2+-selective chemodosimeter derived from 8-hydroxyquinoline. Organic letters 8, 3413-3416.

[41] Zhao, Y., Lin, Z., He, C., Wu, H. and Duan, C. (2006). A "Turn-On" fluorescent sensor for selective Hg(II) detection in aqueous media based on metal-induced dye formation. Inorganic chemistry 45, 10013-10015.

[42] Blanusa, M., Varnai, V.M., Piasek, M. and Kostial, K. (2005). Chelators as antidotes of metal toxicity: therapeutic and experimental aspects. Current medicinal chemistry 12, 2771-2794.

[43] Maiorino, R.M., Aposhian, M.M., Xu, Z.F., Li, Y., Polt, R.L. and Aposhian, H.V. (1993). Determination and metabolism of dithiol chelating agents. XV. The meso-2,3-dimercaptosuccinic acid-cysteine (1:2) mixed disulfide, a major urinary metabolite of DMSA in the human, increases the urinary excretion of lead in the rat. J Pharmacol Exp Ther 267, 1221-1226.

[44] Fang, X. and Fernando, Q. (1994). Synthesis, structure, and properties of rac-2,3-dimercaptosuccinic acid, a potentially useful chelating agent for toxic metals. Chem Res Toxicol 7, 148-156.

[45] Fang, X., Hua, F. and Fernando, Q. (1996). Comparison of rac- and meso-2,3-dimercaptosuccinic acids for chelation of mercury and cadmium using chemical speciation models. Chem Res Toxicol 9, 284-290.

[46] Garza-Ocanas, L., Torres-Alanis, O. and Pineyro-Lopez, A. (1997). Urinary mercury in twelve cases of cutaneous mercurous chloride (calomel) exposure: effect of sodium 2,3-dimercaptopropane-1-sulfonate (DMPS) therapy. J Toxicol Clin Toxicol 35, 653-655.